REPORT 1146

AERODYNAMIC FORCES AND LOADINGS ON SYMMETRICAL CIRCULAR-ARC AIRFOILS WITH PLAIN LEADING-EDGE AND PLAIN TRAILING-EDGE FLAPS[1]

By Jones F. Cahill, William J. Underwood, Robert J. Nuber, and Gail A. Cheesman

SUMMARY

An investigation has been made in the Langley two-dimensional low-turbulence tunnel and in the Langley two-dimensional low-turbulence pressure tunnel of 6- and 10-percent-thick symmetrical circular-arc airfoil sections at low Mach numbers and several Reynolds numbers. The airfoils were equipped with 0.15-chord plain leading-edge flaps and 0.20-chord plain trailing-edge flaps. The section lift and pitching-moment characteristics were determined for both airfoils with the flaps deflected individually and in combination. The section drag characteristics were obtained for the 6-percent-thick airfoil with the flaps partly deflected as low-drag-control flaps and for both airfoils with the flaps neutral. Surface pressures were measured on the 6-percent-thick airfoil section with the flaps deflected either individually or in appropriate combination to furnish flap load and hinge-moment data applicable to the structural design of the airfoil.

The experimental results showed maximum lift coefficients of 1.95 and 2.03 for the optimum combinations of deflection of leading-edge flaps and trailing-edge flaps as compared with 0.73 and 0.67 for the plain 6- and 10-percent-thick airfoils, respectively. Scale effect on the maximum lift coefficients was, in general, small. The aerodynamic center was ahead of the quarter-chord point and moved toward the leading edge when either the leading-edge flap or the trailing-edge flap was deflected. Deflecting the leading-edge flap was more effective in extending the low-drag range to higher section lift coefficients than deflecting the trailing-edge flap. The maximum flap normal-force and hinge-moment coefficients were, respectively, 4.74 and 2.24 for the leading-edge flap as compared with 1.48 and −0.61 for the trailing-edge flap.

A generalized method is developed that permits the determination of the chordwise pressure distribution over sharp-edge airfoils with plain leading-edge flaps and plain trailing-edge flaps of arbitrary size and deflection.

INTRODUCTION

Thin sharp-edge wings designed to minimize wave resistance have been proposed for use on high-speed aircraft. If, however, the aircraft is to land safely or to fly satisfactorily in the low-speed range, means must be provided for increasing the naturally low maximum lift of the sharp-edge airfoils. Because leading-edge separation appears to be the limiting factor, the use of leading-edge high-lift devices is indicated as a possible means for improving the maximum-lift characteristics. An investigation has accordingly been made in the Langley two-dimensional low-turbulence tunnel and in the Langley two-dimensional low-turbulence pressure tunnel of the aerodynamic forces on 6- and 10-percent-thick symmetrical circular-arc airfoil sections and of the aerodynamic loadings on the 6-percent-thick airfoil section at a low Mach number and several Reynolds numbers. The airfoils were equipped with 0.15-chord plain leading-edge flaps and 0.20-chord plain trailing-edge flaps.

The section lift and pitching-moment characteristics were determined for both airfoils with the high-lift devices deflected individually and in combination. The section drag characteristics were obtained for the 6-percent-thick airfoil with the flaps partly deflected as low-drag-control flaps and for both airfoils with the flaps neutral. Surface pressures were measured on the 6-percent-thick airfoil section with the flaps deflected either individually or in appropriate combination to furnish flap load and hinge-moment data applicable to the structural design of the airfoil.

In an effort to provide the designer with additional section-load information, a generalized method has been developed that permits the determination of the chordwise pressure distribution over sharp-edge airfoils with plain leading-edge flaps and plain trailing-edge flaps of arbitrary size and deflection.

COEFFICIENTS AND SYMBOLS

c_l	airfoil section lift coefficient, l/qc
$c_{l_{b\delta}}$	change in ideal lift coefficient caused by flap deflection
c_{l_a}	airfoil section additional lift coefficient due to angle of attack, $c_l - c_{l_{b\delta}}$
$\Delta c_{l_{max}}$	increment of maximum section lift coefficient due to flap deflection
c_d	airfoil section drag coefficient, d/qc
$c_{m_{c/4}}$	airfoil section pitching-moment coefficient about quarter chord, Pitching moment about quarter chord$/qc^2$

[1] Based on recently declassified NACA RM L6K22, "Two-Dimensional Wind-Tunnel Investigation at High Reynolds Numbers of Two Symmetrical Circular-Arc Airfoil Sections With High-Lift Devices," by William J. Underwood and Robert J. Nuber, 1947; NACA RM L7H04, "Aerodynamic Load Measurements Over Leading-Edge and Trailing-Edge Plain Flaps on a 6-Percent-Thick Symmetrical Circular-Arc Airfoil Section," by William J. Underwood and Robert J. Nuber, 1947; and NACA RM L50H17a, "A Method for Predicting the Low-Speed Chordwise Pressure Distribution Over Sharp-Edge Airfoil Sections With Plain Flaps at the Leading and Trailing Edges," by Robert J. Nuber and Jones F. Cahill, 1950.

321695—55——58

$c_{m_{ac}}$ airfoil section pitching-moment coefficient about aerodynamic center, Pitching moment about aerodynamic center/qc^2
c_n flap section normal-force coefficient, n/qc_f
c_c flap section chord-force coefficient, x'/qc_f
c_h flap section hinge-moment coefficient, h/qc_f^2
l airfoil lift per unit span
d drag per unit span
m pitching moment per unit span
n flap normal force per unit span, positive upward
x' flap-chord force per unit span, positive toward trailing edge
h flap hinge moment per unit span, positive when trailing edge tends to deflect downward or leading edge upward
S surface-pressure coefficient, in incompressible flow, $\frac{H_0-p}{q}=\left(\frac{v}{V}\right)^2$
P pressure-difference coefficient across airfoil, $\frac{p_U-p_L}{q}$
p local static pressure
H_0 free-stream total pressure
q free-stream dynamic pressure, $\rho V^2/2$
V free-stream velocity
v local velocity on surface of basic uncambered airfoil at zero angle of attack
v' incremental local velocity on airfoil surface due to separation
v_b effective local velocity on surface of basic airfoil at any given lift coefficient
Δv_a additional local velocity on airfoil surface due to departure from ideal lift coefficient
c airfoil chord with all flaps neutral
c_f flap chord
t airfoil thickness
x distance behind leading edge, in.
y distance above or below chord, in.
$E=\frac{c_f}{c}$
α_0 airfoil section angle of attack, deg
$\Delta\alpha_{c_{l_{max}}}$ increment of section angle of attack at maximum lift due to flap deflection
δ flap deflection, positive when deflected below chord line, deg
ρ free-stream density
R Reynolds number
M Mach number

Subscripts:

N leading-edge flap
F trailing-edge flap
i ideal
U upper surface
L lower surface
$b\delta$ refers to conditions at ideal lift coefficient with flap deflected
a refers to difference between conditions at ideal lift coefficient and any arbitrary lift coefficient

MODELS

Two symmetrical circular-arc airfoil sections with thicknesses of 6 percent and 10 percent are discussed. Ordinates of the 6- and 10-percent-thick circular-arc airfoil sections are given in tables I and II, respectively. Both of the circular-arc airfoil models had a 24-inch chord and a 35.5-inch span and were made of steel. Each model was equipped with a 0.20-chord plain trailing-edge flap and a 0.15-chord plain leading-edge flap which were pivoted on leaf hinges mounted flush with the lower surface. The flaps of the 6-percent-thick airfoil were made of brass and those of the 10-percent-thick airfoil were made of duralumin. Sketches of the models are presented in figure 1. After the force tests were complete, pressure orifices were installed on the 6-percent-thick model at the midspan in a single chordwise row. The chordwise positions of these orifices are given in figure 2. Model end plates were used to facilitate setting the deflection of the plain leading-edge flap and plain trailing-edge flap. Figure 3 shows photographs of the model with and without model end plates.

The models were designed so that trailing-edge-flap deflections δ_F up to 60° and leading-edge-flap deflections δ_N up to 50° could be obtained. The flaps were sealed at the hinge line by having the flap skirt in rubbing contact with the flap. When the trailing-edge flap of the 6-percent-thick airfoil was deflected beyond 50°, the gap between the flap and skirt was sealed with modeling clay to prevent leakage.

For all tests, the surfaces of the models were finished with No. 400 carborundum paper to produce smooth surfaces; slight discontinuities, however, still existed at the leaf hinges on the lower surfaces and at the line of contact between the flaps and flap skirts.

TESTS

A summary of the tests made on the two airfoil sections is given in table III showing the model configurations and

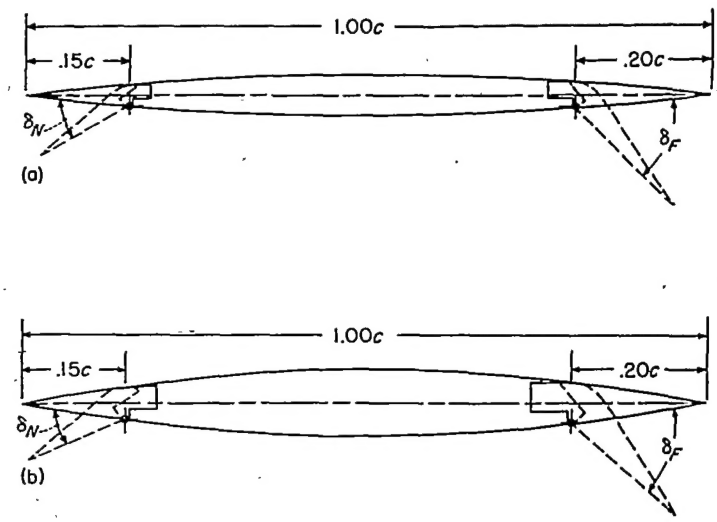

(a) 6-percent-thick airfoil.
(b) 10-percent-thick airfoil.

FIGURE 1.—Symmetrical circular-arc airfoils with plain leading-edge flaps and plain trailing-edge flaps.

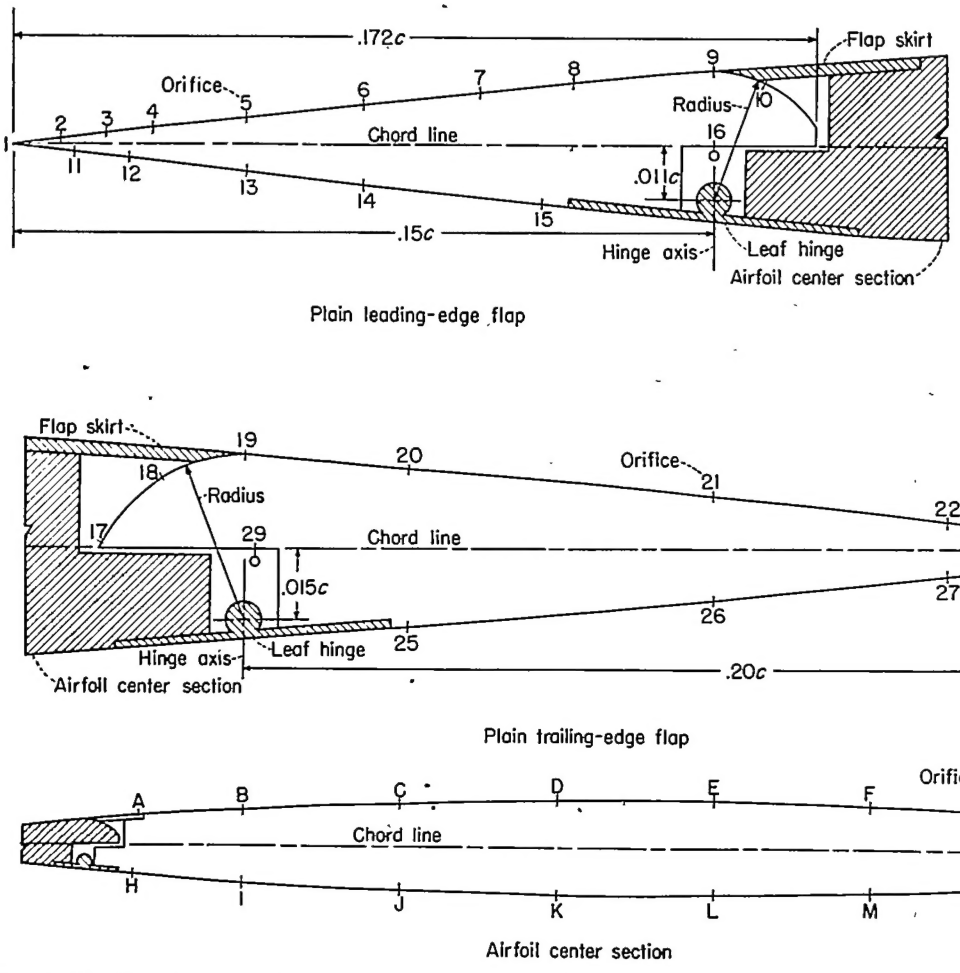

FIGURE 2.—Location of pressure orifices on 6-percent-thick airfoil with a 0.15-chord plain leading-edge flap and a 0.20-chord plain trailing-edge flap.

Plain Leading-Edge Flap

Orifice	x/c	y/c
1	0	0
2	1	.11
3	2	.23
4	3	.35
5	5	.57
6	7.5	.84
7	10	1.08
8	12	1.28
9	15	1.47
10	16.1	1.17
11	1.3	−.15
12	2.6	−.30
13	5	−.57
14	7.5	−.83
15	11.4	−1.21
16	15	−.11

Plain Trailing-Edge Flap

Orifice	x/c	y/c
17	77.03	0.25
18	78.3	1.54
19	80	1.87
20	85	1.53
21	90	1.08
22	95	.57
23	97.5	.29
24	100	0
25	85	−1.53
26	90	−1.08
27	95	−.57
28	97.5	−.29
29	80.3	−.15

Airfoil Center Section

Orifice	x/c
A	18.3
B	25
C	35
D	45
E	55
F	65
G	74
H	18.1
I	25
J	35
K	45
L	55
M	65
N	75

the figures in which the data are presented. The airfoil lift, drag, and pitching moment were measured and corrected to free-air conditions by the methods described in reference 1. The flap section normal-force, chord-force, and hinge-moment coefficients were obtained from mechanical integration of the pressure distributions. Lift measurements of the models with the flaps neutral, with and without model end plates, indicated that the model end plates had no significant effect on the measured characteristics.

RESULTS AND DISCUSSION

AIRFOILS WITH FLAPS NEUTRAL

The section aerodynamic characteristics of the 6- and 10-percent-thick symmetrical circular-arc airfoils with the flaps neutral are presented in figure 4.

The maximum section lift coefficients are 0.73 and 0.67 for the 6- and 10-percent-thick airfoils, respectively. This decrease in maximum section lift coefficient with increasing airfoil thickness is opposite to the trends that are shown by

the data for NACA 6-series airfoils (ref. 1) through the same thickness range, but it is believed to be explainable in the following manner: As the thickness of the NACA 6-series airfoils is increased from 6 to 10 percent, the corresponding increase in the airfoil leading-edge radius results in improved air-flow conditions around the leading edge at the high angles of attack. The increase in trailing-edge angle that results from increasing thickness tends to decrease the maximum section lift coefficient due to an increase in boundary-layer thickness on the upper surface. The favorable effect of a large leading-edge radius appears to predominate in this thickness range for the NACA 6-series airfoils and higher values of maximum lift are produced. For the circular-arc airfoils, however, the leading edges of both the 6- and 10-percent-thick airfoils are sharp and the air-flow conditions around the leading edges at high angles of attack are about the same. The effect of an increase in trailing-edge angle with increasing thickness therefore is a decrease of maximum lift.

The lift-curve slopes are 0.097 and 0.090 for the 6- and 10-percent-thick airfoils, respectively. Because the air-flow

(a) With model end plates.

FIGURE 3.—Front of a symmetrical circular-arc airfoil with and without model end plates in the Langley two-dimensional low-turbulence pressure tunnel.

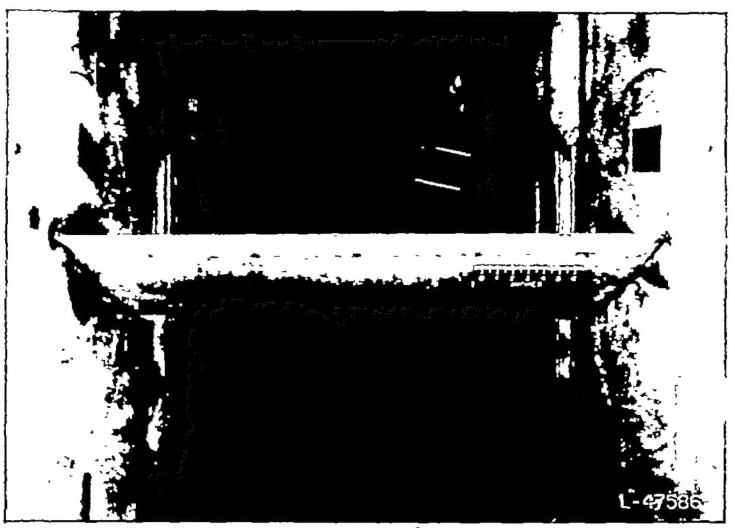

(b) Without model end plates.

FIGURE 3.—Concluded.

conditions around the leading edge of both circular-arc airfoils are probably very nearly alike through the complete range of angle of attack, the thicker boundary layer of the 10-percent-thick airfoil is probably the cause of the decrease in the lift-curve slope. The slope of the lift curve for the 10-percent-thick airfoil was measured at small positive or negative values of the lift coefficient to avoid including the slight jog in the lift curve that occurs near zero lift. This jog in the lift curve has been noticed before in connection with sharp leading-edge airfoils (ref. 2) and appeared when the trailing-edge angle became large. Although a similar phenomenon may have existed on the 6-percent-thick airfoil, it was not of sufficient magnitude to be noticeable in the lift curve. The data (fig. 4) show no appreciable scale effect on the lift characteristics of either circular-arc airfoil with the flaps neutral through the range of Reynolds number investigated.

The variation of the quarter-chord pitching-moment coefficient of both the 6- and 10-percent-thick circular-arc airfoils indicates a forward position of the aerodynamic center with respect to the quarter-chord point of the airfoil. This variation of the pitching moment probably results from the relative thickening of the boundary layer near the trailing edge on the upper surface with increasing angle of attack. The aerodynamic center of the 10-percent-thick airfoil is more forward than that of the 6-percent-thick airfoil. This shift in aerodynamic-center position is in fair quantitative agreement with data presented in reference 3 which show that increases in trailing-edge angle or in the thickness of the rear portion of an airfoil cause the aerodynamic-center position to move forward. As is usually true when an airfoil stalls, the center of pressure of the circular-arc airfoils moves toward the rear and the quarter-chord moment coefficient increases negatively in the normal manner. The small negative pitching moment of both models at zero lift is attributed to asymmetrical loading resulting from very small model irregularities.

For airfoils having sharp leading edges, the drag coefficient increases fairly rapidly as the angle of attack departs from zero. In general, the drag coefficients decrease with increasing Reynolds number in approximately the manner expected for fully developed turbulent flow on both surfaces. In the case of the 6-percent-thick airfoil, however, laminar flow apparently was obtained over a fairly extensive portion of the upper surface at zero and negative angles of attack at Reynolds numbers of 3×10^6 and 6×10^6, as indicated by the lower drag for these conditions as compared with the drag obtained at a Reynolds number of 9×10^6.

AIRFOILS WITH FLAPS DEFLECTED INDIVIDUALLY

The lift and pitching-moment characteristics of the two symmetrical circular-arc airfoils with the plain trailing-edge flaps and plain leading-edge flaps deflected individually are presented in figures 5 and 6, respectively.

The maximum section lift coefficients of the 6- and 10-percent-thick airfoils increased and the angles of attack for maximum lift decreased as the 0.20-chord trailing-edge flaps were deflected. The values of the maximum lift coefficients (fig. 5) for both airfoils were substantially equivalent at corresponding flap deflections.

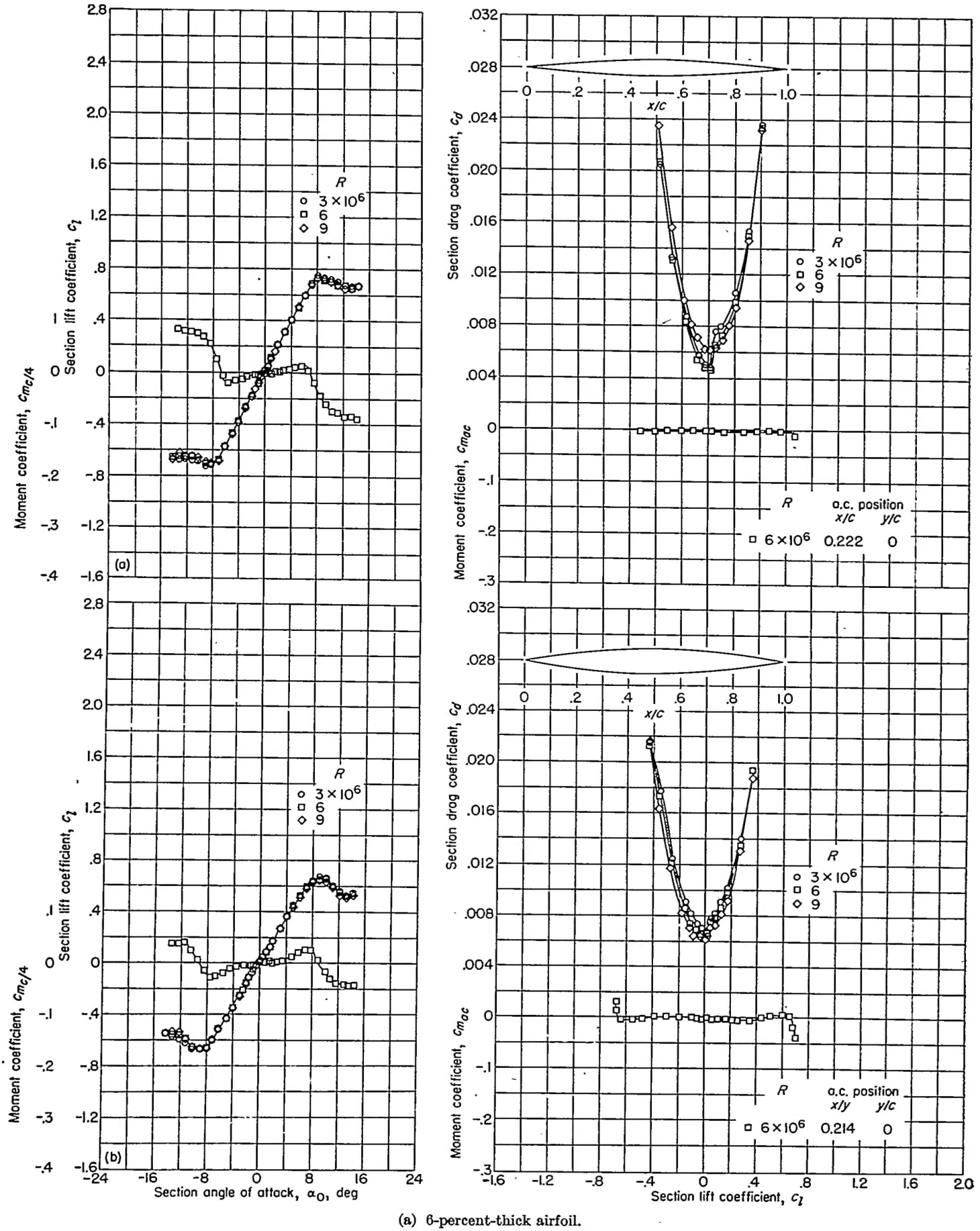

(a) 6-percent-thick airfoil.
(b) 10-percent-thick airfoil.

FIGURE 4.—Aerodynamic characteristics of two symmetrical circular-arc airfoils with flaps neutral.

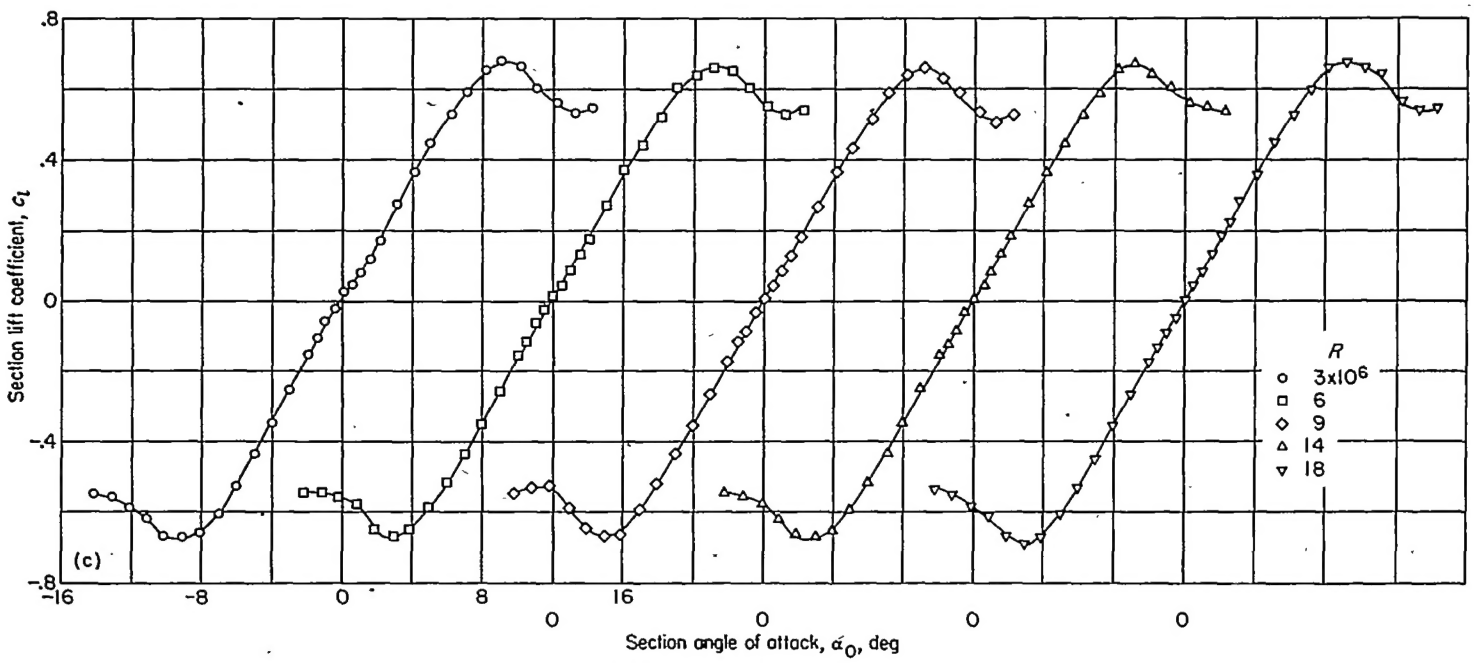

(c) 10-percent-thick airfoil.

FIGURE 4.—Concluded.

Deflecting the 0.15-chord leading-edge flaps increased the maximum section lift coefficients and increased the angles of attack for maximum lift (fig. 6) primarily by alleviating the negative pressure peaks that cause leading-edge separation near maximum lift. These pressure peaks are alleviated because the flow approaching the leading edge is more nearly alined at high angles of attack when the leading-edge flap is deflected. The maximum section lift coefficients for the 6- and 10-percent-thick airfoils at the optimum deflection of the leading-edge flap, 30°, are 1.17 and 1.15, respectively. The optimum flap deflection is defined as the flap deflection for highest maximum lift. At corresponding deflections of the 0.15-chord leading-edge flap, the maximum section lift coefficients of both airfoils are essentially the same. At angles of attack well below those for maximum lift, the leading-edge flaps act as spoilers on the lower surface of the airfoils and cause some reduction in lift. These losses in lift increase as the flap deflection is increased.

The variation of the increment in maximum section lift coefficient $\Delta c_{l_{max}}$ and increment in angle of attack at maximum lift $\Delta\alpha_{c_{l_{max}}}$ for both models with deflection of the leading-edge or trailing-edge flaps individually is summarized in figure 7. From figure 7, it can be seen that the leading-edge-flap deflection for maximum lift, the optimum deflection, occurs at approximately 30° for both the 6- and 10-percent-thick airfoils. No optimum deflection was obtained for the trailing-edge flap because the highest test deflection was still the most effective. The maximum section lift coefficients of both airfoils are approximately the same at corresponding flap deflections, but the increments of maximum section lift coefficient obtained with flap deflection differ because of the lower maximum section lift coefficient of the 10-percent-thick airfoil with the flaps neutral. (See fig. 4.) Positive increments of the angle of attack for maximum lift resulted when the leading-edge flap was deflected, but negative increments resulted when the trailing-edge flap was deflected (fig. 7).

The pitching-moment characteristics of the two models (figs. 5 and 6) show that the aerodynamic center at low α_0 (near the ideal lift coefficient) continues to move toward the leading edge as either the leading-edge or trailing-edge flaps are deflected. At higher angles of attack, the center of pressure always moves to the rear and causes the variation of pitching moment with angle of attack to become stable. The increments in angle of attack and lift coefficient at which this change in stability occurs show approximately the same variation with flap deflection as is shown in figure 7 for maximum lift.

AIRFOILS WITH FLAPS DEFLECTED IN COMBINATION

The section lift characteristics of the two symmetrical circular-arc airfoils with the plain leading-edge flaps and plain trailing-edge flaps deflected in various combinations are presented in figure 8. The flap deflections that resulted in the highest maximum section lift coefficient were δ_N=30°, δ_F=60° (fig. 8 (a)) and δ_N=36°, δ_F=60° (fig. 8 (c)) for the 6- and 10-percent-thick airfoils, respectively. The data for the 10-percent-thick airfoil with the trailing-edge flap deflected 60° indicate no important changes in the maximum section lift coefficient with small departures from the optimum deflection of the leading-edge flap. A comparison between the lift characteristics of the two airfoils with the leading-edge flap deflected 30° and the trailing-edge flap deflected 60° (fig. 8) with those for the airfoil with the leading-edge flap neutral and the trailing-edge flap deflected 60° (fig. 5) shows that the maximum section lift coefficients were increased 0.32 and 0.30 (to 1.95 and 2.03) and the angles of attack for maximum lift were increased 6.5° and 6°, respectively, for the 6- and 10-percent-thick airfoils by deflection of the leading-edge flap.

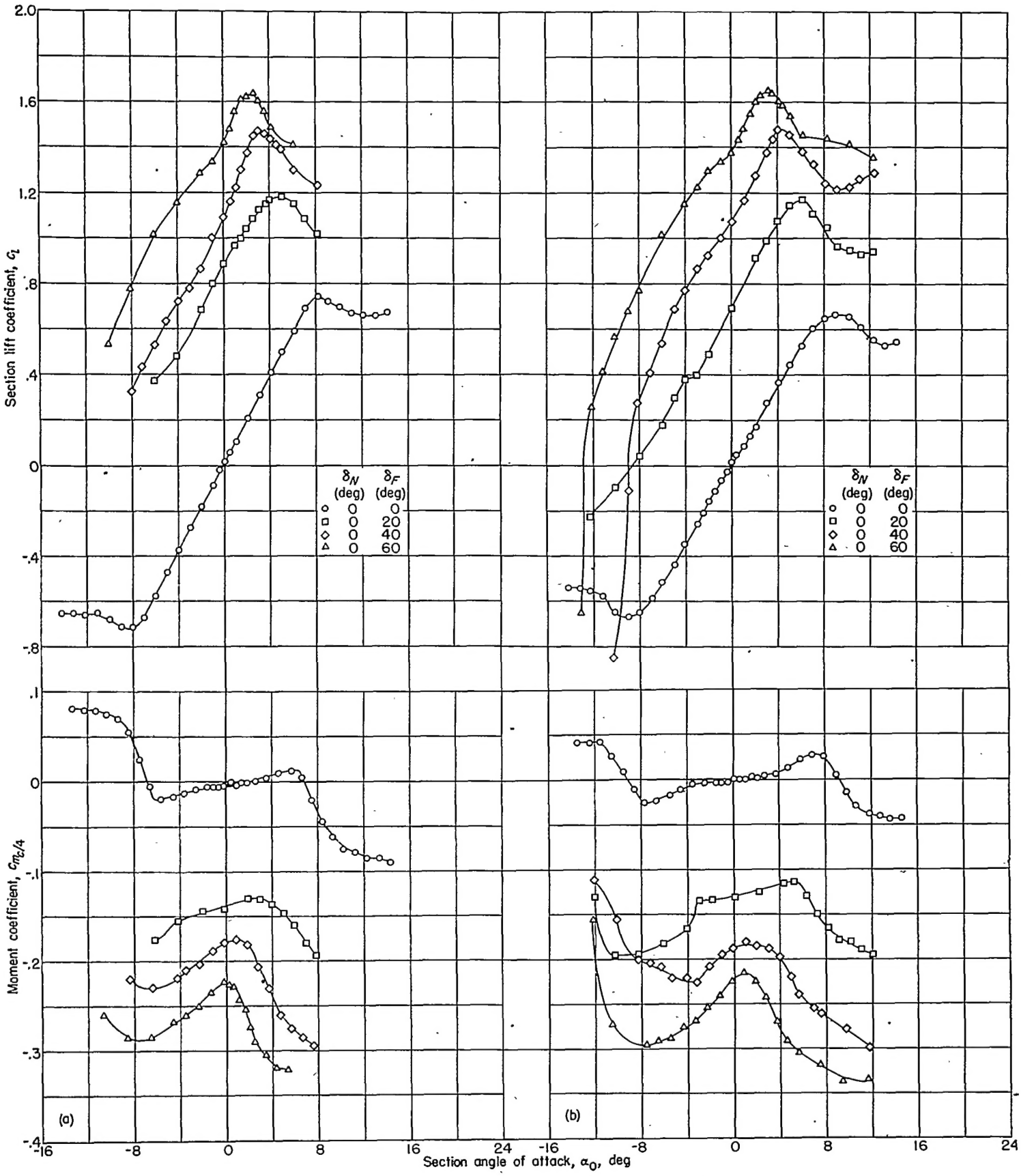

(a) 6-percent-thick airfoil. (b) 10-percent-thick airfoil.

FIGURE 5.—Section lift and pitching-moment characteristics of two symmetrical circular-arc airfoils for various deflections of the 0.20-chord plain trailing-edge flap; $R=6\times10^6$.

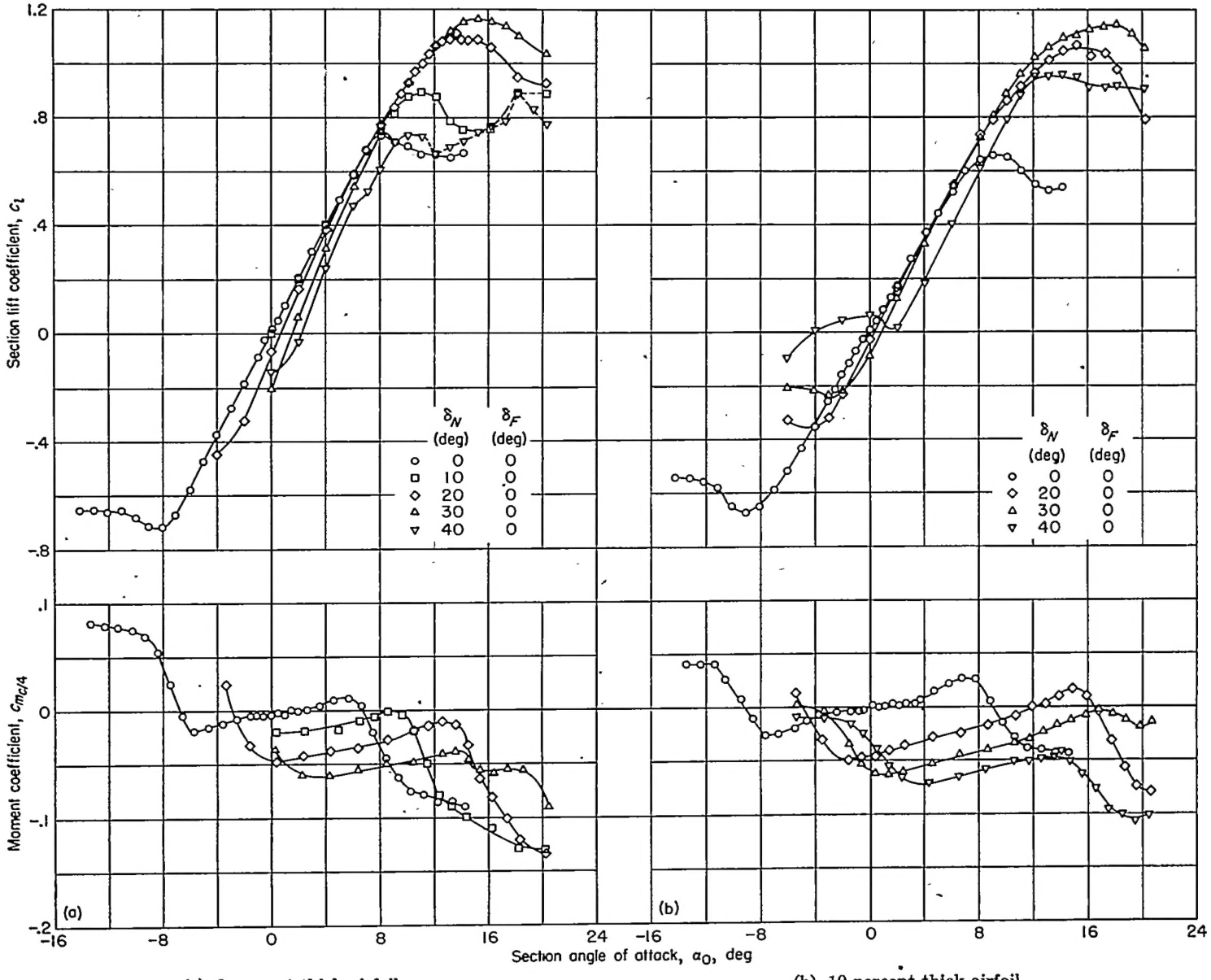

(a) 6-percent-thick airfoil. (b) 10-percent-thick airfoil.

FIGURE 6.—Section lift and pitching-moment characteristics of two symmetrical circular-arc airfoils for various deflections of the 0.15-chord plain leading-edge flap; $R=6\times10^6$.

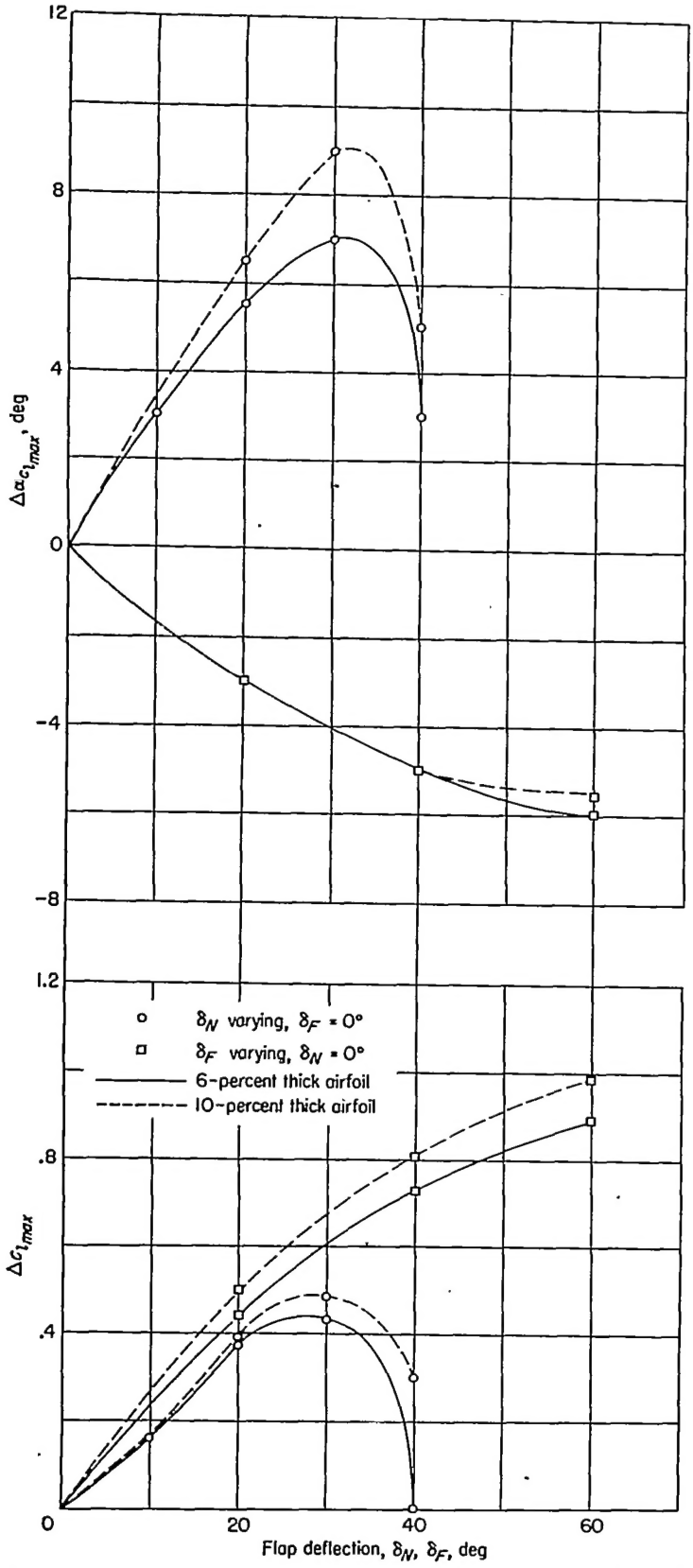

FIGURE 7.—Variation of the increment in maximum section lift coefficient and angle of stall with deflection of the plain leading-edge flap and plain trailing-edge flap; $R=6\times10^6$.

The section lift characteristics of the two models with the plain leading-edge flaps and plain trailing-edge flaps deflected 30° and 60°, respectively, obtained at Reynolds numbers of 3×10^6, 6×10^6, and 9×10^6 are presented in figure 9. At Reynolds numbers between 3×10^6 and 9×10^6, the data (fig. 9 (a)) show no appreciable scale effect on the maximum lift coefficient of the 6-percent-thick airfoil. The section lift characteristics of the 6-percent-thick airfoil with the leading- and trailing-edge flaps deflected 27° and 60°, respectively, are presented in figure 10 for Reynolds numbers from 0.70×10^6 to 2.29×10^6. In this range of Reynolds numbers, the maximum section lift characteristics of the 6-percent-thick airfoil are independent of scale. In the case of the 10-percent-thick airfoil (fig. 9 (b)), however, some adverse scale effect (nearly 0.1) is indicated in the maximum section lift coefficient at Reynolds numbers between 3×10^6 and 6×10^6. Similarly, some adverse scale effect (fig. 8 (c)) is indicated in the maximum section lift coefficient at Reynolds numbers between 3×10^6 and 9×10^6 with the leading- and trailing-edge flaps deflected 36° and 60°, respectively. At Reynolds numbers above 9×10^6, however, the maximum section lift coefficient of this combination remained approximately constant.

The section pitching-moment characteristics of the two airfoils with the leading- and trailing-edge flaps deflected 30° and 60°, respectively, (fig. 9) show that the aerodynamic center remains ahead of the quarter-chord point for angles of attack greater than zero. In addition, the combined action of the leading- and trailing-edge flaps caused the moment coefficients to increase negatively with increasing lift coefficient until the angle of attack was high enough to alleviate the spoiler action of the leading-edge flap. As the lift coefficient was increased beyond this point, the moment became less negative until approximately 2.5° beyond the angle of attack for maximum lift, whereupon the moment curve breaks.

LOW-DRAG-CONTROL FLAPS

The lift and drag characteristics of the 6-percent-thick symmetrical circular-arc airfoil with the leading- and trailing-edge flaps deflected are presented in figure 11. Deflecting the leading-edge flap to 10° decreased the section drag coefficient of the 6-percent-thick airfoil at a lift coefficient of 0.3 about 40 percent by delaying the formation of a negative pressure peak at the leading edge which causes separation. In general, the leading-edge flap was more effective in extending the low drag range to higher section lift coefficients than was the trailing-edge flap.

AIRFOIL LOADING

Pressure coefficients obtained from orifice static-pressure measurements made on the 6-percent-thick symmetrical circular-arc airfoil with the plain leading- and trailing-edge flaps deflected in various combinations and at several angles of attack are presented in table IV.

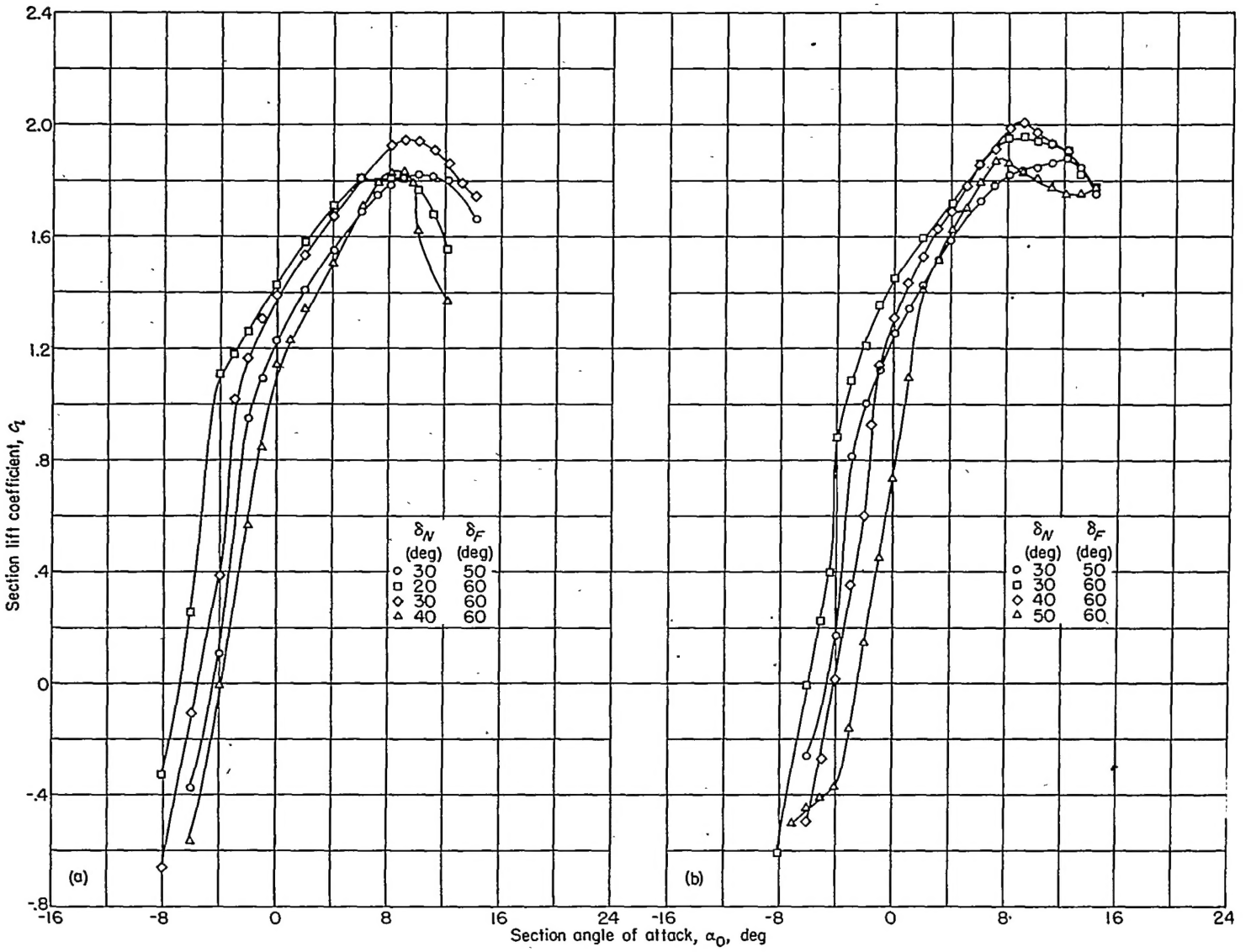

(a) 6-percent-thick airfoil. $R=6\times10^6$. (b) 10-percent-thick airfoil. $R=6\times10^6$.

FIGURE 8.—Section lift characteristics of two symmetrical circular-arc airfoils for various deflections of the plain leading-edge flap and plain trailing-edge flap.

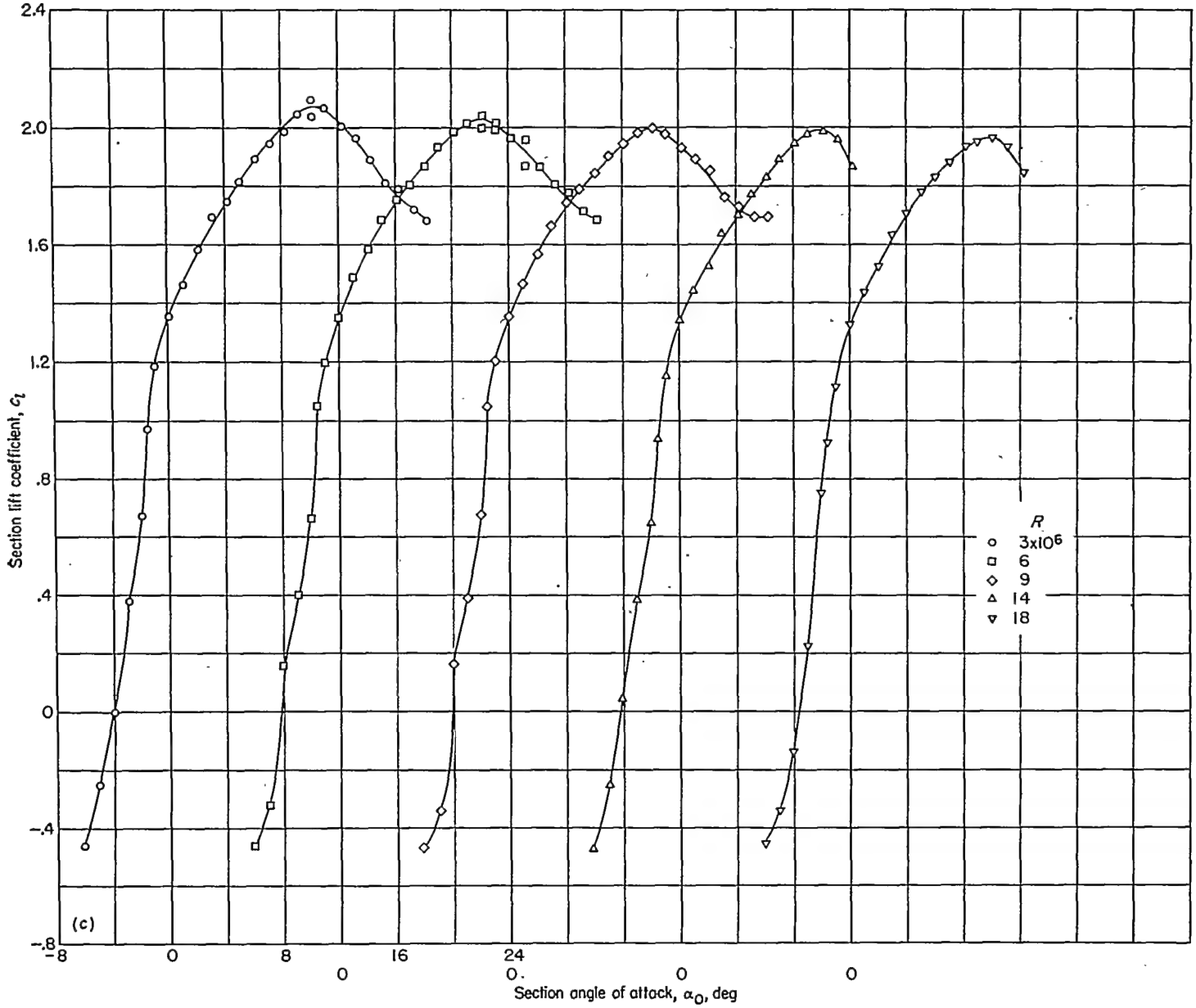

(c) 10-percent-thick airfoil. $\delta_N=36°$, $\delta_F=60°$.

FIGURE 8.—Concluded.

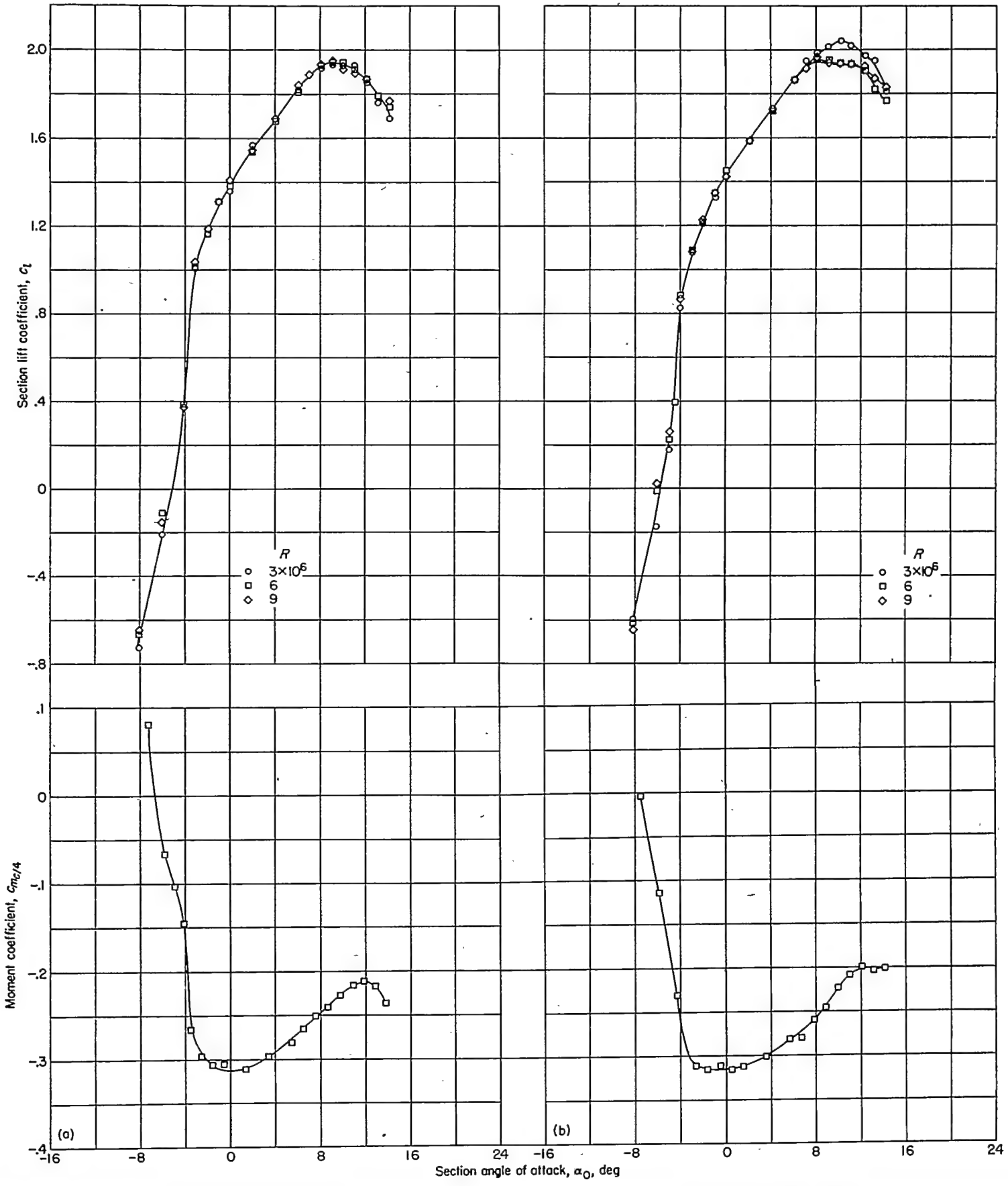

(a) 6-percent-thick airfoil. (b) 10-percent-thick airfoil.

FIGURE 9.—Section lift and pitching-moment characteristics of two symmetrical circular-arc airfoils with the plain leading-edge flap deflected 30° and the plain trailing-edge flap deflected 60°.

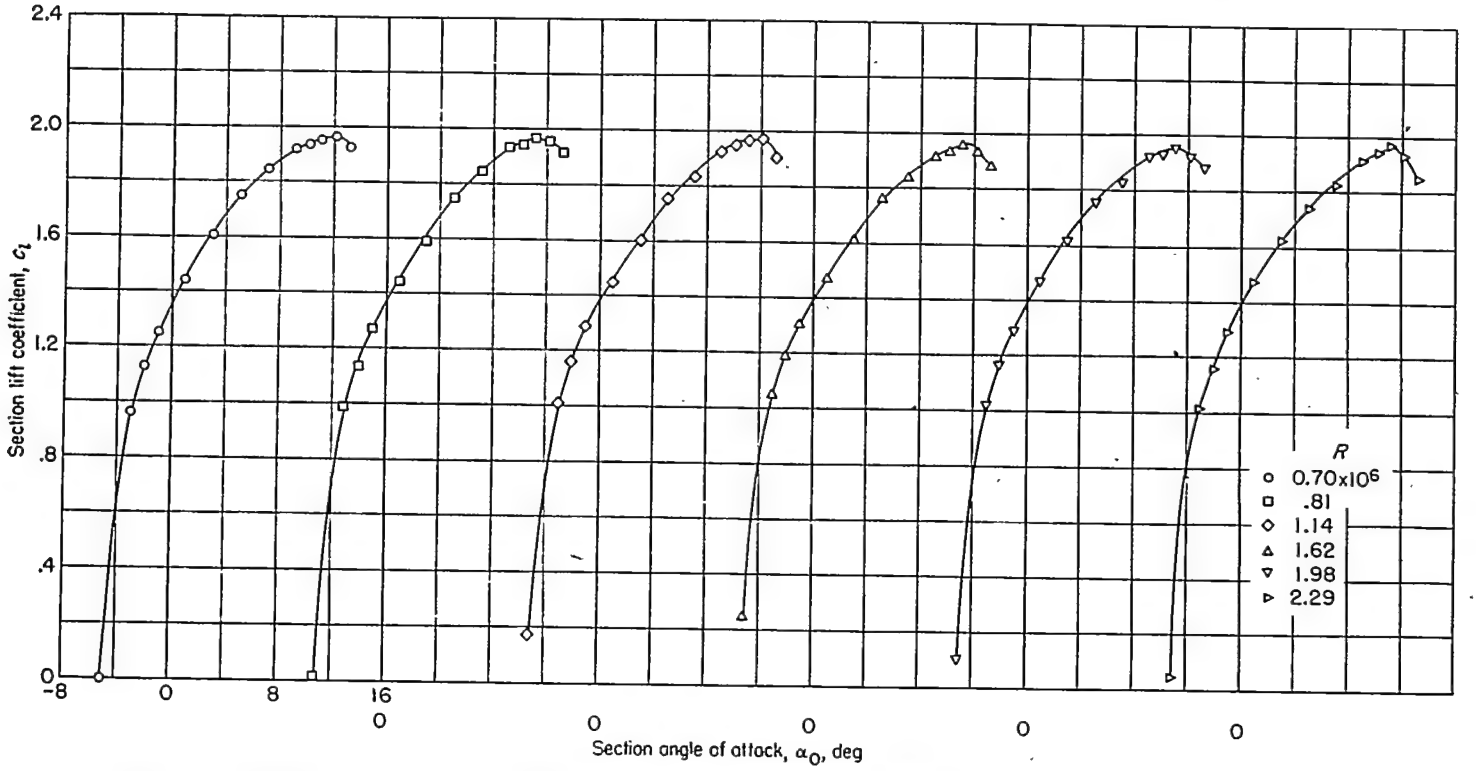

FIGURE 10.—Section lift characteristics at several values of the Reynolds number for 6-percent-thick symmetrical circular-arc airfoil with plain leading-edge flap and plain trailing-edge flap; $\delta_N=27°$, $\delta_F=60°$.

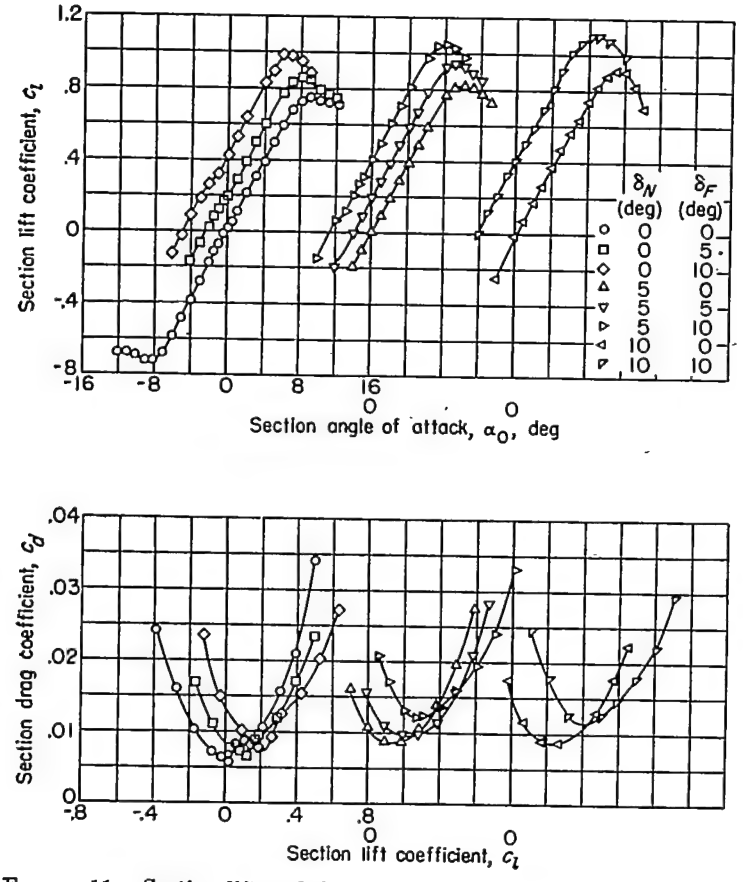

FIGURE 11.—Section lift and drag characteristics of a 6-percent-thick circular-arc airfoil for various deflections of the plain leading-edge flap and plain trailing-edge flap; $R=2.1\times10^6$.

The flap section normal-force, chord-force, and hinge-moment characteristics with the flaps deflected obtained from integrations of these pressure distributions are presented in figures 12 to 16. The loads on the leading-edge and trailing-edge flaps varied qualitatively in the same manner which would be indicated by the thin-airfoil theory. As is shown subsequently, however, separation at the sharp leading edge caused rather large changes in the pressure distributions, and the quantitative agreement between the experimental loads and those predicted by thin-airfoil theory is not good. For a given flap configuration, the normal force and moment on the leading-edge flap increased rapidly in a positive direction with increasing lift coefficient; whereas, in comparison, the normal force and moment on the trailing-edge flap remained almost constant. For a given lift coefficient, increasing the downward deflection of either flap produced downward increments in both the normal force and moment on the leading-edge flap in contrast to the usual characteristic of the conventional trailing-edge flap where the increments of the normal force and moment increase in the upward direction with increased trailing-edge-flap deflection. Deflection of the leading-edge flap had very little effect on normal-force and hinge-moment characteristics of the trailing-edge flap. The magnitude of the loads and moments on the plain trailing-edge flap are of a similar magnitude to those of the plain flaps on an NACA 0009 airfoil (ref. 4). As shown in figure 16 for a combined deflection of the leading-edge and trailing-edge flaps ($\delta_N=27°$; $\delta_F=60°$), the maximum flap normal-force and hinge-moment coefficients were, respectively, 4.74 and 2.24 for the leading-edge flap as compared with 1.48 and −0.61 for the trailing-edge flap.

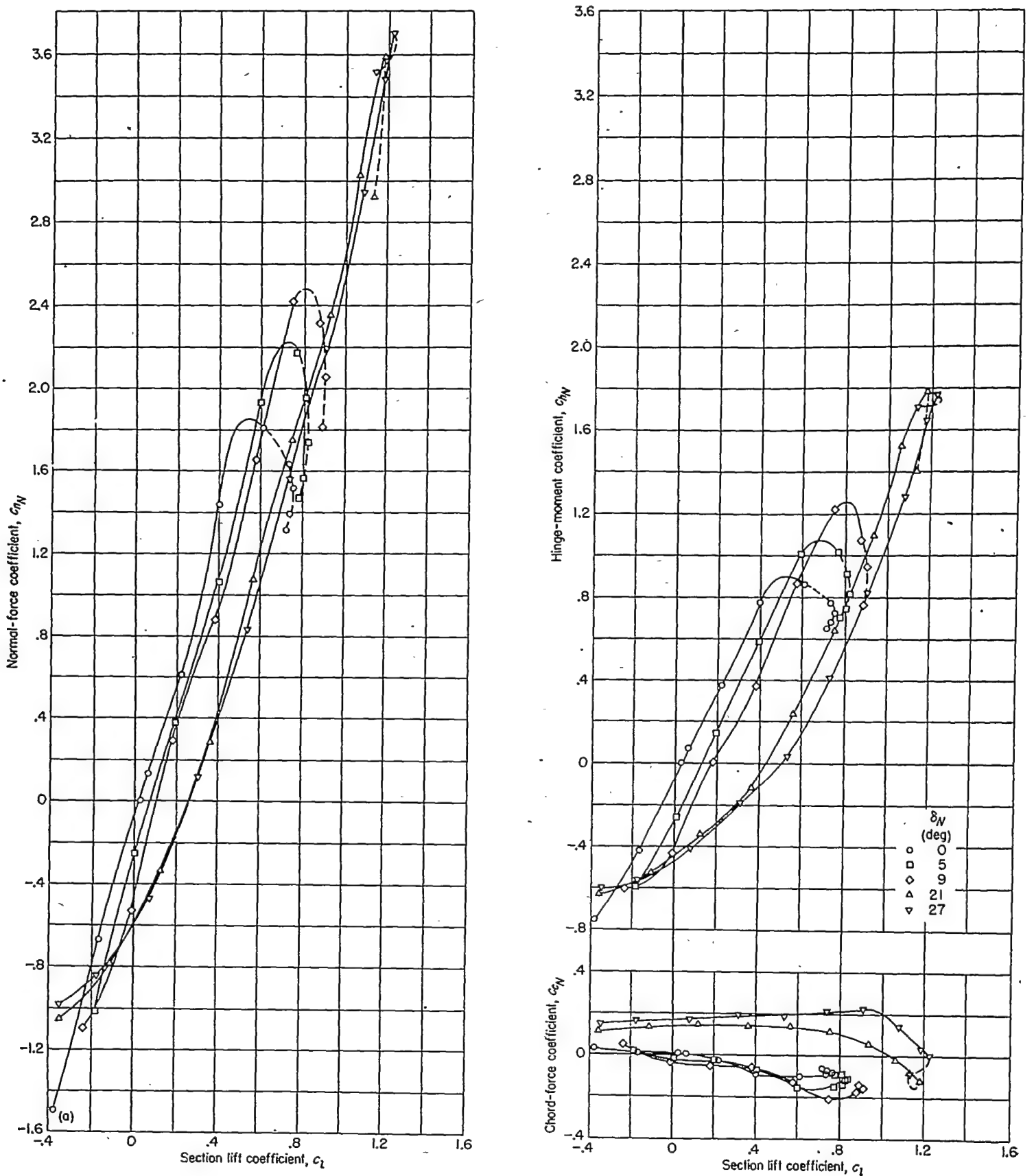

(a) Plain leading-edge flap.

FIGURE 12.—Flap-section load and hinge-moment characteristics of a 6-percent-thick symmetrical circular-arc airfoil for various deflections of the 0.15-chord plain leading-edge flap; $R=2.1\times10^6$; $\delta_f=0°$.

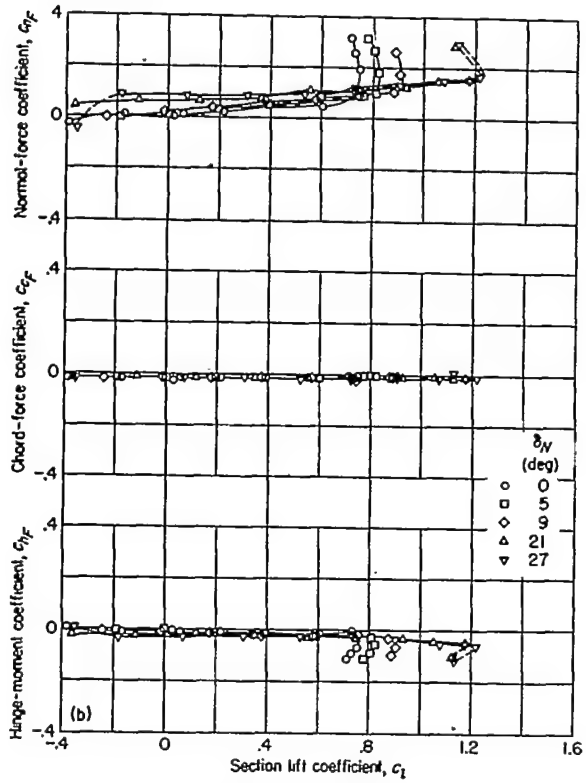

(b) Plain trailing-edge flap.

FIGURE 12.—Concluded.

The chord-force coefficients of both flaps are negative in sign with the exception of the leading-edge-flap chord forces at deflections of 21° and 27°. The chordwise forces due to skin friction have not been included in these results. This omission is considered to be of minor importance because of the large magnitude of the normal-force coefficients. The pressure chord force, however, especially for the leading-edge flap, should not be neglected if the resultant air load is to be obtained.

The variation of the maximum flap loads and hinge moments at or below maximum lift with increasing deflection of either the leading-edge flap or trailing-edge flap is summarized in figures 17 and 18. In figure 17, it is shown that deflecting the leading-edge flap has no appreciable effect on the maximum normal-force and hinge-moment coefficients of the plain trailing-edge flap. Large increases in the corresponding coefficients of the leading-edge flap, however, are evident as the leading-edge flap is deflected. In contrast, deflecting the plain trailing-edge flap increased the maximum normal force and moment of both the leading-edge and trailing-edge flaps. The magnitudes of the maximum normal-force and moment coefficients of the plain trailing-edge flap are shown to increase more rapidly than the corresponding forces and moments of the leading-edge flap regardless of the deflection of the leading-edge flap (figs. 17 and 18).

Typical pressure-distribution diagrams are presented in figures 19 and 20 where the flap pressure coefficients are plotted against the projected chordwise position of the flap orifices on the airfoil chord. Use of the projected position accounts for the shorter effective chord in figure 20 as the flaps were deflected. The load-distribution diagram for the optimum maximum-lift configuration, presented in figure 21, shows the comparatively larger load over the leading-edge flap than over the trailing-edge flap. This load over the leading-edge flap is the result of the additional normal load that occurs as the airfoil-flap configuration departs from the ideal angle of attack or lift coefficient. Thin-airfoil theory indicates that this additional normal load is infinite at the leading-edge but decreases rapidly with distance along the chord to zero at the trailing edge. Actually, because of the bubble of separation at the leading edge, the load has a finite value. A study of table IV shows that this local separation, as indicated by approximately constant values of the pressure coefficients on the upper surface near the leading edge, occurs for all the configurations investigated at an angle of attack well below that for maximum lift.

In order to obtain some indication of the flow pattern existing in the neighborhood of the leading edge of sharp-edge airfoils when supporting a finite lift load, observations were made of the local velocity and of the action of tufts in the airstream near the leading edge of the 6-percent-thick airfoil at several angles of attack. At 2° angle of attack, where a fairly sharp, well-defined peak occurs in the pressure distribution near the leading edge, no evidence of a separation bubble was apparent in the data obtained. The velocity distributions in the flow field above the airfoil and the pressure distribution at the airfoil upper surface for angles of attack of 4° and 6° are shown in figure 22. Pressure distributions computed from approximate potential-flow relations are also shown in this figure. At these angles of attack, where local regions of separated flow are indicated by the nearly constant values of surface pressure coefficient near the leading edge, the flow surveys show that a reversed flow existed just above the surface of the airfoil. The pressure coefficients are much lower than the computed values at the leading edge but are higher than the computed values in a region just behind the leading edge. The chordwise extent of the region of reversed flow coincides approximately with the extent of the region in which the experimental pressure coefficients are higher than the computed coefficients. Farther downstream the flow reattaches to the surface of the airfoil, no reverse flow is observed, and the pressure coefficients are slightly less than those computed. The existence of this reversed flow near the surface of the airfoil suggests the presence of a "captured" vortex imbedded in the flow, similar to that occurring on highly swept wings which experience leading-edge separation. Although the presence of this vortex causes an increase in loading over a portion of the airfoil, its effect is not large enough to cause an increase in lift-curve slope, the decreases in loading ahead of and behind the vortex apparently compensating for any increase in loading at the vortex. As the angle of attack is increased from 4° to 6°, the extent of both the flat spot in the pressure distribution and the region of reversed flow increases in the chordwise direction. Further increases in angle of attack cause the extent of this separated region to increase until it encloses the whole chord of the airfoil at maximum lift. The upper boundary of the reduced velocity in the flow over the airfoil is also shown in figure 22 and indicates very large losses in momentum occurring in the flow as a result of the local separation. These large losses in the flow are of course responsible for the very rapid variation in drag coefficient with lift coefficient shown in figure 4.

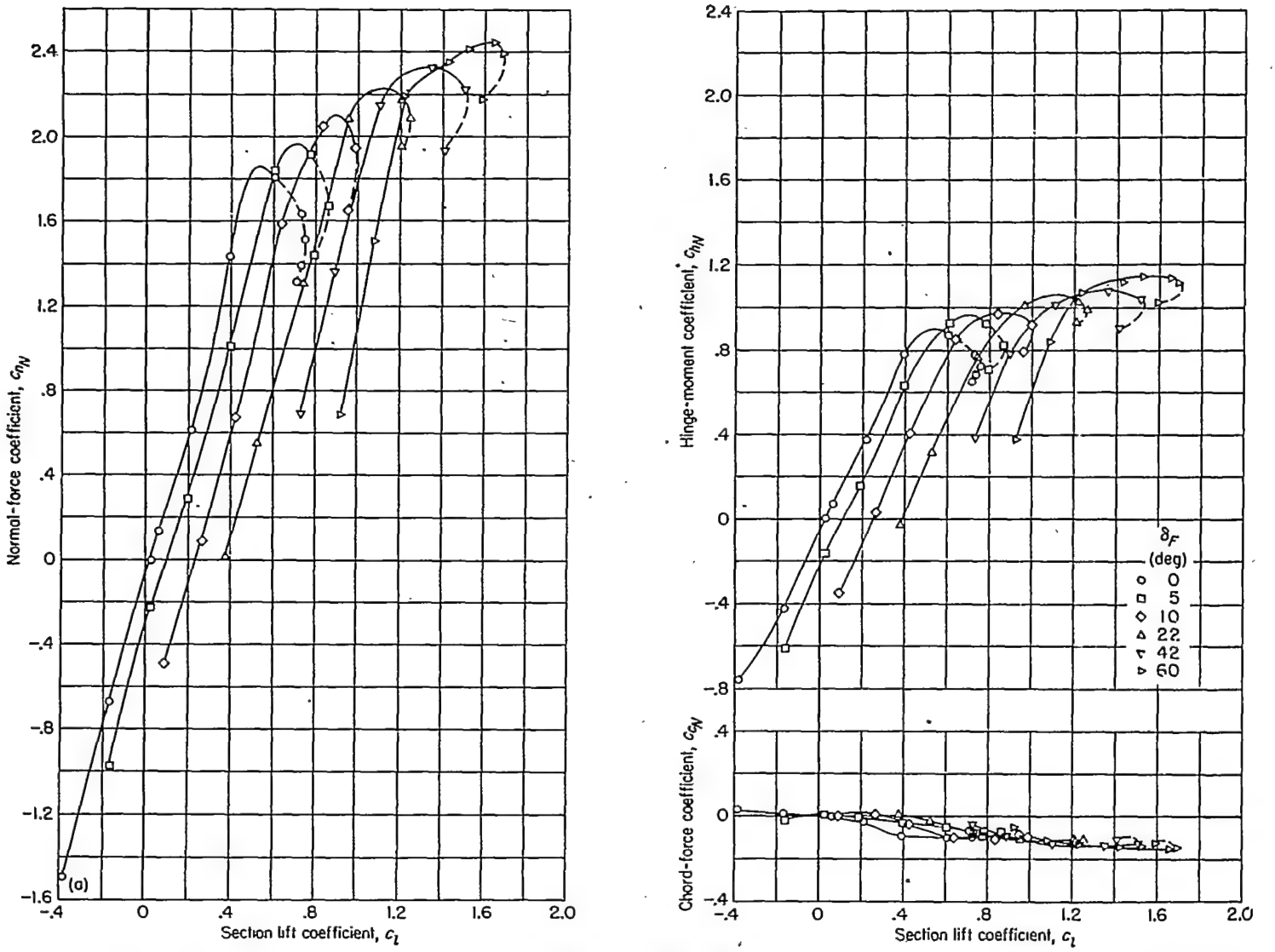

(a) Plain leading-edge flap.

FIGURE 13.—Flap-section load and hinge-moment characteristics of a 6-percent-thick symmetrical circular-arc airfoil for various deflections of the 0.20-chord plain trailing-edge flap; $R=2.1\times10^6$; $\delta_N=0°$.

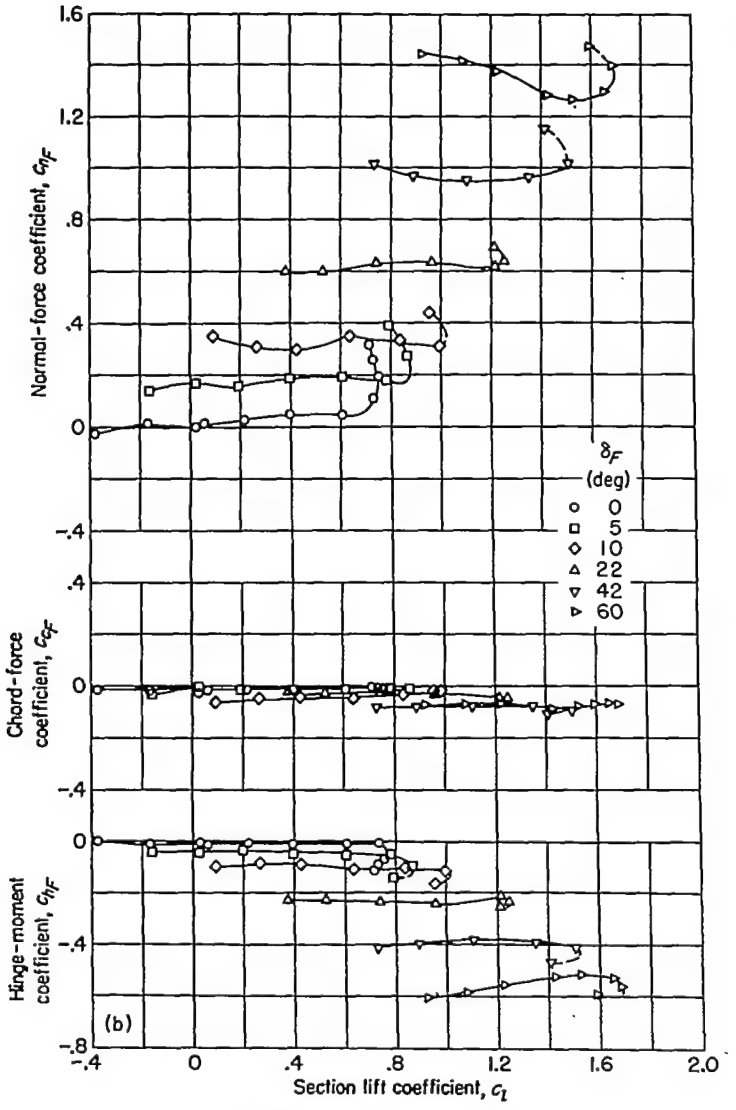

(b) Plain trailing-edge flap.

FIGURE 13.—Concluded.

METHOD FOR PREDICTING THE LOW-SPEED CHORDWISE PRESSURE DISTRIBUTION

DERIVATION OF THE METHOD

Velocity distributions as calculated by potential-flow methods generally bear little resemblance to those obtained experimentally on sharp-edge airfoils because of the existence of extensive regions of separated flow. If the velocity distributions about sharp-edge airfoils with flaps are to be analyzed, the resultant distributions can be broken down into various component parts as is done in the case of airfoils in potential flow (ref. 1). The most generally used breakdown considers the resultant velocity distribution to be made up of the following three components:

(1) Distribution of velocity about the basic symmetrical airfoil at zero angle of attack, v/V

(2) Incremental-additional-velocity distribution due to departure of the airfoil from the ideal lift coefficient, $\Delta v_a/V$ (The ideal lift coefficient is defined as the lift coefficient at which the stagnation point occurs at the leading edge.)

(3) Mean-line velocity distribution

(a) Caused by airfoil camber, $\Delta v/V$

(b) Caused by flap deflection, $(\Delta v/V)_{\delta_f}$

In the present report, the only type of mean-line velocity distribution considered is that resulting from flap deflection, since the data used in the analysis are for a symmetrical airfoil section. It is believed, however, that the method may also be applicable to cambered sections.

In terms of the three component velocities, the complete velocity distribution about an airfoil at any lift coefficient is given approximately by

$$\sqrt{S_U}=\frac{v}{V}+\frac{\Delta v_a}{V}+\left(\frac{\Delta v}{V}\right)_{\delta_f} \tag{1}$$

$$\sqrt{S_L}=\frac{v}{V}-\frac{\Delta v_a}{V}-\left(\frac{\Delta v}{V}\right)_{\delta_f} \tag{2}$$

For the basic thickness form at zero lift, the velocity distribution v/V can, in any case, be calculated by the methods of references 5 and 6. In the absence of flow separation, the component $\Delta v_a/V$ is usually taken to be a linear function of the additional lift coefficient c_{l_a}, that is, the difference between any arbitrary lift coefficient and the ideal lift coefficient, and can be calculated by thick-airfoil theory. If extensive regions of separation do not exist, the components resulting from airfoil camber $\Delta v/V$ or flap deflection $(\Delta v/V)_{\delta_f}$ can also be calculated. The methods of thin-airfoil theory (refs. 7 and 8) are usually employed for this purpose.

For sharp-edge airfoils for which flow separation limits the applicability of potential-flow methods, the problem of developing a general method of determining the velocity distribution resolves itself into a determination of the manner in which the various component distributions vary with c_{l_a} and δ. First, the velocity distribution about the basic thickness form at zero lift must be determined; that is, by definition

$$\frac{v}{V}=\frac{\sqrt{S_U}+\sqrt{S_L}}{2} \tag{3}$$

The value of v/V for the symmetrical airfoil at zero lift can, of course, be calculated by potential-flow methods; however, the extent of the separated flow on the upper and lower surfaces and, therefore, the effective value of v/V which must be used in equations (1) and (2) varies with lift coefficient and flap deflection. Consequently, the value of v/V for the symmetrical airfoil at zero lift, determined theoretically, must be corrected by an increment v'/V which is a function of lift coefficient and flap deflection. The value of v'/V can be determined from the experimental data. Next, the manner in which the additional velocity distribution $\Delta v_a/V$ varies with the additional lift coefficient must be found. The use of the experimental pressure-distribution data and the following relation obtained from equations (1) and (2) provides the solution:

$$\frac{\Delta v_a}{V}=\frac{\sqrt{S_U}-\sqrt{S_L}}{2}-\left(\frac{\Delta v}{V}\right)_{\delta_f} \tag{4}$$

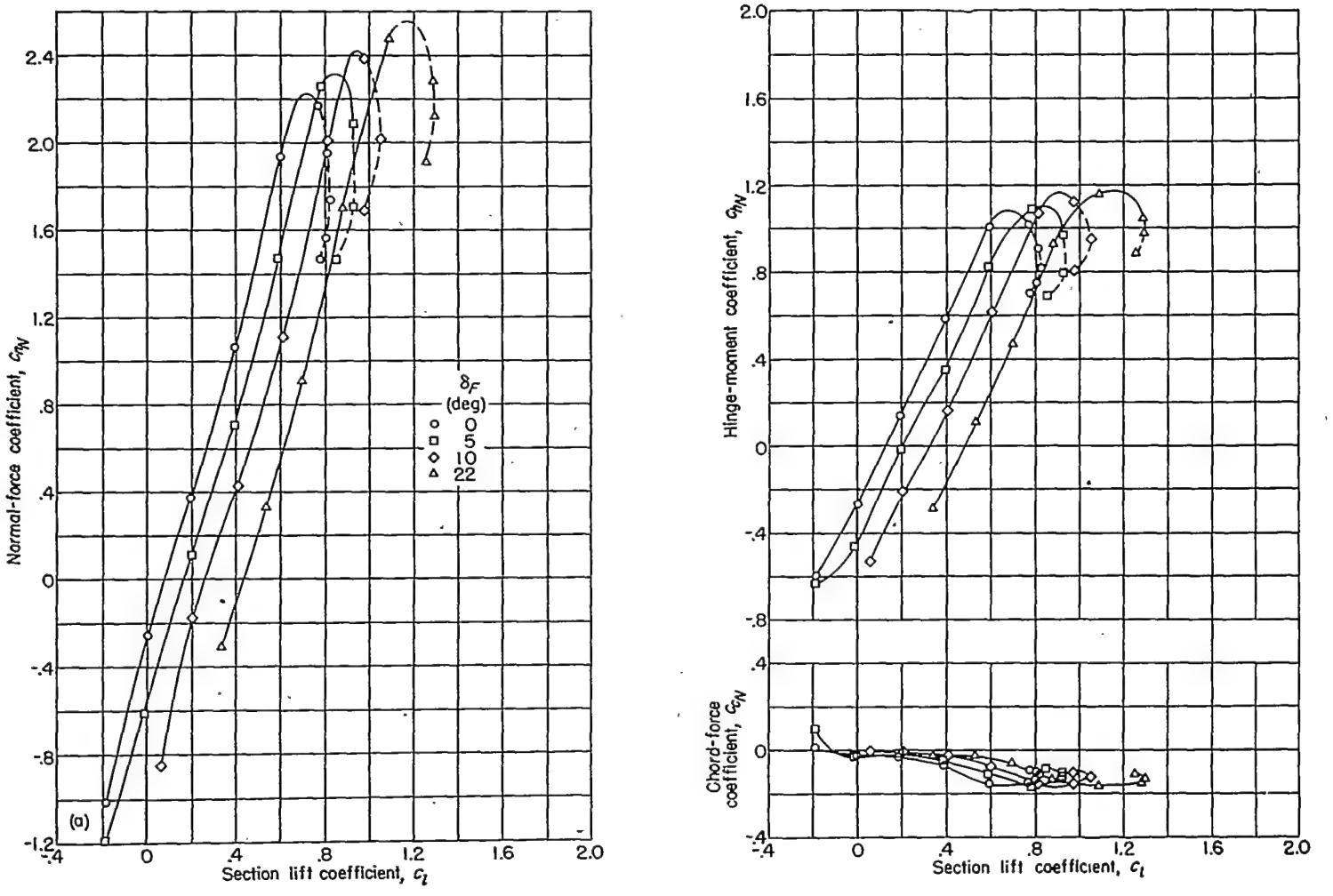

(a) Plain leading-edge flap.

FIGURE 14.—Flap-section load and hinge-moment characteristics of a 6-percent-thick symmetrical circular-arc airfoil for various deflections of the 0.20-chord plain trailing-edge flap; $R=2.1\times10^6$; $\delta_N=5°$.

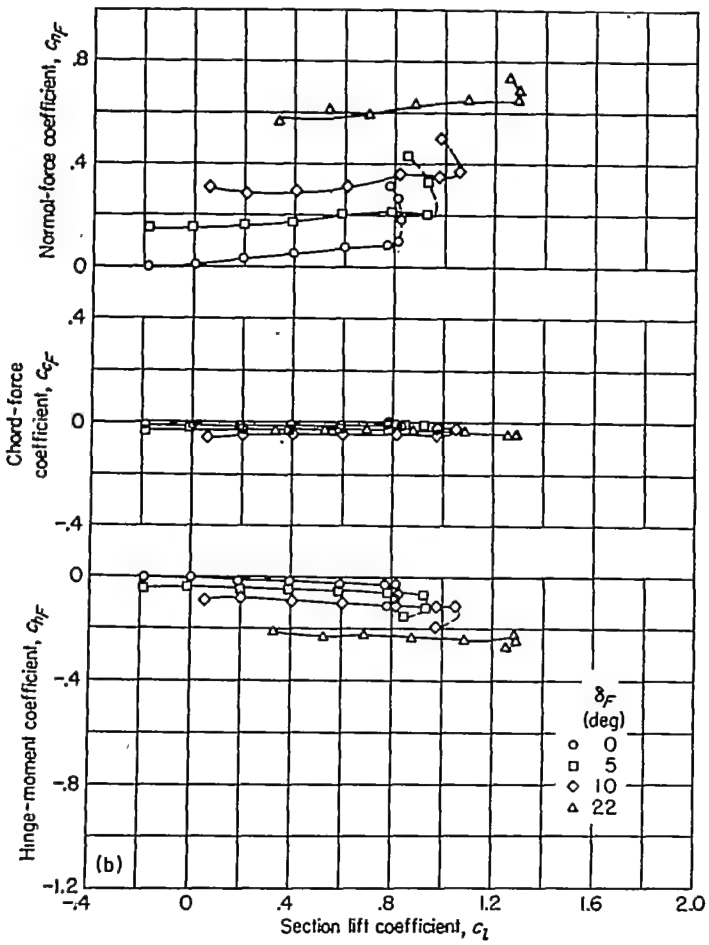

(b) Plain trailing-edge flap.

FIGURE 14.—Concluded.

Finally, the extent to which the theoretical velocity distribution due to flap deflection is realized experimentally must be determined. In order to determine the variation of $\Delta v_a/V$ with lift coefficient and to compare the experimental and theoretical velocity distributions, the ideal lift coefficient must be known. For any combination of leading-edge and trailing-edge deflections, the ideal lift coefficient can be calculated by the methods of reference 7; however, because of flow separation, a correlation must be made between the theoretical and experimental ideal lift coefficients.

Ideal lift coefficient.—The change in ideal lift coefficient is equal to the sum of two component changes, one resulting from leading-edge-flap deflection and the other from trailing-edge-flap deflection. Each of these components may be calculated separately and added linearly. For each leading-edge- and trailing-edge-flap deflection investigated, the ideal lift coefficient $c_{l_{b\delta}}$ has been determined from the experimental data. The results are compared in figure 23 with those calculated from thin-airfoil theory. As shown in figure 23, the theoretical coefficients $c_{l_{b\delta}}$ for the leading-edge flap are identical with those obtained experimentally. In calculating the ideal lift coefficients $c_{l_{b\delta_N}}$ resulting from deflection of a leading-edge flap, the theoretical value may therefore be used.

For trailing-edge-flap deflections above 10°, the experimentally determined values of the ideal lift coefficient $c_{l_{b\delta_F}}$ are considerably lower than indicated by the theory. In order to determine the change in ideal lift coefficient associated with deflection of trailing-edge flaps of different chords, the method used by Allen in reference 9 to obtain $c_{l_{b\delta_F}}$ was applied to a large amount of experimental data from various sources. In this method, the ideal normal-force coefficient is related to the pitching-moment increment resulting from flap deflection and the center of pressure of the flap load for given values of flap-chord ratio and flap deflection. Values of $c_{l_{b\delta_F}}$ (the normal-force coefficient was taken to be essentially the same as the lift coefficient) obtained by this method are plotted in figure 24 against trailing-edge-flap deflection for flap-chord ratios ranging between 10 and 50 percent. The values of the quarter-chord pitching-moment increment required for the determination of these curves were obtained from numerous experimental data. These ideal lift coefficients (fig. 24) represent average values obtained from a series of tests of plain flaps on a large number of conventional airfoil sections. Similar computations were also made for the 0.20-chord flap on the circular-arc airfoil used in the present analysis and, as expected, the results agreed with the corresponding data in figure 24. For any profile with plain flaps, therefore, the results of figure 24 can be used for the determination of the ideal lift coefficient.

Mean-line velocity distribution.—The distribution of velocity over the surface of the airfoil resulting from flap deflection $(\Delta v/V)_{b\delta}$ was computed from the experimental data for various flap deflections by means of the following equation:

$$\left(\frac{\Delta v}{V}\right)_{b\delta}=\frac{\left(\frac{v}{V}\right)_{i_U}-\left(\frac{v}{V}\right)_{i_L}}{2}$$

This expression was obtained by subtracting equation (2) from equation (1) because, by definition, $\Delta v_a/V$ is zero at the ideal lift coefficient. The data thus obtained for various deflections of the leading-edge flap were found to be very nearly independent of flap deflection when expressed in the form of $\left(\frac{\Delta v}{V}\right)_{b\delta_N}\Big/c_{l_{b\delta_N}}$. A comparison of the mean value of $\left(\frac{\Delta v}{V}\right)_{b\delta_N}\Big/c_{l_{b\delta_N}}$ plotted against percent chord as determined by theory and experiment (fig. 25 (a)) shows good agreement. It is concluded, therefore, that the mean-line velocity distribution resulting from deflection of leading-edge flaps of various chords can be calculated theoretically with a sufficiently high degree of accuracy. Because of the effects of separation near the trailing edge, however, the experimental velocity distributions resulting from deflection of the plain trailing-edge flap differed markedly from those predicted by the theory, particularly for large flap deflections. A different distribution for each trailing-edge-flap deflection was determined, therefore, and the results are presented in figure 25(b) in the form of $(\Delta v/V)_{b\delta_F}$ plotted against percent chord.

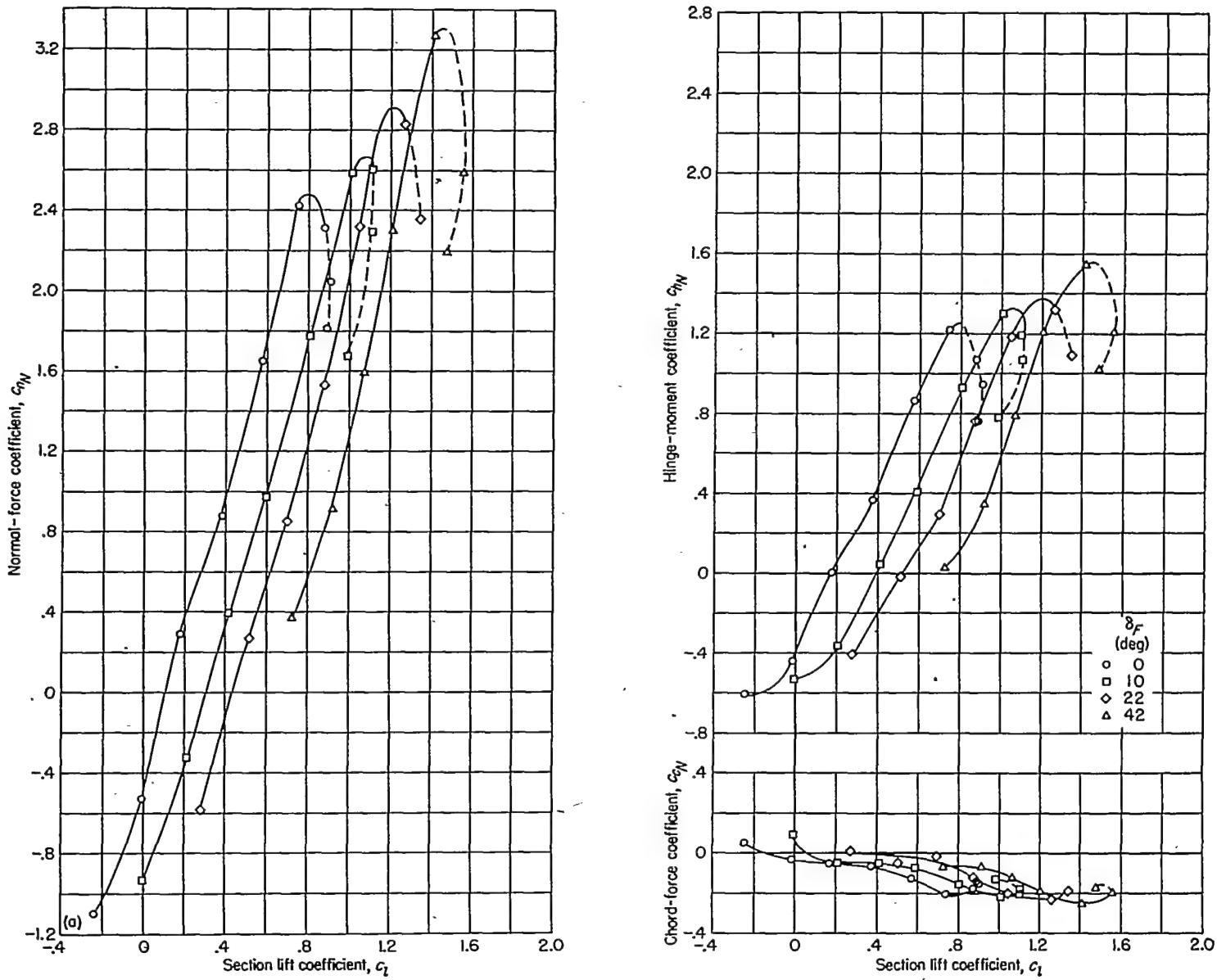

(a) Plain leading-edge flap.

FIGURE 15.—Flap-section load and hinge-moment characteristics of a 6-percent-thick symmetrical circular-arc airfoil for various deflections of the 0.20-chord plain trailing-edge flap; $R=2.1\times10^6$; $\delta_N=9°$.

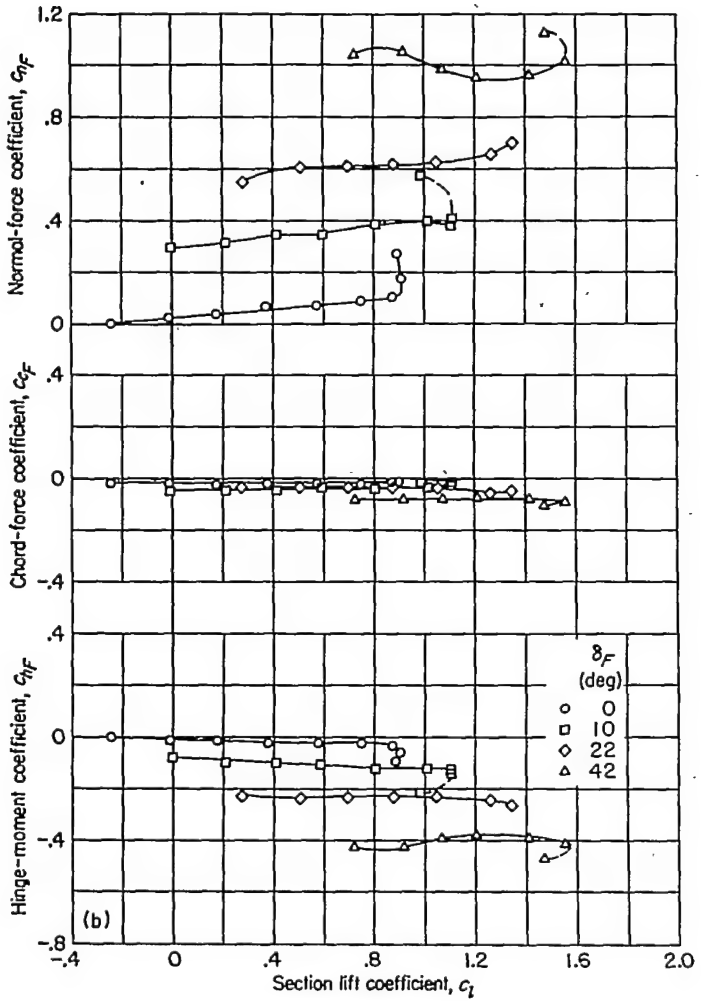

(b) Plain trailing-edge flap.

FIGURE 15.—Concluded.

As a basis for extending the analysis to apply to sharp-edge airfoils having trailing-edge flap-chord ratios other than 0.20, the normal-force distribution $P_{b\delta_F}/c_{l_{b\delta_F}}$ was determined from the pressure distribution at the ideal lift coefficient for several trailing-edge flap deflections by the following relation:

$$\frac{P_{b\delta_F}}{c_{l_{b\delta_F}}}=\frac{\left(\frac{v}{V}\right)_{i_U}^2-\left(\frac{v}{V}\right)_{i_L}^2}{c_{l_{b\delta_F}}}=\frac{4\left(\frac{\Delta v}{V}\right)_{b\delta}\left(\frac{v}{V}\right)}{c_{l_{b\delta_F}}}$$

When compared with the distributions presented in reference 9 for a 0.20-chord trailing-edge flap, good agreement was obtained. It is probable, therefore, that the normal-force distribution $P_{b\delta_F}/c_{l_{b\delta_F}}$ and, consequently, the velocity distribution may be determined with satisfactory precision for any desired trailing-edge flap-chord ratio and deflection from table V (taken from ref. 9, table III).

Additional velocity distribution.—The values of the local incremental velocity ratio $\Delta v_a/V$ were determined from the experimental data and equation (4). When plotted as a function of the additional lift coefficient ($c_{l_a}=c_l-c_{l_{b\delta}}$), these values were found to be essentially independent of both leading-edge-flap and trailing-edge-flap deflections. Average values of $\Delta v_a/V$ are plotted against c_{l_a} in figure 26 for various chordwise positions. It is thought that these values of $\Delta v_a/V$ (fig. 26) can be used for various flap-chord ratios because, after the leading edge has caused separation of the flow, any differences in airfoil contour behind that point would have only secondary effects on $\Delta v_a/V$.

Effective basic velocity distribution.—The theoretical velocity distribution v/V about any symmetrical airfoil at zero lift can be calculated by the general methods of references 5 and 6. The effective values of v/V which must be employed in equations (1) and (2), however, vary with both additional lift coefficient and trailing-edge-flap deflection because of separation phenomena. The increment v'/V which must be added to the theoretical basic velocity distribution was determined from the following relation:

$$\frac{v'}{V}=\frac{\left(\frac{v}{V}\right)_U+\left(\frac{v}{V}\right)_L}{2}-\frac{v}{V} \tag{5}$$

Since v'/V is a function of both trailing-edge-flap deflection and lift coefficient, it may be broken down into two components $(v'/V)_F$ and $(v'/V)_a$, respectively. The values of $(v'/V)_F$ were determined first from equation (5) by using the experimental pressure distributions at the design lift coefficient. Values of the total change in basic velocity distribution $\frac{v'}{V}=\left(\frac{v'}{V}\right)_F+\left(\frac{v'}{V}\right)_a$ were determined from equation (5) by using the experimental pressure distributions at various lift coefficients. The values of $(v'/V)_F$ were subtracted from the results thus obtained to obtain $(v'/V)_a$. It should be pointed out that deflection of the leading-edge flap had no appreciable effect on the shape of these velocity distributions when expressed as a function of c_{l_a}.

For various chordwise positions, values of $(v'/V)_F$ are presented in figure 27 as a function of trailing-edge-flap deflection. Forward of the 40-percent-chord station, values of this component of velocity were found to be negligibly small. The chordwise position of $(v'/V)_F$ is expressed in terms of $\frac{\frac{x}{c}}{1-E_F}$ and $\frac{1-\frac{x}{c}}{E_F}$ for points ahead of and behind the hinge, respectively. In this form, the results are correlated so that they may be applied to sharp-edge airfoils having trailing-edge flaps of varying chord. This method of correlation is thought to be justified since the distribution of $(v'/V)_F$ is a result of separation at the flap hinge and has been shown (ref. 9) to be similar for various hinge locations.

The results of the determination of $(v'/V)_a$ are shown in figure 28. As would be expected, the values are independent of flap deflection when expressed in terms of c_{l_a}.

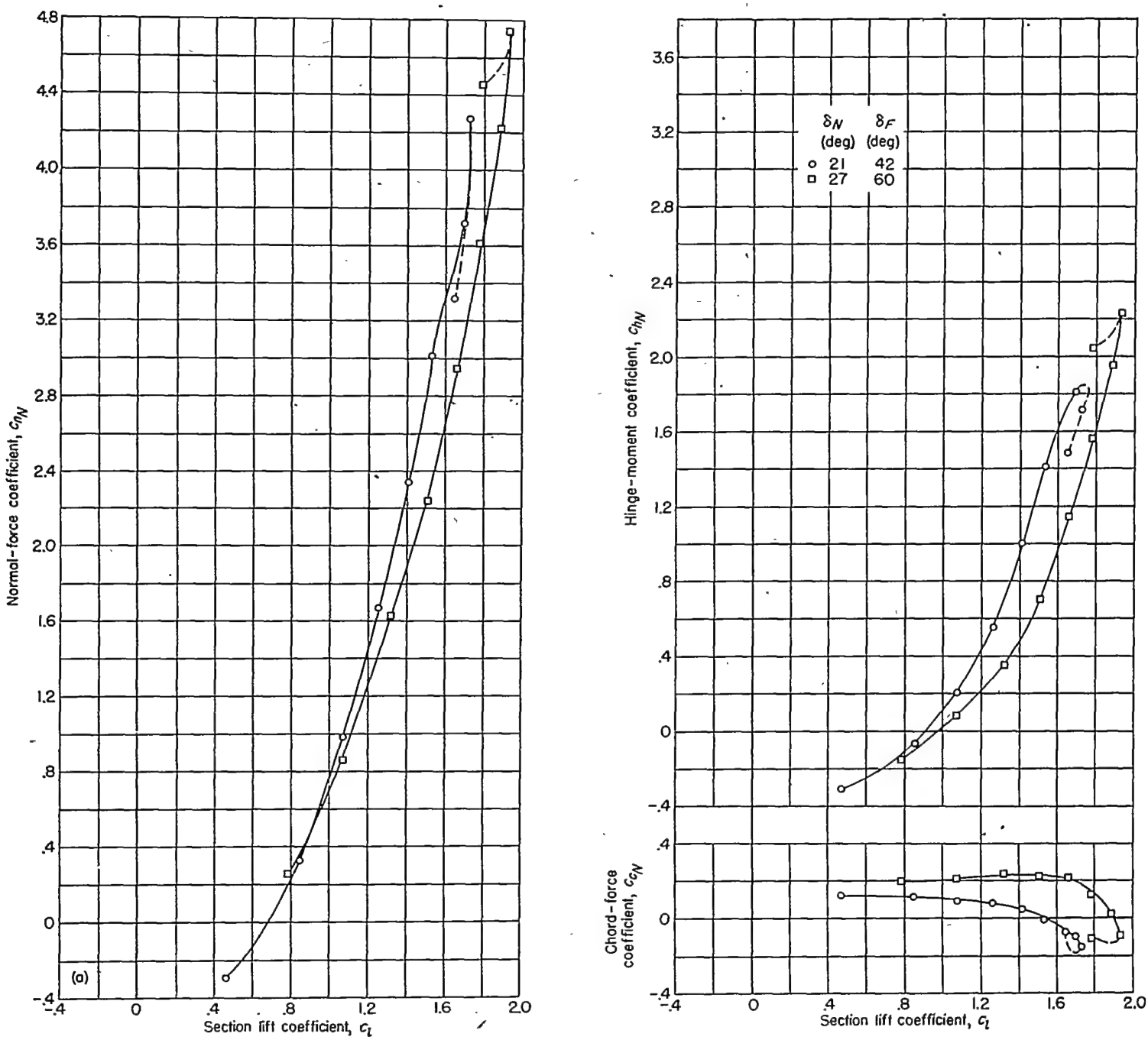

(a) Plain leading-edge flap.

FIGURE 16.—Section flap load and hinge-moment characteristics of a 6-percent-thick symmetrical circular-arc airfoil for various deflections of the 0.15-chord plain leading-edge flap and 0.20-chord plain trailing-edge flap; $R=2.1\times10^6$.

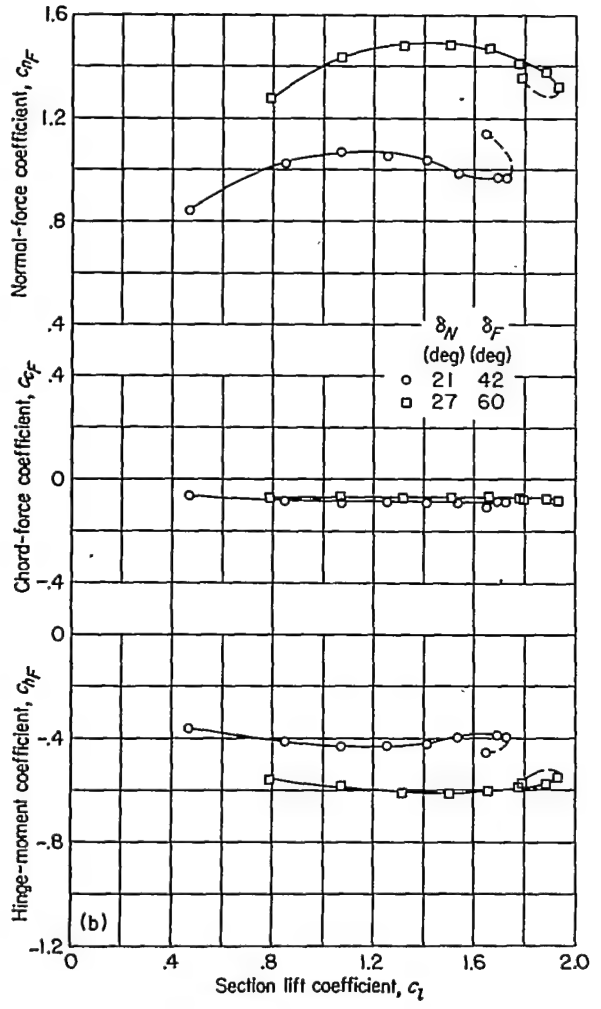

(b) Plain trailing-edge flap.

FIGURE 16.—Concluded.

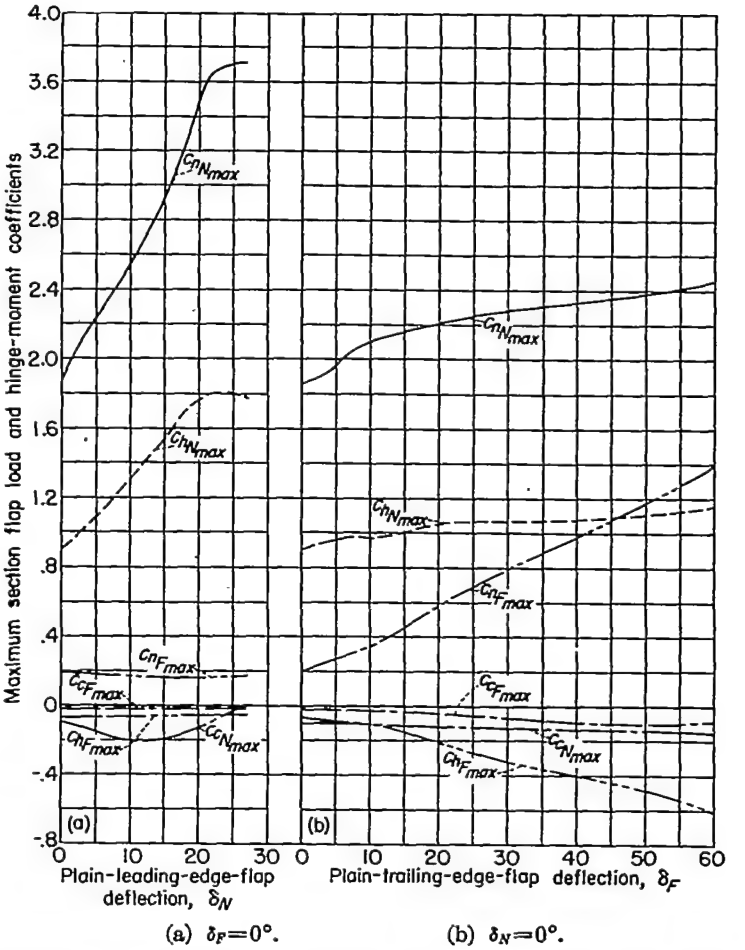

(a) $\delta_F=0°$. (b) $\delta_N=0°$.

FIGURE 17.—Variation of maximum section flap load and hinge-moment coefficients of a 6-percent-thick symmetrical circular-arc airfoil for various deflections of the 0.15-chord plain leading-edge flap and 0.20-chord plain trailing-edge flap; $R=2.1\times10^6$.

OUTLINE OF THE METHOD

A method has been developed for the calculation of the low-speed chordwise pressure distribution over various sharp-edge airfoils equipped with plain leading-edge and trailing-edge flaps of arbitrary size and deflection. The assumption has been made that for sharp-edge airfoils the separation phenomena controlling those components of the pressure distribution which cannot be calculated from potential-flow theory do not vary appreciably with variations in the detailed shape of the airfoil.

If the airfoil section for which calculations are to be made satisfies the conditions of the assumptions, the following data may be noted in preparation for the calculation:

E_N leading-edge flap-chord ratio, $(c_f/c)_N$
δ_N leading-edge-flap deflection, deg
E_F trailing-edge flap-chord ratio, $(c_f/c)_F$
δ_F trailing-edge-flap deflection, deg
c_l section lift coefficient
x/c chordwise locations at which the pressure is to be calculated

The calculations are made in the following manner:

(1) Find change in ideal lift coefficient caused by leading-edge-flap deflection $c_{l_{b\delta_N}}$ from the following equation (derived from ref. 9):

$$c_{l_{b\delta_N}}=\frac{\pi}{45}\sqrt{E_N(1-E_N)}\,\delta_N$$

(2) Find change in ideal lift coefficient caused by trailing-edge-flap deflection $c_{l_{b\delta_F}}$ from figure 24.

(3) Find additional lift coefficient c_{l_a}

$$c_{l_a}=c_l-\left(c_{l_{b\delta_N}}+c_{l_{b\delta_F}}\right)$$

(4) Find incremental additional velocity $\Delta v_a/V$ from figure 26.

(5) Obtain airfoil basic velocity at x/c, v/V from references 5 and 6 or from the following equation (ref. 10) for circular-arc airfoils:

$$\frac{v}{V}=\frac{4}{n^2}\left(\frac{\cosh\eta-\cos\frac{n\pi}{2}}{\cosh\frac{2\eta}{n}+1}\right)$$

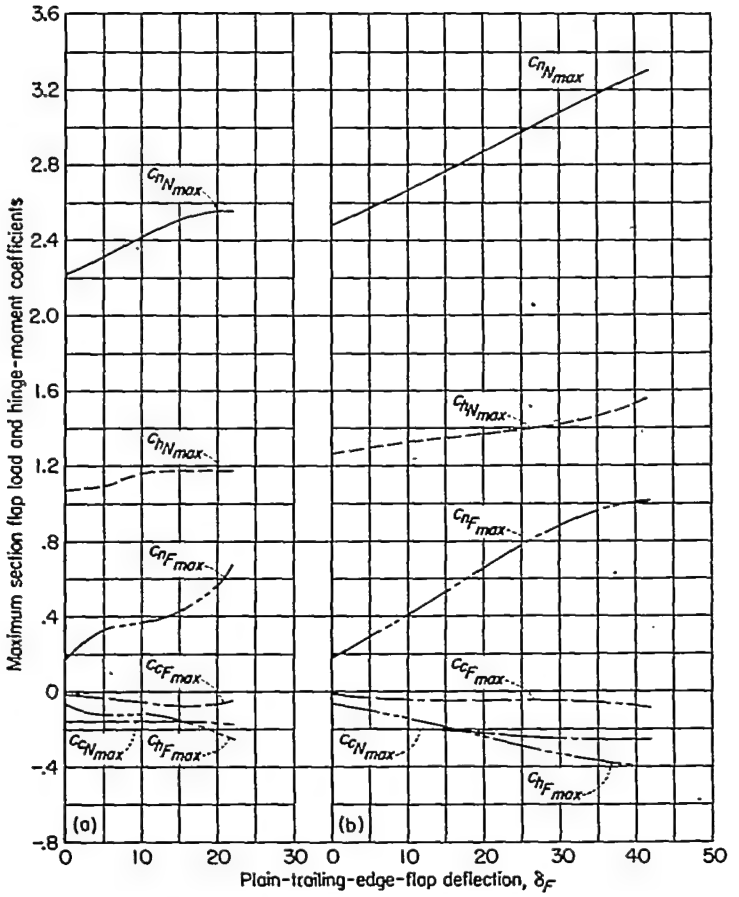

(a) $\delta_N=5°$. (b) $\delta_N=9°$.

FIGURE 18.—Variation of maximum section flap load and hinge-moment coefficients with plain-trailing-edge-flap deflections of a 6-percent-thick symmetrical circular-arc airfoil for various deflections of the 0.15-chord plain leading-edge flap; $R=2.1\times10^6$.

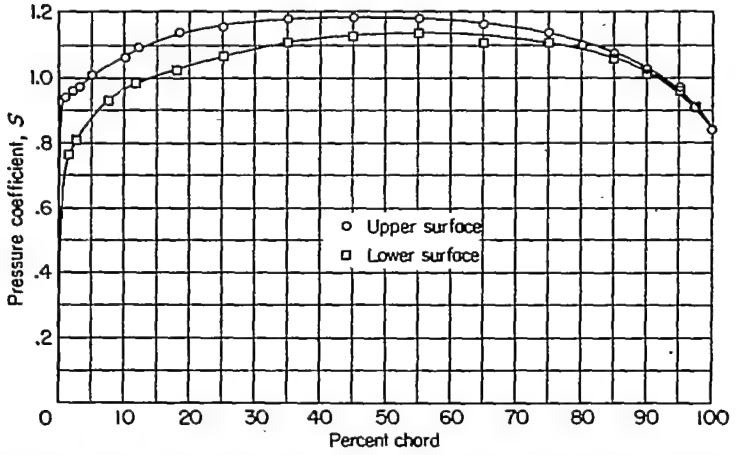

FIGURE 19.—Chordwise variation of pressure coefficient for the 6-percent-thick symmetrical circular-arc airfoil with the flaps neutral; $R=2.1\times10^6$; $M=0.15$; $\alpha_0=0.5°$. See table IV (a).

where

$$n=2-\frac{4}{\pi}\tan^{-1}\frac{t}{c}$$

$$\eta=\log_e\left(\frac{x/c}{1-\frac{x}{c}}\right)$$

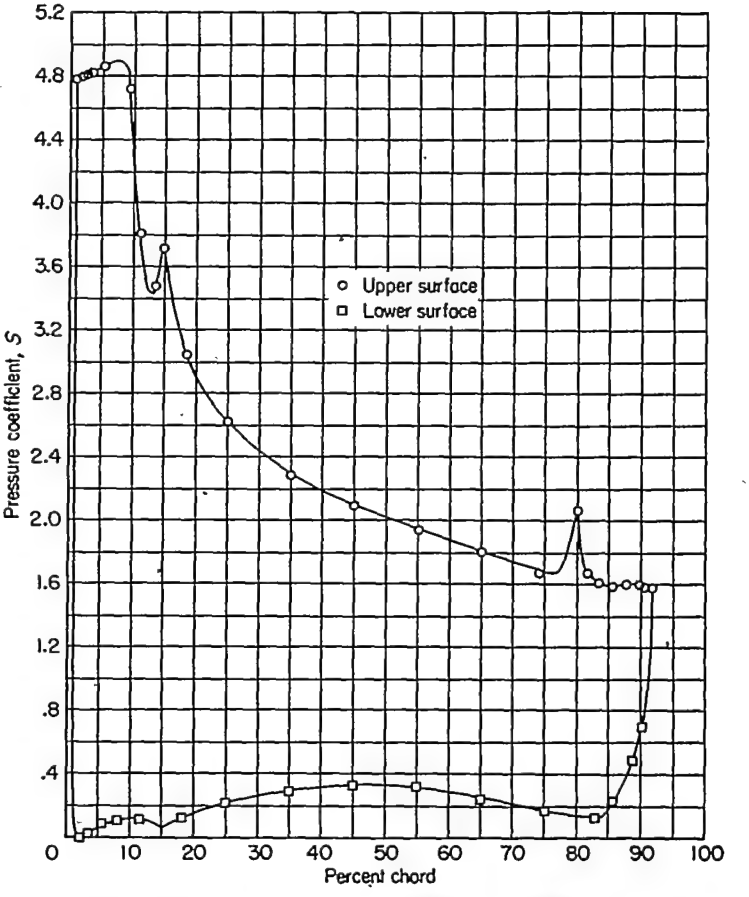

FIGURE 20.—Chordwise variation of pressure coefficient for the 6-percent-thick symmetrical circular-arc airfoil with the plain leading-edge flap deflected 27° and the plain trailing-edge flap deflected 60°; $R=2.1\times10^6$; $M=0.15$; $\alpha_0=10.2°$. See table IV (r).

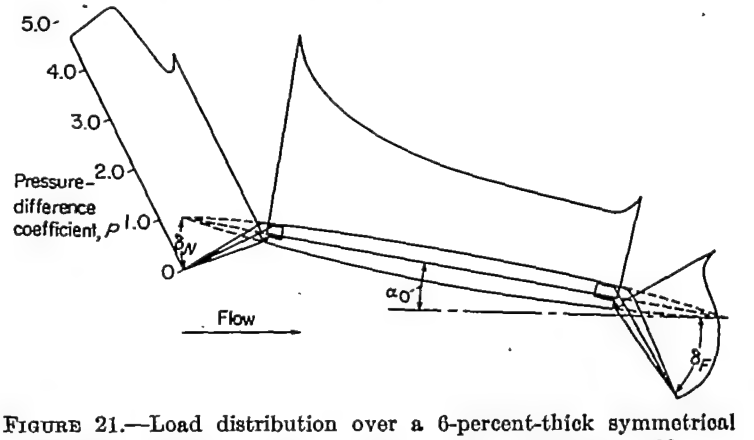

FIGURE 21.—Load distribution over a 6-percent-thick symmetrical circular-arc airfoil; $\alpha_N=27°$; $\delta_F=60°$. $R=2.1\times10^6$; $\alpha_0=10.2°$.

(6) Find the pressure-difference coefficient due to the leading-edge flap $P_{\delta\delta_N}$ from the following equation (derived from ref. 9):

$$P_{\delta\delta_N}=\frac{1}{45}\delta_N\log_e\left[\frac{\sqrt{(1-E_N)\left(1-\frac{x}{c}\right)}+\sqrt{E_N\,x/c}}{\sqrt{(1-E_N)\left(1-\frac{x}{c}\right)}-\sqrt{E_N\,x/c}}\right]$$

(7) Find the pressure-difference coefficient due to the trailing-edge flap $P_{\delta\delta_F}$ from table V and step (2).

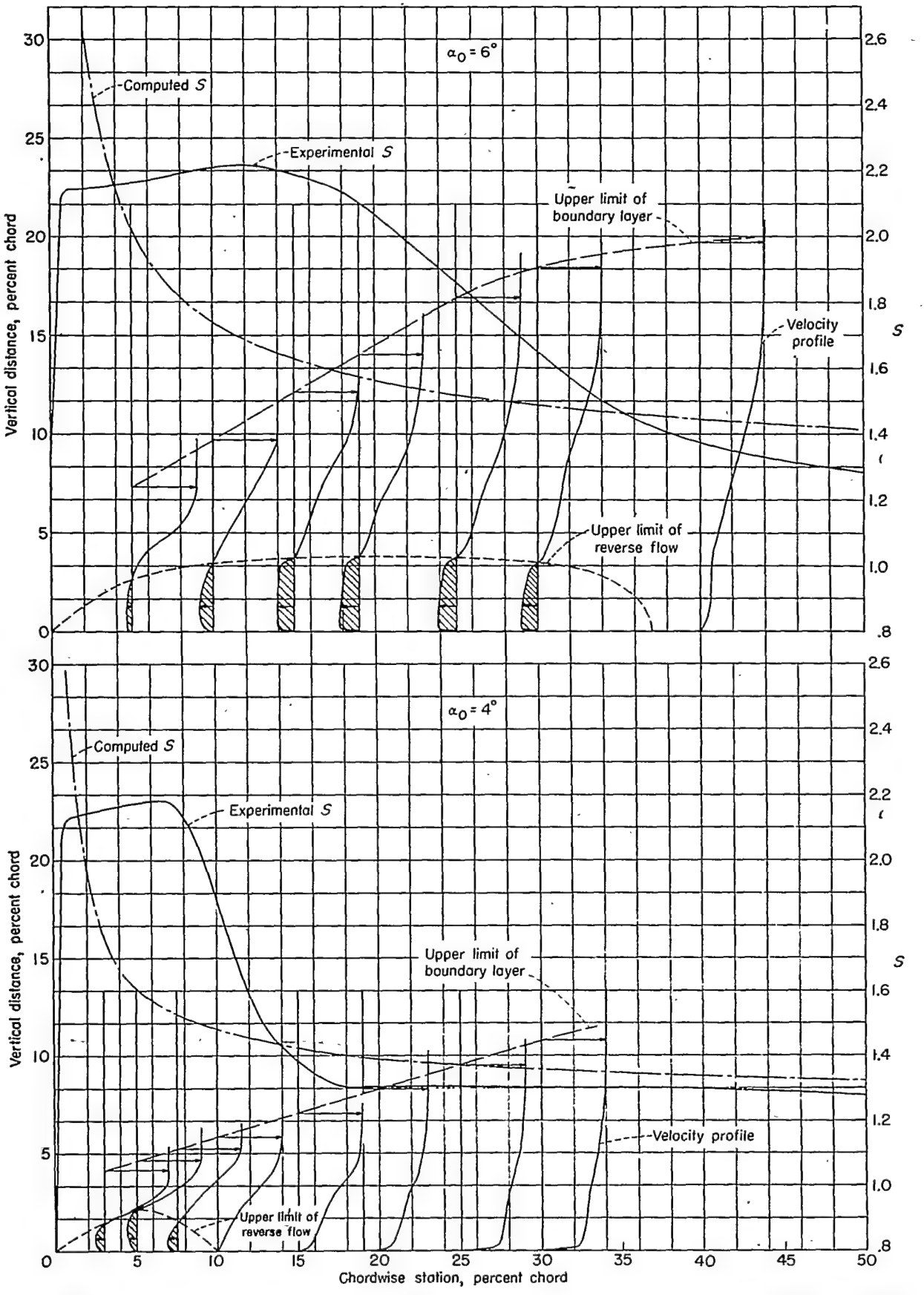

FIGURE 22.—Pressure distributions and velocity profiles over the upper surface of a 6-percent-thick symmetrical circular-arc airfoil at two angles of attack; $\delta_F = \delta_N = 0°$.

321005—55——59

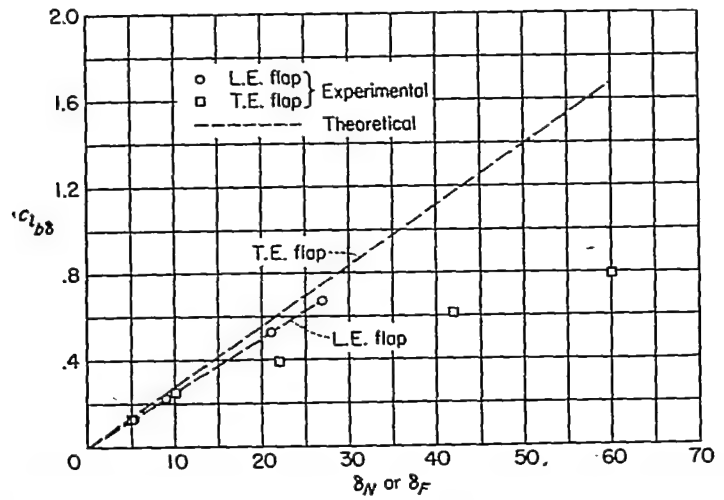

FIGURE 23.—Variation of change in ideal lift coefficient with deflection of the 0.15-chord plain leading-edge flap and 0.20-chord plain trailing-edge flap on the 6-percent-thick symmetrical circular-arc airfoil.

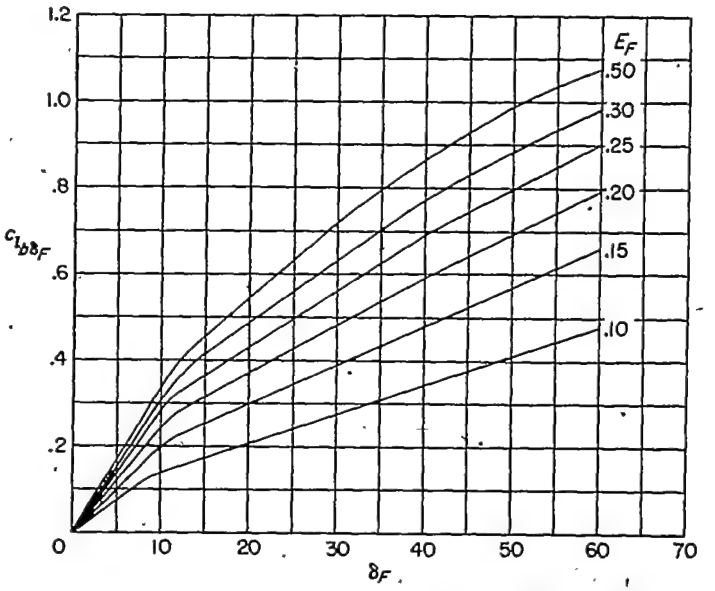

FIGURE 24.—Variation of change in ideal lift coefficient with plain-trailing-edge-flap deflection.

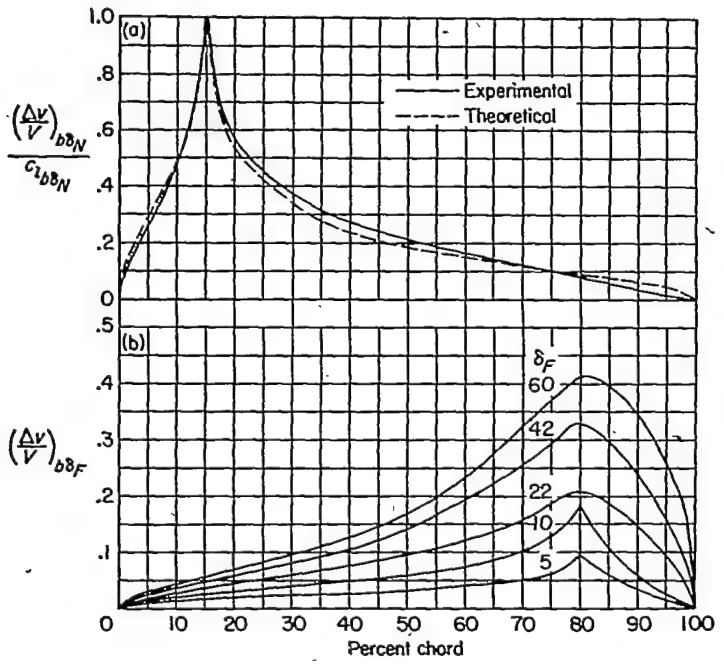

(a) 0.15-chord plain leading-edge flap.
(b) 0.20-chord plain trailing-edge flap.

FIGURE 25.—Mean-line velocity distribution for various flap deflections.

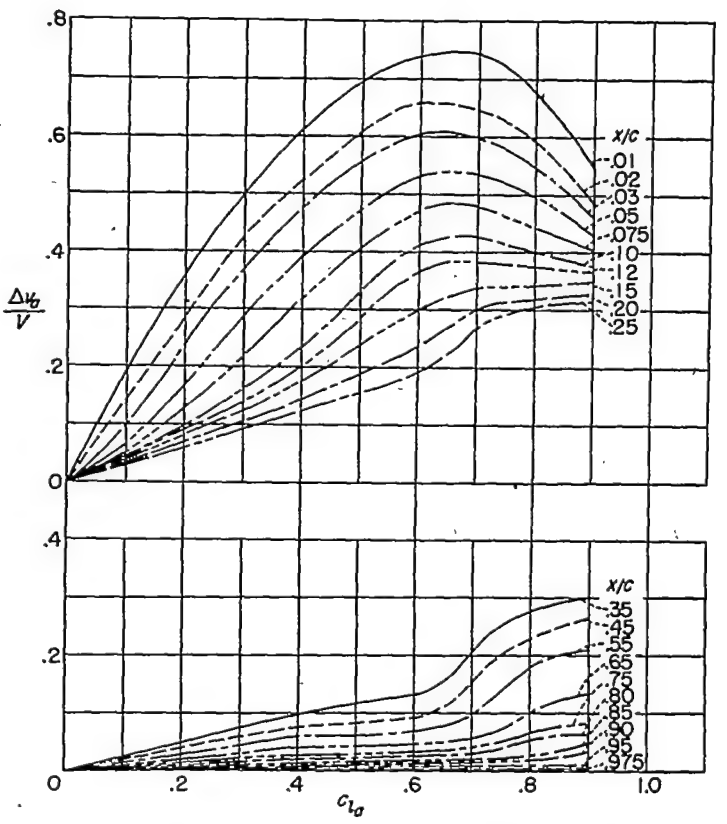

FIGURE 26.—Variation of incremental-additional-velocity ratio with additional lift coefficient.

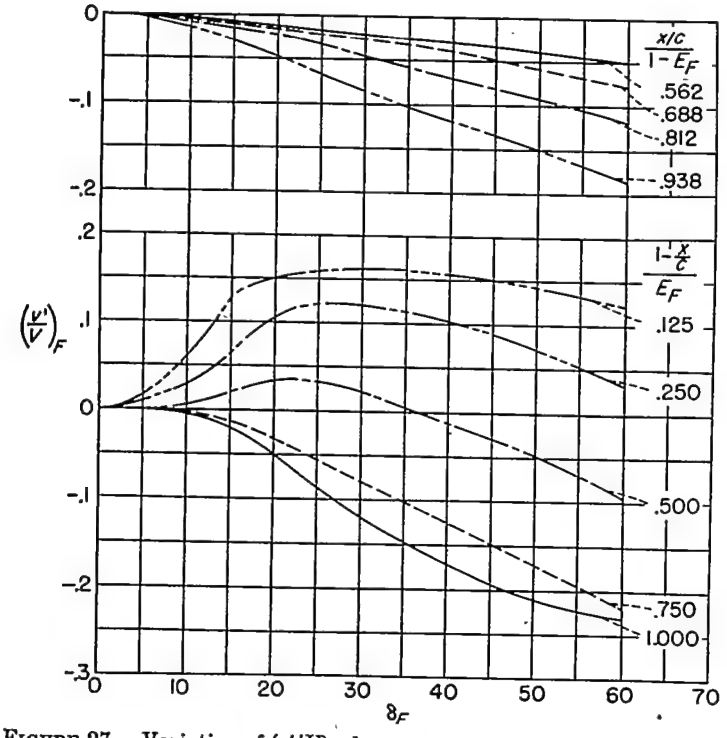

FIGURE 27.—Variation of $(v'/V)_F$ due to separation in the region of the trailing edge with plain-trailing-edge-flap deflection.

(8) Find incremental velocity due to separation at the leading edge $(v'/V)_a$ from figure 28.

(9) Find incremental velocity due to separation at the trailing edge $(v'/V)_F$ from figure 27.

(10) Add the incremental velocities obtained in steps (4), (5), (8), and (9) to obtain the effective velocity on the surface of the basic airfoil at the desired lift coefficient, v_b/V.

(11) Add the pressure-difference coefficients obtained in steps (6) and (7), $P_{b\delta}$.

(12) Substitute values from steps (10) and (11) into the following equations obtained from reference 11:

$$S_U=\left(\frac{v_b}{V}+\frac{P_{b\delta}}{4\frac{v_b}{V}}\right)^2$$

$$S_L=\left(\frac{v_b}{V}-\frac{P_{b\delta}}{4\frac{v_b}{V}}\right)^2$$

EXAMPLE

In order to demonstrate the method, the following example is presented. It is required to determine the pressure coefficients S at 55 percent of the chord of a 6-percent-thick symmetrical circular-arc airfoil section with a 10-percent-chord plain leading-edge flap deflected 30° and a 30-percent-chord plain trailing-edge flap deflected 40°. The section lift coefficient is assumed to be 1.65.

The airfoil section obviously satisfies the general assumptions of the method. The following data are then assembled:

$$E_N=0.1 \qquad \delta_N=30°$$

$$E_F=0.3 \qquad \delta_F=40°$$

$$c_l=1.65 \qquad \frac{x}{c}=0.55$$

(1) $c_{l_{b\delta_N}}=\frac{\pi}{45}\sqrt{(0.1)(1-0.1)}(30)=0.628$

(2) From figure 24,

$$c_{l_{b\delta_F}}=0.772$$

(3) $c_{l_a}=1.65-(0.628+0.772)=0.25$

(4) From figure 26,

$$\frac{\Delta v_a}{V}=0.034$$

(5) The basic velocity distribution for the 6-percent-thick symmetrical circular-arc airfoil at zero lift has been computed and plotted in figure 29. At $\frac{x}{c}=0.55$

$$\frac{v}{V}=1.078$$

(6) $P_{b\delta_N}=\frac{30}{45}\log_e\left[\frac{\sqrt{(1-0.1)(1-0.55)}+\sqrt{(0.1)(0.55)}}{\sqrt{(1-0.1)(1-0.55)}-\sqrt{(0.1)(0.55)}}\right]$
$=0.516$

(7) From table V, for $\frac{x/c}{1-E_F}=0.786$,

$$\frac{P_{b\delta_F}}{c_{l_{b\delta_F}}}=1.265$$

then

$$P_{b\delta_F}=(1.265)(0.772)=0.977$$

(8) From figure 28,

$$\left(\frac{v'}{V}\right)_a=-0.006$$

(9) From figure 27,

$$\left(\frac{v'}{V}\right)_F=-0.062$$

(10) $\frac{v_b}{V}=0.034+1.078-0.006-0.062=1.044$

(11) $P_{b\delta}=0.516+0.977=1.493$

(12) $S_U=\left[1.044+\frac{1.493}{4(1.044)}\right]^2=1.97$

$$S_L=\left[1.044-\frac{1.493}{4(1.044)}\right]^2=0.47$$

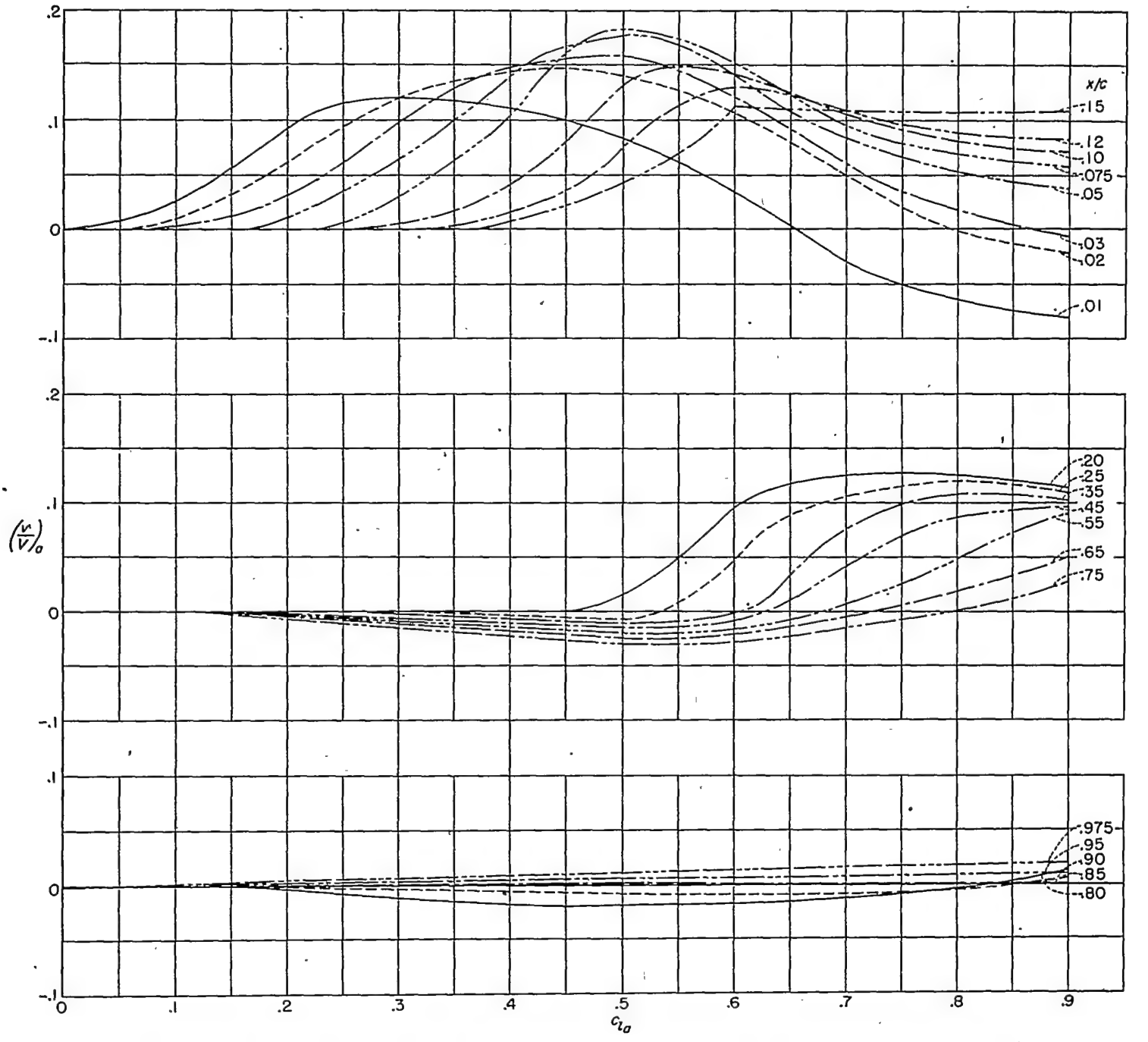

FIGURE 28.—Variation of $(v'/V)_a$ due to separation near the leading edge with additional lift coefficient.

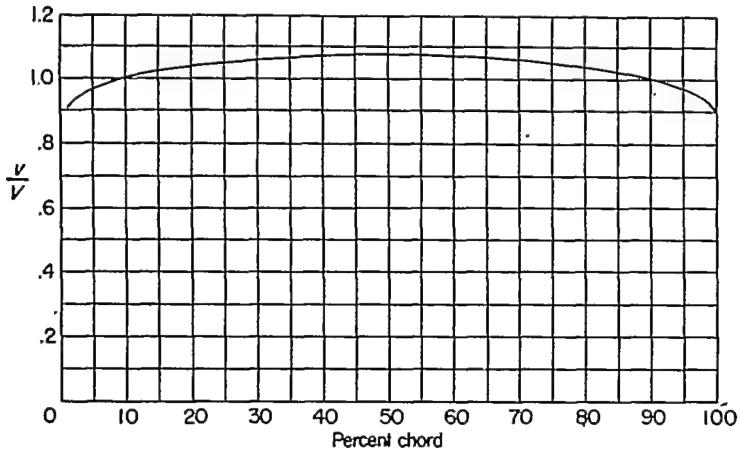

FIGURE 29.—Velocity distribution for the 6-percent-thick symmetrical circular-arc airfoil section; $\alpha_0=0°$; $\delta_N=\delta_F=0°$.

ACCURACY AND LIMITATIONS OF METHOD

In order to justify the method of correlation employed in the development of the present method, the calculated pressure distributions over the 6-percent-thick symmetrical circular-arc airfoil section and the integrated flap normal-force and hinge-moment coefficients for several individual and combined deflections of the plain leading-edge and plain trailing-edge flaps are compared with those obtained experimentally in figures 30 to 32. The flap pressure coefficients (fig. 30) are plotted against the projected chordwise position of the flap orifices on the airfoil chord. The dispersion of the normal-force and hinge-moment results shown in figures 31 and 32 may be considered typical of the accuracy to be expected from the present method. In every case the calculated values of the flap loadings are shown to provide a reasonable quantitative prediction of the experimental loads. For individual deflections of the leading-edge and trailing-edge flaps, the normal-force and hinge-moment characteristics as a rule are within 10 percent of the experimental values. For combined deflections of the leading-edge and trailing-edge flaps, the predicted values of the loads and hinge moments over the trailing-edge flap remain within 10 percent; whereas for the leading-edge flap, the method tends to underestimate these characteristics to a larger degree, depending upon the magnitude of the flap deflections.

The flap hinges were located on the lower surface of the airfoil and the flaps were in contact with the flap skirts so that, in effect, there was no leakage of air between the upper and lower surfaces. Changes in the vertical location of the hinge line are believed to have negligible effects on the airfoil characteristics. If leakage at the flap hinge were present, however, the effects may be such as to alter the separation phenomena particularly at low trailing-edge-flap deflections.

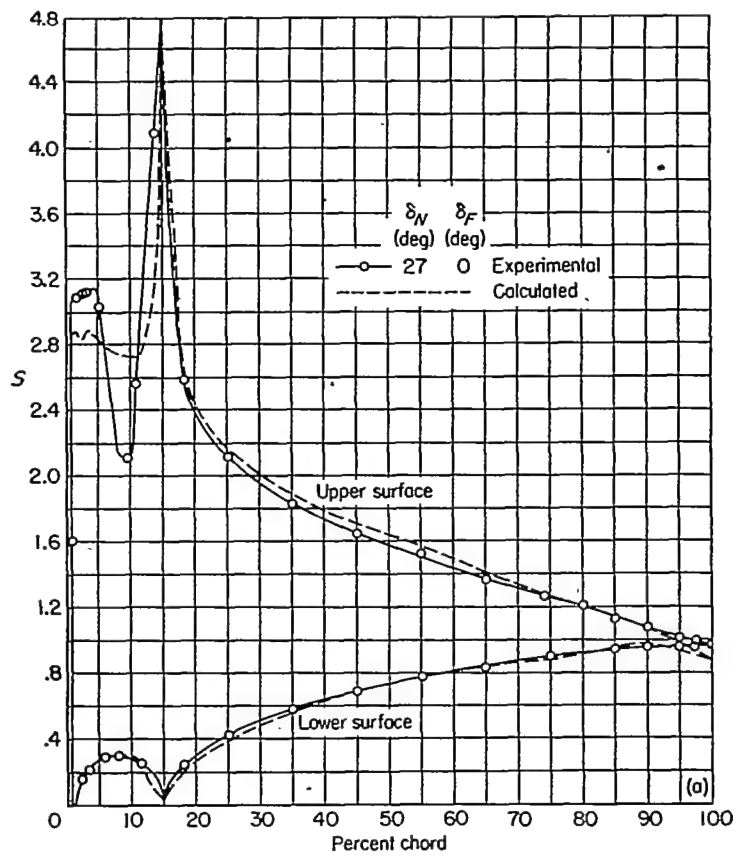

(a) $\alpha_0=12.2°$.

FIGURE 30.—Variation of surface pressure coefficient with percent chord for the 6-percent-thick symmetrical circular-arc airfoil section with 0.15-chord plain leading-edge flap and 0.20-chord plain trailing-edge flap.

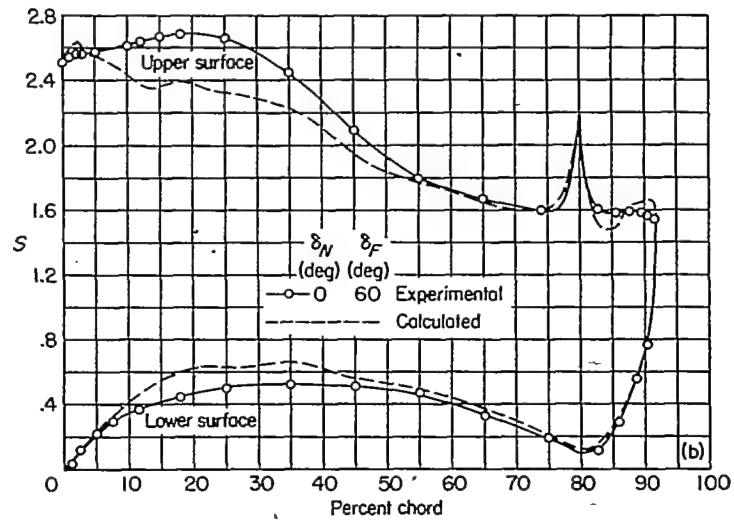

(b) $\alpha_0=1.0°$.

FIGURE 30.—Continued.

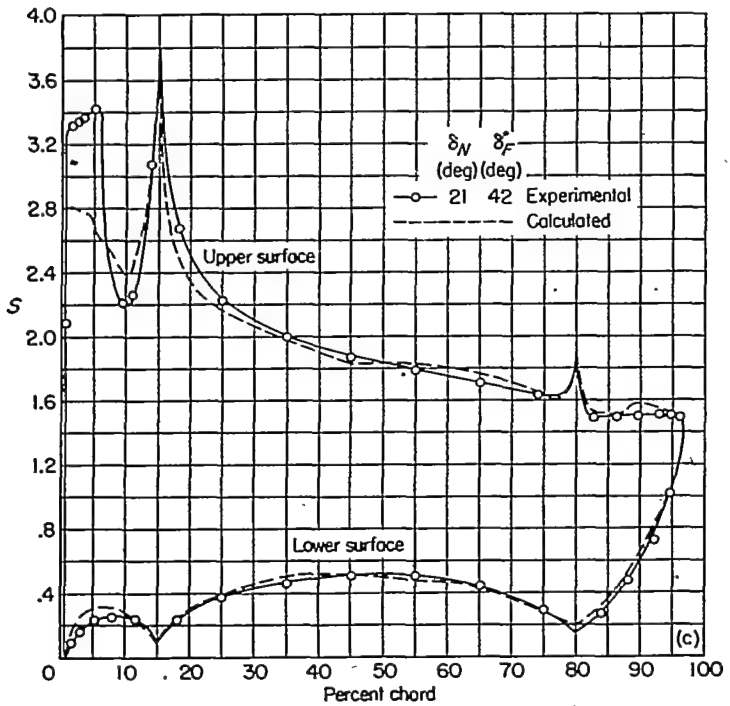

(c) $\alpha_0 = 6.1°$.

FIGURE 30.—Concluded.

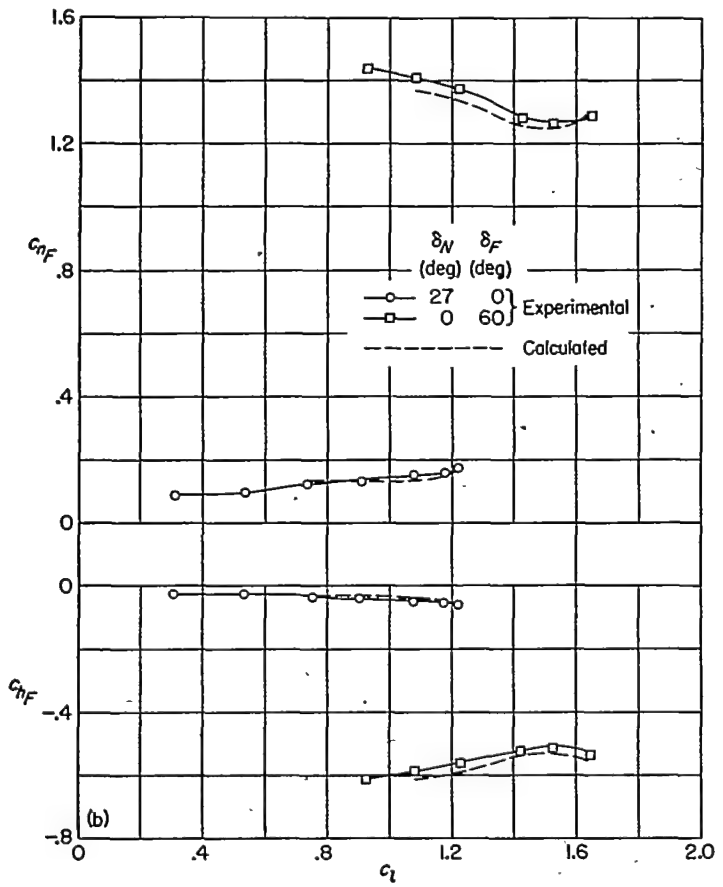

(b) 0.20-chord plain trailing-edge flap.

FIGURE 31.—Concluded.

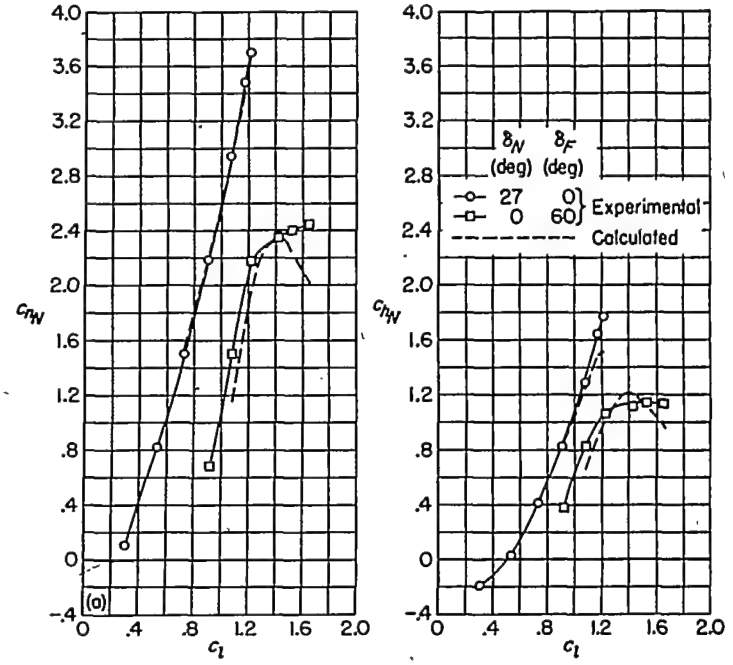

(a) 0.15-chord plain leading-edge flap.

FIGURE 31.—Flap-section normal-force and hinge-moment characteristics of a 6-percent-thick symmetrical circular-arc airfoil section for individual deflections of the plain leading-edge flap and plain trailing-edge flap.

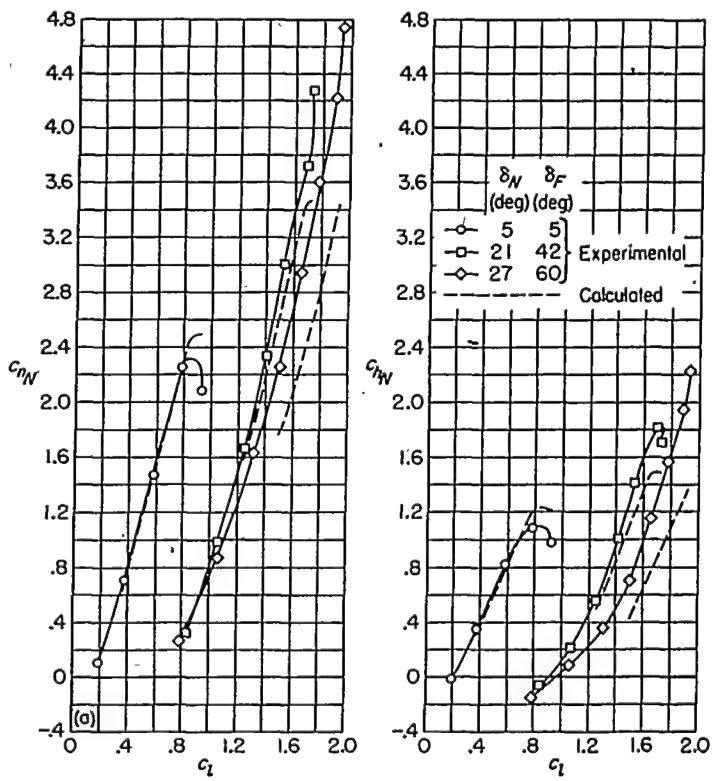

(a) 0.15-chord plain leading-edge flap.

FIGURE 32.—Flap-section normal-force and hinge-moment characteristics of a 6-percent-thick symmetrical circular-arc airfoil section for combined deflections of the plain leading-edge flap and plain trailing-edge flap.

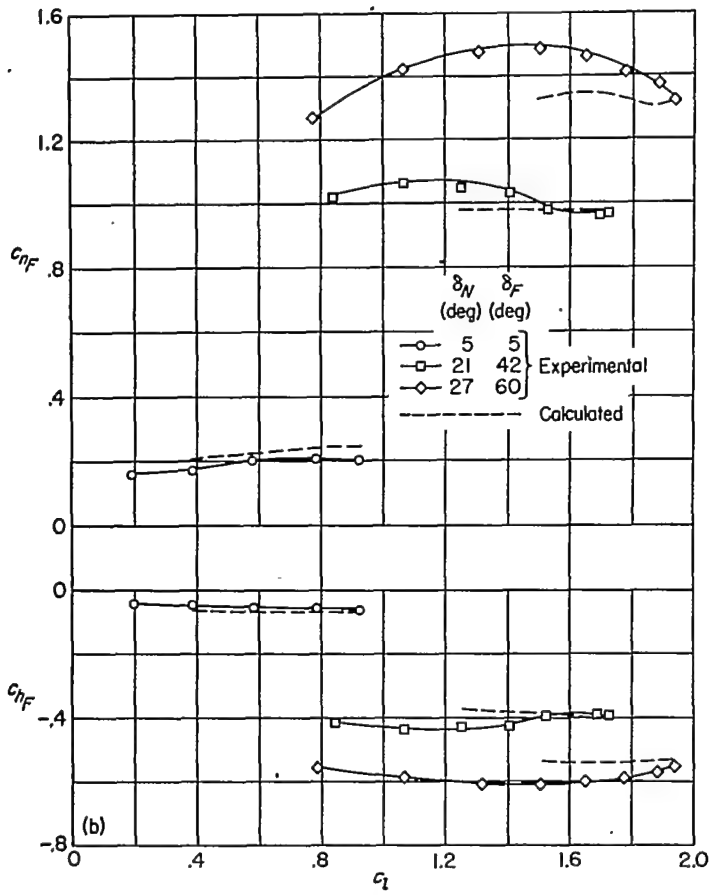

(b) 0.20-chord plain trailing-edge flap.

FIGURE 32.—Concluded.

Although there may be some tendency of increased Reynolds number to alter the conditions of the boundary layer, the effects of scale will probably be insignificant particularly in view of the negligible variations in section lift coefficient associated with sharp-edge airfoils. (See figs. 9 and 10, and ref. 12.)

CONCLUSIONS

A two-dimensional wind-tunnel investigation was made of two symmetrical circular-arc airfoils 6- and 10-percent thick, with plain leading- and trailing-edge flaps at Reynolds numbers from 0.70×10^6 to 18×10^6. The results obtained indicated the following conclusions:

1. Maximum lift coefficients of 1.95 and 2.03 were obtained for the optimum combination of leading- and trailing-edge-flap deflection for the 6- and 10-percent-thick airfoils, respectively. The corresponding maximum lift coefficients for the plain airfoils were 0.73 and 0.67, respectively.

2. The optimum combinations of flap deflection for the 6- and 10-percent-thick airfoils were found to be $\delta_N=30°$, $\delta_F=60°$ and $\delta_N=36°$, $\delta_F=60°$, respectively, where δ_N represents the leading-edge-flap and δ_F the trailing-edge-flap deflections. The results for the 10-percent-thick airfoil with the trailing-edge flap deflected 60° indicate no important changes in the maximum section lift coefficient with small departures from the optimum deflection of the leading-edge flap.

3. The scale effects on the maximum lift coefficient were, in general, small, the largest change being a decrease of about 0.1 for the 10-percent-thick airfoil for Reynolds numbers from 3×10^6 to 9×10^6.

4. The section pitching-moment characteristics indicated that the aerodynamic center was ahead of the quarter-chord point and moved toward the leading edge when either the leading-edge flap or the trailing-edge flap was deflected.

5. Deflecting the leading-edge flap was more effective in extending the low-drag range to higher section lift coefficients than deflecting the trailing-edge flap.

6. The leading-edge-flap section normal-force and hinge-moment coefficients increased rapidly in a positive direction with increasing lift coefficient; for a given lift coefficient, however, increasing the downward deflection of either flap produced downward increments in the leading-edge flap force and moment coefficients.

7. The trailing-edge flap section normal-force and hinge-moment coefficients are of a similar magnitude to those for a plain trailing-edge flap on a subsonic type of airfoil.

8. The maximum flap normal-force and hinge-moment coefficients were, respectively, 4.74 and 2.24 for the leading-edge flap as compared with 1.48 and −0.61 for the trailing-edge flap.

9. A method for predicting the pressure distribution over sharp-edge airfoils equipped with plain trailing-edge and leading-edge flaps has been developed from a generalization of the pressure-distribution measurements made for this investigation. A comparison of the measured flap loads with those obtained by the generalized method indicates that the methods by which the data were generalized give overall results which are in reasonable agreement with experiment.

LANGLEY AERONAUTICAL LABORATORY,
NATIONAL ADVISORY COMMITTEE FOR AERONAUTICS,
LANGLEY FIELD, VA., *April 16, 1953*.

REFERENCES

1. Abbott, Ira H., Von Doenhoff, Albert E., and Stivers, Louis S., Jr.: Summary of Airfoil Data. NACA Rep. 824, 1945. (Supersedes NACA WR L–560.)
2. Lindsey, W. F., Daley, Bernard N., and Humphreys, Milton D.: The Flow and Force Characteristics of Supersonic Airfoils at High Subsonic Speeds. NACA TN 1211, 1947.
3. Purser, Paul E., and Johnson, Harold S.: Effects of Trailing-Edge Modifications on Pitching-Moment Characteristics of Airfoils. NACA WR L–664, 1944. (Formerly NACA CB L4I30.)
4. Street, William G., and Ames, Milton B., Jr.: Pressure-Distribution Investigation of an N.A.C.A. 0009 Airfoil With a 50-Percent-Chord Plain Flap and Three Tabs. NACA TN 734, 1939.
5. Theodorsen, T., and Garrick, I. E.: General Potential Theory of Arbitrary Wing Sections. NACA Rep. 452, 1933.
6. Theodorsen, Theodore, and Naiman, Irven: Pressure Distributions for Representative Airfoils and Related Profiles. NACA TN 1016, 1946.
7. Glauert, H.: Theoretical Relationships for an Aerofoil With Hinged Flap. R. & M. No. 1095, British A.R.C., 1927.
8. Glauert, H.: A Theory of Thin Aerofoils. R. & M. No. 910, British A.R.C., 1924.
9. Allen, H. Julian: Calculation of the Chordwise Load Distribution Over Airfoil Sections With Plain, Split, or Serially Hinged Trailing-Edge Flaps. NACA Rep. 634, 1938.
10. Milne-Thomson, L. M.: Theoretical Hydrodynamics. Second ed., Macmillan and Co., Ltd., 1949, pp. 167–168.
11. Allen, H. Julian: A Simplified Method for the Calculation of Airfoil Pressure Distribution. NACA TN 708, 1939.
12. Powter, G. J., and Young, A. D.: Wind Tunnel Tests on a 7.5 Per Cent Thick Bi-Convex Wing With Leading and Trailing Edge Flaps. Rep. No. Aero. 2157, British R.A.E., Sept. 1946.

TABLE I.—ORDINATES FOR THE 6-PERCENT-THICK SYMMETRICAL CIRCULAR-ARC AIRFOIL

[Stations and ordinates given in percent of airfoil chord]

Upper surface		Lower surface	
Station	Ordinate	Station	Ordinate
0	0	0	0
5	.572	5	−.572
10	1.082	10	−1.082
15	1.533	15	−1.533
20	1.922	20	−1.922
25	2.252	25	−2.252
30	2.521	30	−2.521
35	2.731	35	−2.731
40	2.880	40	−2.880
45	2.970	45	−2.970
50	3.000	50	−3.000
55	2.970	55	−2.970
60	2.880	60	−2.880
65	2.731	65	−2.731
70	2.521	70	−2.521
75	2.252	75	−2.252
80	1.922	80	−1.922
85	1.533	85	−1.533
90	1.082	90	−1.082
95	.572	95	−.572
100	0	100	0
Radius of circular arc: 4.182c			

TABLE II.—ORDINATES FOR THE 10-PERCENT-THICK SYMMETRICAL CIRCULAR-ARC AIRFOIL

[Stations and ordinates given in percent of airfoil chord]

Upper surface		Lower surface	
Station	Ordinate	Station	Ordinate
0	0	0	0
5	.958	5	−.958
10	1.812	10	−1.812
15	2.562	15	−2.562
20	3.211	20	−3.211
25	3.759	25	−3.759
30	4.207	30	−4.207
35	4.554	35	−4.554
40	4.802	40	−4.802
45	4.951	45	−4.951
50	5.000	50	−5.000
55	4.951	55	−4.951
60	4.802	60	−4.802
65	4.554	65	−4.554
70	4.207	70	−4.207
75	3.759	75	−3.759
80	3.211	80	−3.211
85	2.562	85	−2.562
90	1.812	90	−1.812
95	.958	95	−.958
100	0	100	0
Radius of circular arc: 2.525c			

TABLE III.—SUMMARY OF TESTS OF CIRCULAR-ARC AIRFOIL SECTIONS

Airfoil thickness	Tunnel (a)	δ_N (deg)	δ_F (deg)	R	Measurements	Source of data
0.06c	TDT	0	0	3, 6, and 9×10⁶	Lift—Drag	Figure 4 (a)
0.10c	TDT	0	0	3, 6, and 9×10⁶	Lift—Drag	Figure 4 (b)
0.10c	TDT	0	0	14 and 18×10⁶	Lift	Figure 4 (c)
0.06c	TDT	0	0, 20, 40, 60	6×10⁶	Lift—Pitching moment	Figure 5 (a)
0.10c	TDT	0	0, 20, 40, 60	6×10⁶	Lift—Pitching moment	Figure 5 (b)
0.06c	TDT	0, 10, 20, 30, 40	0	6×10⁶	Lift—Pitching moment	Figure 6 (a)
0.10c	TDT	0, 20, 30, 40	0	6×10⁶	Lift—Pitching moment	Figure 6 (b)
0.06c	TDT	30	50	6×10⁶	Lift	Figure 8 (a)
0.06c	TDT	20, 30, 40	60	6×10⁶	Lift	Figure 8 (a)
0.10c	TDT	30	50	6×10⁶	Lift	Figure 8 (b)
0.10c	TDT	30, 40, 50	60	6×10⁶	Lift	Figure 8 (b)
0.10c	TDT	36	60	3, 6, 9, 14, and 18×10⁶	Lift	Figure 8 (c)
0.06c	TDT	30	60	3, 6, and 9×10⁶	Lift—Pitching moment	Figure 9 (a)
0.10c	TDT	30	60	3, 6, and 9×10⁶	Lift—Pitching moment	Figure 9 (b)
0.06c	LTT	27	60	0.7 and 2.3×10⁶	Lift	Figure 10
0.06c	LTT	0	0, 5, 10	2.1×10⁶	Lift—Drag	Figure 11
0.06c	LTT	5	0, 5, 10	2.1×10⁶	Lift—Drag	Figure 11
0.06c	LTT	10	0, 10	2.1×10⁶	Lift—Drag	Figure 11
0.06c	LTT	0, 5, 9, 21, 27	0	2.1×10⁶	Pressure distribution	Table IV
0.06c	LTT	0	5, 10, 22, 42, 60	2.1×10⁶	Pressure distribution	Table IV
0.06c	LTT	5	5, 10, 22	2.1×10⁶	Pressure distribution	Table IV
0.06c	LTT	9	10, 22, 42	2.1×10⁶	Pressure distribution	Table IV
0.06c	LTT	21	42	2.1×10⁶	Pressure distribution	Table IV
0.06c	LTT	27	60	2.1×10⁶	Pressure distribution	Table IV

* TDT Langley two-dimensional low-turbulence pressure tunnel.
LTT Langley two-dimensional low-turbulence tunnel.

TABLE IV.—PRESSURE COEFFICIENTS FOR THE AIRFOIL WITH THE LEADING-EDGE FLAP AND TRAILING-EDGE FLAP DEFLECTED IN VARIOUS COMBINATIONS AND AT SEVERAL ANGLES OF ATTACK

[R=2.1×10^6; M=0.15]

(a) δ_N=0°, δ_F=0°

Orifice	x/c	Pressure coefficients for section angle of attack—								
		0°	0.5°	2.0°	4.1°	6.1°	8.1°	[a] 9.1°	10.2°	12.2°
1	0	0.17	0	0.11	0.78	1.36	1.42	1.33	1.25	1.24
2	1	.81	.94	1.96	2.13	2.14	1.94	1.82	1.73	1.64
3	2	.87	.96	1.72	2.14	2.15	1.94	1.83	1.73	1.64
4	3	.89	.98	1.39	2.15	2.15	1.95	1.83	1.74	1.64
5	5	.94	1.01	1.17	2.18	2.16	1.96	1.84	1.74	1.65
6	7.5	.98	1.04	1.19	2.19	2.18	1.97	1.85	1.75	1.65
7	10	1.01	1.06	1.21	1.88	2.21	1.98	1.86	1.75	1.65
8	12	1.04	1.10	1.22	1.59	2.22	2.00	1.87	1.76	1.66
9	15	1.03	1.02	1.14	1.38	2.18	2.00	1.87	1.77	1.67
[b] 10	16.1	1.02	.98	.90	.79	.74	.69	.68	.68	.55
A	18.3	1.07	1.14	1.25	1.31	2.14	2.03	1.90	1.79	1.67
B	25	1.12	1.16	1.25	1.31	1.86	2.02	1.91	1.81	1.69
C	35	1.16	1.18	1.25	1.31	1.47	1.93	1.89	1.81	1.71
D	45	1.17	1.18	1.24	1.29	1.32	1.76	1.81	1.78	1.72
E	55	1.17	1.18	1.23	1.26	1.26	1.69	1.71	1.73	1.72
F	65	1.16	1.17	1.20	1.22	1.22	1.44	1.59	1.72	1.71
G	74	1.13	1.14	1.16	1.17	1.17	1.32	1.49	1.61	1.71
[b] 17	77.03	1.10	1.10	1.10	1.10	1.11	1.23	1.37	1.49	1.61
[b] 18	78.3	1.10	1.10	1.10	1.10	1.11	1.23	1.36	1.48	1.60
[b] 19	80	1.10	1.10	1.12	1.13	1.14	1.26	1.42	1.54	1.67
20	85	1.06	1.08	1.09	1.09	1.09	1.22	1.38	1.53	1.69
21	90	1.02	1.03	1.04	1.04	1.05	1.18	1.34	1.49	1.66
22	95	.97	.97	.96	.97	1.01	1.15	1.29	1.44	1.60
23	97.5	.92	.92	.92	.93	.98	1.13	1.28	1.39	1.56
24	100	.83	.84	.85	.86	.94	1.11	1.24	1.35	1.50
11	1.3	.87	.77	.50	.26	.15	.11	.11	.12	.09
12	2.6	.89	.81	.69	.37	.26	.22	.21	.21	.19
13	5	.95	.89	.72	.52	.40	.35	.35	.35	.33
14	7.5	.98	.93	.78	.61	.50	.45	.44	.44	.42
15	11.4	1.01	.98	.85	.69	.59	.54	.55	.55	.53
H	18.1	1.05	1.02	.93	.79	.71	.66	.67	.67	.66
I	25	1.09	1.07	.99	.88	.79	.76	.77	.77	.77
J	35	1.12	1.11	1.04	.94	.88	.85	.87	.88	.88
K	45	1.15	1.13	1.07	1.00	.95	.93	.95	.97	.99
L	55	1.15	1.14	1.09	1.02	.99	.99	1.02	1.04	1.07
M	65	1.12	1.11	1.09	1.02	1.01	1.02	1.06	1.09	1.13
N	75	1.10	1.11	1.09	1.04	1.04	1.06	1.11	1.15	1.21
25	85	1.05	1.06	1.05	1.02	1.04	1.09	1.15	1.20	1.29
26	90	1.01	1.02	1.02	1.00	1.03	1.09	1.16	1.23	1.33
27	95	.94	.96	.96	.95	1.00	1.09	1.17	1.26	1.38
28	97.5	.89	.93	.93	.93	.78	1.09	1.19	1.29	1.42
[b] 16	15	1.02	.99	.89	.77	.68	.64	.63	.63	.62
[b] 29	80.3	1.07	1.07	1.06	1.03	1.02	1.08	1.13	1.20	1.28

[a] Angle of attack for maximum lift.
[b] Internal pressure.

TABLE IV.—PRESSURE COEFFICIENTS—Continued

(b) δ_N=5°, δ_F=0°

Orifice	x/c	Pressure coefficients for section angle of attack—							
		−2.0°	0°	2.0°	4.1°	6.1°	8.1°	9.1°	[a] 10.2°
1	0	1.78	1.83	0.02	0.34	1.26	1.67	1.56	1.39
2	1	.28	.49	.99	2.14	2.47	2.37	2.15	1.97
3	2	.42	.63	1.01	2.16	2.48	2.37	2.15	1.97
4	3	.50	.69	1.03	2.08	2.49	2.38	2.16	1.98
5	5	.62	.80	1.03	1.46	2.53	2.40	2.18	1.98
6	7.5	.74	.90	1.15	1.37	2.56	2.42	2.19	2.00
7	10	.83	.98	1.19	1.37	2.29	2.50	2.21	2.02
8	12	.93	1.07	1.27	1.45	1.92	2.46	2.24	2.04
9	15	1.07	1.19	1.38	1.54	1.67	2.42	2.25	2.05
[b] 10	16.1	1.29	.88	.81	.69	.60	.55	.53	.53
A	18.3	1.03	1.15	1.33	1.49	1.55	2.29	2.23	2.05
B	25	1.05	1.15	1.28	1.41	1.48	2.02	2.14	2.03
C	35	1.09	1.16	1.27	1.37	1.44	1.63	1.93	1.94
D	45	1.11	1.17	1.26	1.33	1.39	1.42	1.69	1.82
E	55	1.13	1.18	1.24	1.30	1.34	1.33	1.49	1.67
F	65	1.12	1.15	1.20	1.25	1.27	1.26	1.36	1.54
G	74	1.11	1.13	1.17	1.19	1.21	1.20	1.27	1.44
[b] 17	77.03	1.09	1.09	1.10	1.11	1.12	1.14	1.18	1.33
[b] 18	78.3	1.09	1.09	1.10	1.11	1.12	1.13	1.18	1.32
19	80	1.07	1.09	1.13	1.15	1.17	1.16	1.22	1.37
20	85	1.07	1.07	1.09	1.10	1.12	1.13	1.18	1.34
21	90	1.04	1.03	1.04	1.05	1.06	1.08	1.15	1.29
22	95	.99	.97	.97	.98	.99	1.04	1.12	1.26
23	97.5	.94	.93	.92	.93	.95	1.01	1.10	1.23
24	100	.87	.85	.85	.87	.90	.98	1.07	1.20
11	1.3	1.80	1.71	.72	.38	.19	.11	.11	.11
12	2.6	1.81	1.19	.75	.43	.31	.21	.20	.21
13	5	1.83	1.04	.83	.60	.44	.35	.34	.34
14	7.5	1.81	1.04	.84	.65	.52	.42	.41	.41
15	11.4	1.61	.99	.84	.69	.57	.49	.48	.47
H	18.1	1.23	.99	.85	.64	.65	.67	.63	.69
I	25	1.12	1.07	.96	.85	.76	.69	.68	.69
J	35	1.17	1.11	1.02	.94	.86	.80	.79	.80
K	45	1.20	1.14	1.07	.99	.93	.88	.88	.89
L	55	1.19	1.15	1.09	1.03	.97	.94	.94	.96
M	65	1.16	1.13	1.09	1.05	1.00	.93	.93	1.01
N	75	1.12	1.11	1.03	1.05	1.01	1.01	1.03	1.07
25	85	1.07	1.06	1.05	1.03	1.01	1.03	1.06	1.11
26	90	1.04	1.02	1.02	1.01	1.00	1.03	1.06	1.12
27	95	.98	.96	.96	.96	.97	1.01	1.06	1.15
28	97.5	.94	.91	.93	.94	.94	1.00	1.06	1.16
[b] 16	15	1.29	.88	.80	.69	.63	.50	.50	.50
[b] 29	80.3	1.08	1.06	1.05	1.04	1.01	1.01	1.05	1.10

[a] Angle of attack for maximum lift.
[b] Internal pressures.

TABLE IV.—PRESSURE COEFFICIENTS—Continued

(c) $\delta_N=9°$, $\delta_F=0°$

Orifice	x/c	Pressure coefficients for section angle of attack—								
		−2.0°	0°	2.0°	4.1°	6.1°	8.1°	10.2°	[a] 11.2°	12.2°
1	0	1.70	1.62	1.00	0.04	0.28	1.89	1.92	1.65	0.88
2	1	.18	.35	.69	1.55	2.42	2.81	2.45	2.19	1.98
3	2	.33	.51	.80	1.19	2.45	2.82	2.46	2.20	1.99
4	3	.40	.53	.85	1.20	2.46	2.83	2.46	2.20	1.99
5	5	.55	.71	.96	1.26	2.36	2.86	2.48	2.21	2.00
6	7.5	.69	.85	1.06	1.33	1.68	2.90	2.51	2.24	2.01
7	10	.80	.96	1.17	1.40	1.53	2.74	2.53	2.26	2.03
8	12	.94	1.10	1.31	1.53	1.64	2.35	2.53	2.27	2.04
9	15	1.25	1.43	1.66	1.90	1.94	1.96	2.49	2.27	2.06
[b] 10	16.1	1.18	.92	.63	.62	.51	.42	.38	.39	.40
A	18.3	1.07	1.20	1.34	1.53	1.67	1.75	2.37	2.21	2.03
B	25	1.06	1.16	1.29	1.43	1.55	1.62	2.17	2.14	2.01
C	35	1.09	1.17	1.27	1.37	1.47	1.53	1.83	1.97	1.94
D	45	1.11	1.18	1.25	1.33	1.40	1.45	1.57	1.78	1.85
E	55	1.12	1.18	1.24	1.29	1.34	1.38	1.42	1.62	1.75
F	65	1.12	1.16	1.20	1.24	1.28	1.30	1.31	1.49	1.65
G	74	1.11	1.13	1.16	1.18	1.21	1.23	1.23	1.39	1.56
[b] 17	77.03	1.07	1.09	1.10	1.11	1.12	1.12	1.16	1.29	1.44
[b] 18	78.3	1.07	1.09	1.10	1.11	1.12	1.12	1.16	1.28	1.43
19	80	1.07	1.09	1.12	1.15	1.17	1.18	1.20	1.33	1.49
20	85	1.06	1.07	1.09	1.10	1.11	1.12	1.16	1.29	1.47
21	90	1.04	1.03	1.04	1.04	1.05	1.06	1.12	1.26	1.43
22	95	.99	.98	.96	.96	.98	1.00	1.09	1.22	1.39
23	97.5	.95	.92	.91	.91	.93	.96	1.07	1.20	1.36
24	100	.89	.85	.85	.87	.88	.92	1.04	1.17	1.30
11	1.3	1.71	1.62	.93	.53	.28	.14	.10	.10	.11
12	2.6	1.72	1.64	.90	.59	.37	.24	.19	.19	.20
13	5	1.72	1.62	.89	.66	.49	.35	.30	.30	.31
14	7.5	1.74	1.47	.87	.68	.53	.42	.36	.37	.37
15	11.4	1.75	1.13	.80	.66	.54	.45	.41	.41	.41
H	18.1	1.74	.92	.81	.69	.59	.52	.48	.48	.49
I	25	1.45	1.01	.94	.83	.73	.66	.61	.62	.63
J	35	1.15	1.09	1.01	.91	.84	.77	.74	.75	.77
K	45	1.12	1.12	1.06	.98	.91	.85	.83	.85	.87
L	55	1.14	1.13	1.08	1.01	.96	.90	.90	.92	.96
M	65	1.13	1.12	1.09	1.04	.99	.96	.95	.98	1.02
N	75	1.11	1.10	1.07	1.04	1.01	.99	.99	1.04	1.09
25	85	1.06	1.06	1.04	1.01	1.00	1.00	1.03	1.08	1.15
26	90	1.02	1.02	1.01	.99	.99	.99	1.04	1.10	1.18
27	95	.97	.95	.95	.95	.95	.96	1.04	1.11	1.21
28	97.5	.94	.92	.91	.93	.93	.95	1.04	1.12	1.24
[b] 16	15	1.73	.91	.63	.62	.50	.42	.39	.39	.39
[b] 29	80.3	1.07	1.06	1.05	1.02	1.00	1.00	1.03	1.09	1.16

[a] Angle of attack for maximum lift.
[b] Internal pressures.

TABLE IV.—PRESSURE COEFFICIENTS—Continued

(d) $\delta_N=21°$, $\delta_F=0°$

Orifice	x/c	Pressure coefficients for section angle of attack—								
		0°	2.0°	4.1°	6.1°	8.1°	10.2°	12.2°	[a] 14.2°	16.2°
1	0	1.54	1.31	1.17	0.47	0.16	1.18	2.46	3.44	2.57
2	1	.09	.23	.45	.83	2.20	2.82	3.41	3.82	3.02
3	2	.23	.39	.61	.94	1.65	2.86	3.43	3.84	3.04
4	3	.31	.48	.70	1.00	1.38	2.88	3.45	3.86	3.05
5	5	.47	.65	.87	1.14	1.45	2.67	3.50	3.89	3.08
6	7.5	.71	.87	1.09	1.36	1.64	1.88	3.42	3.94	3.12
7	10	.86	1.05	1.26	1.50	1.80	1.89	2.64	3.77	3.01
8	12	1.10	1.31	1.53	1.78	2.20	2.22	2.24	3.03	2.74
9	15	1.86	2.13	2.40	2.67	3.07	3.18	2.83	2.70	2.55
10	16.1	1.99	2.33	2.74	3.03	3.21	3.10	2.86	2.45	2.15
A	18.3	1.36	1.54	1.75	1.98	2.22	2.38	2.42	2.40	2.30
B	25	1.24	1.38	1.51	1.66	1.83	1.97	2.03	2.07	2.10
C	35	1.21	1.31	1.42	1.51	1.63	1.72	1.77	1.79	1.91
D	45	1.21	1.28	1.36	1.43	1.51	1.58	1.60	1.61	1.80
E	55	1.20	1.26	1.32	1.37	1.43	1.47	1.47	1.47	1.65
F	65	1.18	1.21	1.26	1.29	1.34	1.36	1.35	1.35	1.56
G	74	1.15	1.17	1.20	1.23	1.25	1.26	1.24	1.26	1.50
[b] 17	77.03	1.09	1.10	1.11	1.12	1.14	1.15	1.14	1.17	1.39
[b] 18	78.3	1.09	1.10	1.11	1.12	1.13	1.13	1.13	1.17	1.38
19	80	1.12	1.14	1.16	1.19	1.20	1.20	1.19	1.20	1.43
20	85	1.09	1.10	1.11	1.12	1.12	1.13	1.12	1.17	1.42
21	90	1.05	1.05	1.05	1.05	1.06	1.07	1.07	1.13	1.39
22	95	.99	.98	.98	.98	.98	1.01	1.03	1.11	1.35
23	97.5	.95	.93	.93	.93	.94	.98	1.01	1.10	1.33
24	100	.89	.87	.87	.88	.90	.94	.98	1.07	1.29
11	1.3	1.54	1.31	1.14	.73	.38	.20	.07	.03	.06
12	2.6	1.55	1.32	1.15	.70	.44	.28	.16	.10	.12
13	5	1.55	1.33	1.13	.66	.49	.35	.25	.19	.20
14	7.5	1.56	1.33	1.05	.62	.47	.37	.28	.23	.24
15	11.4	1.57	1.34	.90	.49	.42	.33	.26	.23	.24
H	18.1	1.58	1.37	.68	.47	.39	.32	.26	.24	.25
I	25	1.61	1.23	.72	.67	.56	.51	.45	.40	.42
J	35	1.50	.91	.85	.79	.72	.65	.59	.55	.57
K	45	1.21	.93	.94	.88	.82	.75	.69	.67	.69
L	55	1.04	.99	.99	.94	.88	.83	.78	.78	.80
M	65	1.02	1.02	1.01	.97	.93	.87	.84	.83	.89
N	75	1.01	1.03	1.02	.99	.96	.93	.90	.90	.98
25	85	1.00	1.01	1.00	.98	.97	.96	.94	.96	1.06
26	90	.98	.99	.99	.98	.96	.96	.96	.99	1.11
27	95	.95	.95	.95	.94	.95	.96	.96	1.02	1.16
28	97.5	.93	.93	.92	.92	.93	.95	.93	1.04	1.20
[b] 16	15	1.58	1.35	.78	.33	.32	.34	.28	.24	.24
[b] 29	80.3	1.01	1.02	1.01	.99	.97	.95	.93	.95	1.05

[a] Angle of attack for maximum lift.
[b] Internal pressures.

TABLE IV.—PRESSURE COEFFICIENTS—Continued

(e) $\delta_N=27°$, $\delta_F=0°$

Orifice	x/c	Pressure coefficients for section angle of attack—								
		0°	2.0°	4.1°	6.1°	8.1°	10.2°	12.2°	[a] 15.2°	18.3°
1	0	1.58	1.39	1.14	1.20	0.04	0.35	1.59	3.39	3.41
2	1	.04	.12	.29	.52	1.02	2.41	3.08	3.88	3.09
3	2	.15	.26	.46	.69	1.09	2.29	3.11	3.89	3.71
4	3	.23	.36	.55	.79	1.15	1.88	3.14	3.91	3.72
5	5	.39	.54	.74	.97	1.30	1.53	3.03	3.97	3.76
6	7.5	.60	.75	1.00	1.22	1.52	1.77	2.30	4.01	3.82
7	10	.81	.99	1.21	1.45	1.76	2.02	2.10	3.25	3.54
8	12	1.10	1.31	1.55	1.82	2.16	2.34	2.56	2.64	2.84
9	15	2.04	2.35	2.73	3.14	3.68	4.01	4.10	3.47	2.63
10	16.1	2.26	2.60	3.00	3.43	4.10	4.42	4.43	3.76	2.72
A	18.3	1.38	1.55	1.74	1.95	2.21	2.42	2.59	2.64	2.19
B	25	1.28	1.39	1.54	1.69	1.85	1.99	2.12	2.18	1.85
C	35	1.23	1.32	1.43	1.53	1.64	1.74	1.83	1.80	1.62
D	45	1.23	1.29	1.37	1.45	1.53	1.59	1.64	1.05	1.52
E	55	1.22	1.26	1.32	1.38	1.44	1.47	1.52	1.40	1.49
F	65	1.20	1.23	1.26	1.30	1.34	1.36	1.37	1.35	1.46
G	74	1.16	1.18	1.20	1.23	1.26	1.26	1.27	1.25	1.43
[b] 17	77.03	1.10	1.10	1.11	1.13	1.14	1.15	1.15	1.18	1.38
[b] 18	78.3	1.10	1.10	1.11	1.12	1.12	1.14	1.13	1.17	1.37
19	80	1.14	1.15	1.17	1.19	1.21	1.20	1.21	1.20	1.42
20	85	1.11	1.10	1.11	1.12	1.12	1.12	1.13	1.17	1.42
21	90	1.07	1.05	1.05	1.06	1.06	1.06	1.07	1.13	1.42
22	95	1.01	.99	.98	.98	.97	.98	1.01	1.11	1.42
23	97.5	.97	.94	.93	.92	.93	.96	.99	1.11	1.40
24	100	.94	.88	.87	.88	.89	.92	.98	1.09	1.30
11	1.3	1.58	1.39	1.12	1.15	.56	.29	.15	.04	.03
12	2.6	1.58	1.39	1.12	1.10	.56	.35	.20	.11	.09
13	5	1.59	1.40	1.13	.84	.53	.38	.29	.18	.18
14	7.5	1.59	1.40	1.13	.67	.50	.37	.29	.21	.19
15	11.4	1.60	1.41	1.15	.54	.37	.34	.26	.19	.20
H	18.1	1.61	1.42	1.17	.47	.36	.30	.24	.20	.20
I	25	1.64	1.46	.99	.63	.56	.48	.42	.37	.36
J	35	1.65	1.27	.77	.78	.70	.62	.58	.51	.52
K	45	1.53	.99	.87	.87	.80	.73	.69	.64	.66
L	55	1.30	.95	.94	.92	.87	.81	.77	.73	.77
M	65	1.19	.98	.98	.96	.92	.87	.84	.80	.87
N	75	1.02	1.00	1.00	.98	.95	.91	.90	.88	.97
25	85	.99	.99	.99	.98	.96	.94	.94	.95	1.07
26	90	.98	.98	.98	.98	.95	.95	.95	.98	1.13
27	95	.95	.95	.95	.95	.94	.94	.96	1.01	1.21
28	97.5	.94	.92	.92	.92	.92	.93	.96	1.04	1.20
[b] 16	15	1.58	1.40	1.14	.45	.20	.21	.23	.18	.18
29	80.3	1.01	1.00	1.00	.99	.96	.94	.93	.93	1.05

[a] Angle of attack for maximum lift.
[b] Internal pressures.

TABLE IV.—PRESSURE COEFFICIENTS—Continued

(f) $\delta_N=0°$, $\delta_F=5°$

Orifice	x/c	Pressure coefficients for section angle of attack—							
		−4.1°	−2.0°	0°	2.0°	4.1°	6.1°	[a] 8.1°	10.2°
1	0	1.65	1.60	0.30	0.38	0.79	1.40	1.56	0.93
2	1	.29	.57	1.06	2.10	2.23	2.15	1.92	1.72
3	2	.43	.68	1.06	2.12	2.25	2.16	1.93	1.73
4	3	.50	.74	1.06	2.12	2.25	2.16	1.93	1.73
5	5	.61	.82	1.08	1.97	2.27	2.18	1.94	1.74
6	7.5	.71	.89	1.11	1.46	2.29	2.20	1.95	1.74
7	10	.78	.94	1.13	1.28	2.29	2.23	1.97	1.75
8	12	.83	.98	1.15	1.27	2.21	2.25	1.99	1.77
9	15	.87	.98	1.06	1.15	2.01	2.27	2.01	1.78
[b] 10	16.1	1.08	1.01	.93	.86	.91	.88	.83	.79
A	18.3	.91	1.05	1.19	1.34	1.72	2.26	2.02	1.79
B	25	.98	1.10	1.21	1.34	1.42	2.15	2.03	1.81
C	35	1.05	1.15	1.24	1.34	1.37	1.83	1.99	1.82
D	45	1.11	1.18	1.25	1.34	1.36	1.53	1.88	1.81
E	55	1.15	1.20	1.26	1.33	1.35	1.37	1.74	1.77
F	65	1.17	1.22	1.25	1.31	1.32	1.29	1.59	1.72
G	74	1.21	1.24	1.26	1.29	1.28	1.24	1.47	1.68
[b] 17	77.03	1.19	1.20	1.19	1.20	1.18	1.15	1.31	1.61
[b] 18	78.3	1.19	1.20	1.18	1.19	1.17	1.14	1.31	1.60
19	80	1.36	1.39	1.37	1.39	1.36	1.26	1.39	1.69
20	85	1.16	1.17	1.19	1.20	1.20	1.17	1.36	1.61
21	90	1.09	1.09	1.08	1.10	1.10	1.12	1.32	1.58
22	95	1.00	.99	.99	1.00	1.02	1.07	1.29	1.53
23	97.5	.94	.93	.94	.95	.98	1.05	1.26	1.50
24	100	.85	.84	.89	.90	.93	1.02	1.24	1.44
11	1.3	1.89	1.07	.65	.36	.19	.12	.09	.10
12	2.6	1.91	1.05	.72	.47	.31	.22	.17	.20
13	5	1.90	1.06	.82	.60	.45	.36	.33	.34
14	7.5	1.76	1.07	.86	.68	.54	.45	.43	.43
15	11.4	1.27	1.07	.91	.75	.63	.55	.52	.53
H	18.1	1.21	1.10	.97	.84	.73	.65	.64	.65
I	25	1.23	1.12	1.01	.91	.81	.75	.74	.75
J	35	1.23	1.13	1.05	.96	.88	.83	.83	.85
K	45	1.21	1.13	1.07	1.00	.93	.89	.90	.91
L	55	1.18	1.11	1.06	1.01	.95	.93	.95	1.00
M	65	1.11	1.07	1.04	1.00	.96	.94	.97	1.03
N	75	1.04	1.00	.98	.95	.92	.91	.96	1.05
25	85	.99	.96	.95	.94	.93	.94	1.01	1.11
26	90	.98	.96	.96	.96	.95	.98	1.06	1.20
27	95	.94	.93	.95	.95	.95	1.00	1.12	1.27
28	97.5	.91	.90	.93	.94	.95	1.00	1.15	1.32
[b] 16	15	1.12	1.02	.93	.82	.73	.66	.63	.63
[b] 29	80.3	1.05	1.04	1.02	1.01	1.00	.98	1.09	1.23

[a] Angle of attack for maximum lift.
[b] Internal pressures.

TABLE IV.—PRESSURE COEFFICIENTS—Continued

(g) $\delta_N=0°$, $\delta_F=10°$

Orifice	x/c	Pressure coefficients for section angle of attack—						
		−4.1°	−2.0°	0°	2.0°	4.1°	[a] 6.1°	8.1°
1	0	1.39	0.91	0.58	0.79	1.23	1.56	1.66
2	1	.45	.85	1.98	2.24	2.30	2.17	1.91
3	2	.58	.90	1.80	2.26	2.30	2.17	1.92
4	3	.65	.93	1.48	2.27	2.31	2.18	1.92
5	5	.75	.98	1.20	2.29	2.33	2.19	1.92
6	7.5	.83	1.02	1.21	2.29	2.36	2.21	1.94
7	10	.89	1.06	1.24	2.02	2.39	2.23	1.95
8	12	.94	1.09	1.26	1.70	2.40	2.25	1.97
9	15	.96	1.06	1.12	1.46	2.37	2.28	1.99
[b] 10	16.1	1.04	.99	.88	.83	.87	.81	.77
A	18.3	1.03	1.16	1.31	1.40	2.26	2.28	2.00
B	25	1.09	1.19	1.31	1.40	1.91	2.27	2.02
C	35	1.16	1.23	1.33	1.42	1.52	2.11	2.00
D	45	1.21	1.27	1.34	1.42	1.42	1.85	1.93
E	55	1.26	1.31	1.36	1.42	1.41	1.61	1.83
F	65	1.30	1.32	1.36	1.42	1.39	1.45	1.71
G	74	1.37	1.37	1.38	1.42	1.39	1.35	1.60
[b] 17	77.03	1.40	1.34	1.31	1.34	1.28	1.21	1.40
[b] 18	78.3	1.44	1.38	1.36	1.39	1.32	1.26	1.47
19	80	1.75	1.64	1.58	1.62	1.50	1.33	1.50
20	85	1.33	1.27	1.25	1.30	1.28	1.26	1.49
21	90	1.16	1.13	1.14	1.16	1.17	1.22	1.46
22	95	1.01	1.05	1.08	1.06	1.09	1.18	1.42
23	97.5	.94	1.02	1.06	1.03	1.06	1.16	1.39
24	100	.85	1.00	1.04	1.00	1.03	1.14	1.36
11	1.3	1.85	.82	.47	.24	.14	.09	.09
12	2.6	1.50	.84	.57	.37	.24	.19	.19
13	5	1.10	.90	.69	.50	.39	.32	.31
14	7.5	1.11	.94	.75	.59	.47	.41	.41
15	11.4	1.10	.96	.81	.66	.56	.50	.50
H	18.1	1.11	.99	.87	.75	.66	.62	.61
I	25	1.13	1.02	.93	.82	.75	.70	.71
J	35	1.12	1.04	.96	.88	.82	.79	.80
K	45	1.10	1.04	.98	.91	.87	.84	.87
L	55	1.05	1.01	.98	.91	.88	.87	.91
M	65	.97	.96	.95	.90	.87	.87	.91
N	75	.88	.86	.84	.81	.79	.81	.87
25	85	.84	.85	.84	.82	.82	.84	.92
26	90	.89	.91	.91	.88	.89	.93	1.02
27	95	.89	.94	.96	.93	.94	1.00	1.13
28	97.5	.88	.96	.98	.95	.96	1.04	1.20
[b] 16	15	1.04	.98	.85	.74	.67	.61	.60
[b] 29	80.3	1.27	1.23	1.20	1.20	1.15	1.10	1.27

[a] Angle of attack for maximum lift.
[b] Internal pressures.

TABLE IV.—PRESSURE COEFFICIENTS—Continued

(h) $\delta_N=0°$, $\delta_F=22°$

Orifice	x/c	Pressure coefficients for section angle of attack—						
		−4.1°	−2.0°	0°	2.0°	4.1°	[a] 5.1°	6.1°
1	0	0.74	0.34	0.61	1.08	1.64	2.00	1.98
2	1	.75	1.78	2.19	2.36	2.35	2.27	2.14
3	2	.83	1.23	2.21	2.37	2.36	2.28	2.14
4	3	.86	1.16	2.23	2.38	2.36	2.28	2.14
5	5	.93	1.18	2.22	2.40	2.37	2.29	2.15
6	7.5	.99	1.21	1.92	2.43	2.39	2.32	2.17
7	10	1.04	1.23	1.54	2.46	2.42	2.34	2.19
8	12	1.08	1.24	1.36	2.44	2.44	2.36	2.21
9	15	1.05	1.10	1.23	2.32	2.47	2.38	2.23
[b] 10	16.1	.96	.87	.80	.85	.79	.77	.75
A	18.3	1.16	1.31	1.40	2.14	2.48	2.39	2.24
B	25	1.20	1.32	1.42	1.66	2.46	2.41	2.26
C	35	1.26	1.36	1.43	1.48	2.25	2.32	2.23
D	45	1.31	1.38	1.44	1.48	1.93	2.12	2.13
E	55	1.36	1.41	1.45	1.49	1.67	1.88	1.97
F	65	1.39	1.42	1.45	1.48	1.53	1.67	1.79
G	74	1.42	1.43	1.44	1.47	1.48	1.54	1.65
[b] 17	77.03	1.27	1.25	1.24	1.26	1.28	1.29	1.38
18	78.3	1.42	1.43	1.44	1.47	1.51	1.51	1.58
19	80	1.41	1.41	1.42	1.45	1.54	1.49	1.55
20	85	1.39	1.39	1.40	1.41	1.37	1.41	1.51
21	90	1.43	1.42	1.43	1.42	1.33	1.39	1.50
22	95	1.45	1.43	1.42	1.40	1.29	1.37	1.47
23	97.5	1.44	1.42	1.39	1.37	1.28	1.35	1.46
24	100	1.37	1.36	1.34	1.31	1.25	1.32	1.41
11	1.3	.91	.53	.28	.14	.07	.06	.06
12	2.6	.90	.62	.40	.25	.16	.14	.15
13	5	.94	.72	.53	.39	.29	.27	.28
14	7.5	.96	.78	.61	.47	.37	.37	.36
15	11.4	.96	.82	.67	.56	.46	.45	.45
H	18.1	.99	.87	.74	.65	.55	.55	.55
I	25	1.00	.90	.80	.72	.64	.64	.64
J	35	1.00	.92	.83	.77	.70	.70	.73
K	45	.98	.91	.85	.79	.73	.74	.76
L	55	.93	.88	.83	.78	.74	.75	.77
M	65	.83	.80	.77	.73	.70	.72	.73
N	75	.68	.64	.62	.59	.55	.57	.60
25	85	.67	.65	.63	.60	.59	.61	.64
26	90	.83	.82	.79	.78	.75	.78	.82
27	95	.99	.99	.96	.94	.90	.94	1.00
28	97.5	1.09	1.09	1.07	1.04	1.00	1.04	1.11
[b] 16	15	.95	.85	.73	.65	.57	.56	.56
[b] 29	80.3	1.26	1.23	1.21	1.23	1.24	1.25	1.33

[a] Angle of attack for maximum lift.
[b] Internal pressures.

TABLE IV.—PRESSURE COEFFICIENTS—Continued

(i) $\delta_N=0°$, $\delta_F=42°$

Orifice	x/c	Pressure coefficients for section angle of attack—					
		−4.1°	−2.0°	0°	2.0°	[a] 4.1°	6.1°
1	0	0.34	1.18	2.07	2.38	2.30	2.05
2	1	1.94	2.19	2.38	2.45	2.32	2.07
3	2	1.53	2.21	2.40	2.45	2.33	2.08
4	3	1.26	2.23	2.40	2.46	2.34	2.08
5	5	1.20	2.23	2.42	2.47	2.34	2.09
6	7.5	1.21	2.22	2.46	2.49	2.36	2.10
7	10	1.25	1.53	2.48	2.52	2.37	2.11
8	12	1.28	1.36	2.43	2.54	2.39	2.12
9	15	1.14	1.25	2.27	2.56	2.41	2.14
[b] 10	16.1	.83	.75	.76	.70	.67	.65
A	18.3	1.34	1.40	2.02	2.57	2.43	2.14
B	25	1.37	1.43	1.61	2.52	2.46	2.16
C	35	1.42	1.48	1.51	2.22	2.44	2.19
D	45	1.46	1.50	1.54	1.85	2.31	2.18
E	55	1.50	1.52	1.56	1.64	2.11	2.12
F	65	1.54	1.54	1.56	1.55	1.89	2.00
G	74	1.60	1.56	1.56	1.54	1.74	1.92
[b] 17	77.03	1.58	1.51	1.49	1.50	1.65	1.91
18	78.3	1.89	1.76	1.69	1.69	1.66	1.81
19	80	1.59	1.51	1.47	1.49	1.60	1.81
20	85	1.59	1.51	1.48	1.49	1.58	1.78
21	90	1.61	1.53	1.50	1.50	1.57	1.77
22	95	1.64	1.53	1.51	1.51	1.56	1.74
23	97.5	1.62	1.53	1.50	1.50	1.54	1.71
24	100	1.56	1.50	1.47	1.47	1.50	1.67
11	1.3	.46	.27	.14	.08	.03	.04
12	2.6	.57	.38	.24	.15	.11	.12
13	5	.68	.51	.36	.27	.22	.24
14	7.5	.71	.57	.45	.35	.31	.31
15	11.4	.74	.64	.53	.43	.39	.40
H	18.1	.79	.69	.60	.52	.48	.51
I	25	.82	.73	.66	.58	.54	.57
J	35	.80	.75	.68	.63	.61	.64
K	45	.79	.73	.68	.63	.62	.66
L	55	.71	.68	.63	.60	.59	.64
M	65	.58	.55	.52	.53	.51	.54
N	75	.42	.39	.34	.33	.33	.35
25	85	.34	.34	.31	.30	.31	.33
26	90	.56	.54	.54	.53	.53	.56
27	95	.84	.81	.79	.78	.79	.87
28	97.5	1.02	.93	.91	.91	.95	1.06
[b] 16	15	.79	.69	.59	.53	.49	.50
[b] 29	80.3	1.33	1.27	1.25	1.24	1.38	1.56

[a] Angle of attack for maximum lift.
[b] Internal pressures.

TABLE IV.—PRESSURE COEFFICIENTS—Continued

(j) $\delta_N=0°$, $\delta_F=60°$

Orifice	x/c	Pressure coefficients for section angle of attack—							
		−6.1°	−4.1°	−2.0°	0°	1.0°	2.0°	[a] 3.0°	4.1°
1	0	0.29	1.36	2.23	2.45	2.53	2.50	2.44	2.30
2	1	1.87	2.26	2.46	2.52	2.55	2.53	2.47	2.30
3	2	1.36	2.29	2.48	2.52	2.56	2.53	2.47	2.30
4	3	1.20	2.30	2.49	2.53	2.57	2.54	2.48	2.30
5	5	1.19	2.31	2.51	2.55	2.58	2.55	2.49	2.31
6	7.5	1.21	2.08	2.54	2.56	2.60	2.56	2.49	2.32
7	10	1.25	1.67	2.56	2.60	2.62	2.59	2.52	2.34
8	12	1.28	1.44	2.49	2.62	2.64	2.61	2.54	2.35
9	15	1.13	1.31	2.31	2.64	2.67	2.63	2.57	2.37
[b] 10	16.1	.78	.70	.73	.69	.67	.63	.62	.66
A	18.3	1.34	1.47	2.00	2.63	2.68	2.64	2.57	2.38
B	25	1.39	1.51	1.62	2.47	2.67	2.67	2.61	2.41
C	35	1.45	1.56	1.58	1.99	2.46	2.61	2.61	2.42
D	45	1.51	1.61	1.62	1.69	2.09	2.40	2.51	2.37
E	55	1.58	1.66	1.66	1.61	1.80	2.10	2.31	2.26
F	65	1.64	1.69	1.68	1.61	1.66	1.85	2.06	2.10
G	74	1.66	1.68	1.65	1.59	1.60	1.70	1.86	1.96
17	77.03	2.19	2.12	1.97	2.07	2.08	2.03	2.07	2.04
18	78.3	1.92	1.87	1.81	1.75	1.72	1.70	1.80	1.89
19	80	2.00	1.93	1.82	1.65	1.61	1.64	1.75	1.87
20	85	1.86	1.83	1.72	1.58	1.58	1.61	1.72	1.81
21	90	1.86	1.83	1.73	1.59	1.59	1.62	1.71	1.79
22	95	1.85	1.81	1.71	1.58	1.59	1.61	1.69	1.76
23	97.5	1.82	1.78	1.69	1.57	1.58	1.60	1.66	1.74
24	100	1.79	1.75	1.65	1.55	1.55	1.57	1.64	1.71
11	1.3	.47	.24	.13	.07	.03	.02	.02	.02
12	2.6	.56	.35	.23	.14	.11	.09	.08	.09
13	5	.65	.47	.35	.26	.22	.19	.18	.19
14	7.5	.69	.53	.42	.34	.30	.26	.25	.26
15	11.4	.71	.57	.49	.41	.37	.35	.33	.35
H	18.1	.74	.64	.56	.48	.46	.42	.42	.44
I	25	.75	.67	.59	.53	.51	.48	.48	.49
J	35	.72	.66	.60	.55	.53	.51	.51	.53
K	45	.66	.63	.57	.53	.52	.50	.50	.52
L	55	.55	.51	.49	.49	.48	.47	.46	.47
M	65	.37	.35	.35	.34	.34	.33	.33	.34
N	75	.34	.31	.27	.21	.20	.19	.19	.20
25	85	.31	.28	.18	.11	.12	.14	.13	.15
26	90	.32	.30	.28	.28	.29	.29	.29	.30
27	95	.61	.59	.58	.56	.56	.56	.57	.60
28	97.5	.86	.84	.80	.77	.77	.78	.79	.83
[b] 16	15	.75	.64	.57	.50	.47	.44	.43	.45
[b] 29	80.3	.59	.56	.50	.49	.47	.46	.47	.51

[a] Angle of attack for maximum lift.
[b] Internal pressures.

TABLE IV.—PRESSURE COEFFICIENTS—Continued

(k) $\delta_N=5°$, $\delta_F=5°$

Orifice	x/c	Pressure coefficients for section angle of attack—								
		−4.1°	−2.0°	0°	2.0°	4.1°	6.1°	8.1°	[a] 10.2°	12.2°
1	0	1.77	1.78	1.10	0.54	0.73	1.76	1.83	1.53	1.23
2	1	.20	.36	.71	1.77	2.35	2.58	2.27	1.93	1.72
3	2	.34	.51	.80	1.23	2.37	2.59	2.29	1.94	1.72
4	3	.42	.58	.85	1.19	2.39	2.60	2.29	1.94	1.73
5	5	.55	.71	.94	1.23	2.36	2.62	2.31	1.96	1.74
6	7.5	.69	.82	1.03	1.28	1.80	2.64	2.34	1.97	1.75
7	10	.77	.91	1.10	1.32	1.53	2.64	2.37	1.99	1.76
8	12	.88	1.00	1.17	1.39	1.47	2.50	2.40	2.01	1.77
9	15	1.10	1.09	1.20	1.39	1.44	2.23	2.40	2.03	1.79
[b] 10	16.1	1.73	.97	.86	.78	.70	.70	.68	.64	.62
A	18.3	.99	1.10	1.26	1.46	1.57	1.87	2.36	2.03	1.80
B	25	1.02	1.12	1.25	1.39	1.50	1.59	2.26	2.03	1.82
C	35	1.08	1.16	1.26	1.36	1.45	1.50	1.98	1.99	1.82
D	45	1.13	1.18	1.27	1.35	1.42	1.45	1.69	1.90	1.82
E	55	1.17	1.21	1.27	1.34	1.39	1.41	1.49	1.80	1.80
F	65	1.19	1.22	1.27	1.31	1.35	1.36	1.37	1.67	1.76
G	74	1.22	1.23	1.27	1.30	1.32	1.32	1.30	1.58	1.76
[b] 17	77.03	1.21	1.18	1.20	1.20	1.21	1.20	1.18	1.42	1.59
[b] 18	78.3	1.20	1.18	1.20	1.19	1.20	1.18	1.18	1.40	1.58
19	80	1.39	1.38	1.39	1.28	1.40	1.36	1.28	1.49	1.66
20	85	1.17	1.18	1.20	1.20	1.21	1.21	1.22	1.48	1.69
21	90	1.10	1.09	1.09	1.09	1.11	1.12	1.17	1.44	1.67
22	95	1.02	1.00	.99	1.00	1.02	1.04	1.14	1.40	1.62
23	97.5	.96	.94	.94	.96	.97	1.00	1.12	1.38	1.58
24	100	.88	.89	.90	.92	.93	.96	1.10	1.34	1.53
11	1.3	1.78	1.80	.94	.53	.28	.14	.10	.11	.11
12	2.6	1.79	1.82	.93	.61	.39	.25	.20	.20	.21
13	5	1.81	1.70	.94	.70	.51	.38	.33	.33	.33
14	7.5	1.82	1.36	.94	.74	.57	.46	.40	.40	.41
15	11.4	1.83	1.05	.90	.75	.62	.51	.46	.47	.48
H	18.1	1.71	1.01	.90	.77	.67	.58	.54	.55	.56
I	25	1.36	1.09	1.00	.88	.78	.70	.66	.68	.69
J	35	1.15	1.13	1.05	.95	.87	.80	.77	.79	.82
K	45	1.13	1.14	1.07	.99	.92	.86	.84	.88	.91
L	55	1.12	1.12	1.07	1.00	.95	.90	.90	.94	.99
M	65	1.09	1.08	1.05	1.00	.95	.91	.92	.98	1.04
N	75	1.03	1.01	.98	.95	.92	.90	.91	.99	1.07
25	85	.99	.99	.96	.94	.92	.91	.95	1.05	1.15
26	90	.98	.98	.97	.96	.95	.95	1.00	1.12	1.23
27	95	.95	.95	.95	.95	.95	.96	1.03	1.18	1.33
28	97.5	.92	.94	.93	.94	.94	.96	1.05	1.22	1.38
[b] 16	15	1.68	.96	.82	.73	.62	.55	.51	.51	.51
[b] 29	80.3	1.07	1.04	1.04	1.02	1.01	.99	.99	1.12	1.28

[a] Angle of attack for maximum lift.
[b] Internal pressures.

TABLE IV.—PRESSURE COEFFICIENTS—Continued

(l) $\delta_N=5°$, $\delta_F=10°$

Orifice	x/c	Pressure coefficients for section angle of attack—							
		−4.1°	−2.0°	0°	2.0°	4.1°	6.1°	[a] 8.1°	10.2°
1	0	1.64	1.72	0.70	0.37	1.10	1.59	1.84	1.59
2	1	.29	.51	1.00	2.18	2.57	2.54	2.19	1.91
3	2	.44	.64	1.02	2.20	2.59	2.55	2.20	1.91
4	3	.52	.71	1.05	2.12	2.60	2.56	2.20	1.92
5	5	.64	.83	1.10	1.59	2.63	2.58	2.22	1.92
6	7.5	.77	1.00	1.17	1.41	2.66	2.66	2.25	1.94
7	10	.87	1.07	1.23	1.41	2.37	2.66	2.27	1.96
8	12	.96	1.10	1.31	1.48	1.96	2.66	2.29	1.97
9	15	1.15	1.15	1.34	1.46	1.67	2.61	2.31	1.99
[b] 10	16.1	1.17	.89	.82	.73	.67	.70	.66	.63
A	18.3	1.08	1.21	1.40	1.56	1.62	2.43	2.31	2.00
B	25	1.11	1.22	1.35	1.49	1.57	2.08	2.27	2.01
C	35	1.16	1.25	1.35	1.45	1.54	1.67	2.14	1.99
D	45	1.21	1.28	1.36	1.44	1.50	1.52	1.93	1.94
E	55	1.26	1.31	1.36	1.43	1.48	1.47	1.72	1.86
F	65	1.29	1.32	1.36	1.41	1.45	1.42	1.56	1.77
G	74	1.37	1.37	1.38	1.40	1.44	1.39	1.45	1.70
[b] 17	77.03	1.37	1.34	1.31	1.31	1.32	1.27	1.28	1.50
[b] 18	78.3	1.42	1.38	1.34	1.34	1.37	1.32	1.33	1.55
19	80	1.71	1.61	1.55	1.54	1.59	1.47	1.39	1.60
20	85	1.32	1.27	1.24	1.26	1.29	1.27	1.34	1.59
21	90	1.15	1.13	1.16	1.17	1.17	1.19	1.31	1.57
22	95	1.02	1.06	1.11	1.11	1.09	1.12	1.27	1.53
23	97.5	.95	1.03	1.09	1.10	1.06	1.10	1.26	1.50
24	100	.88	1.01	1.07	1.07	1.02	1.07	1.23	1.45
11	1.3	1.70	1.61	.71	.37	.18	.10	.09	.10
12	2.6	1.71	1.11	.74	.47	.29	.20	.18	.19
13	5	1.73	1.02	.79	.58	.42	.33	.30	.31
14	7.5	1.70	1.01	.82	.63	.49	.40	.38	.38
15	11.4	1.47	.95	.80	.66	.54	1.46	.44	.45
H	18.1	1.09	.94	.81	.70	.60	.53	.53	.53
I	25	1.04	1.01	.90	.80	.71	.64	.64	.66
J	35	1.07	1.04	.95	.87	.79	.74	.74	.77
K	45	1.10	1.05	.98	.91	.83	.80	.81	.84
L	55	1.04	1.02	.97	.91	.85	.83	.85	.90
M	65	.98	.98	.94	.89	.84	.83	.85	.91
N	75	.89	.88	.84	.82	.78	.78	.81	.88
25	85	.87	.87	.85	.83	.80	.79	.85	.95
26	90	.90	.92	.92	.90	.87	.88	.95	1.06
27	95	.91	.95	.97	.96	.93	.95	1.04	1.18
28	97.5	.90	.98	1.00	.99	.95	.98	1.10	1.26
[b] 16	15	1.16	.91	.78	.66	.56	.51	.49	.50
[b] 29	80.3	1.25	1.22	1.19	1.18	1.19	1.15	1.16	1.34

[a] Angle of attack for maximum lift.
[b] Internal pressures.

TABLE IV.—PRESSURE COEFFICIENTS—Continued

(m) $\delta_N=5°$, $\delta_F=22°$

Orifice	x/c	Pressure coefficients for section angle of attack—							
		−4.1°	−2.0°	0°	2.0°	4.1°	6.1°	[a] 7.1°	8.1°
1	0	1.09	0.71	0.34	0.73	1.09	1.43	1.90	1.74
2	1	.43	.86	2.06	2.48	2.63	2.40	2.24	2.09
3	2	.57	.92	.83	2.50	2.69	2.40	2.25	2.09
4	3	.64	.96	1.47	2.51	2.70	2.41	2.25	2.10
5	5	.76	1.03	1.26	2.53	2.72	2.42	2.26	2.11
6	7.5	.88	1.11	1.28	2.16	2.76	2.46	2.29	2.13
7	10	.97	1.18	1.38	1.81	2.79	2.49	2.31	2.15
8	12	1.06	1.25	1.44	1.56	2.73	2.51	2.34	2.17
9	15	1.11	1.26	1.42	1.49	2.55	2.53	2.36	2.19
[b] 10	16.1	.89	.84	.72	.66	.69	.64	.63	.62
A	18.3	1.18	1.35	1.53	1.64	2.20	2.53	2.36	2.20
B	25	1.20	1.33	1.46	1.59	1.80	2.49	2.35	2.21
C	35	1.24	1.36	1.44	1.55	1.61	2.31	2.27	2.18
D	45	1.29	1.38	1.45	1.54	1.57	2.03	2.12	2.10
E	55	1.33	1.40	1.44	1.52	1.55	1.78	1.93	1.98
F	65	1.36	1.41	1.44	1.49	1.51	1.60	1.75	1.85
G	74	1.39	1.42	1.43	1.45	1.48	1.50	1.61	1.73
[b] 17	77.03	1.27	1.28	1.24	1.26	1.28	1.28	1.36	1.47
18	78.3	1.39	1.42	1.40	1.43	1.47	1.50	1.56	1.66
19	80	1.38	1.40	1.39	1.40	1.43	1.49	1.53	1.62
20	85	1.37	1.39	1.37	1.38	1.40	1.39	1.48	1.60
21	90	1.40	1.43	1.40	1.42	1.40	1.37	1.47	1.59
22	95	1.42	1.43	1.40	1.42	1.39	1.34	1.44	1.56
23	97.5	1.40	1.42	1.39	1.40	1.37	1.33	1.43	1.54
24	100	1.36	1.37	1.34	1.36	1.31	1.29	1.39	1.49
11	1.3	1.72	.78	.43	.22	.10	.06	.07	.07
12	2.6	1.87	.79	.52	.34	.20	.14	.14	.15
13	5	1.16	.82	.61	.45	.33	.26	.26	.27
14	7.5	.99	.83	.65	.52	.40	.23	.34	.34
15	11.4	.94	.80	.67	.56	.45	.39	.40	.40
H	18.1	.91	.79	.69	.61	.51	.40	.40	.47
I	25	.98	.88	.78	.71	.62	.56	.57	.59
J	35	.99	.91	.83	.77	.69	.64	.66	.68
K	45	.97	.91	.84	.79	.73	.69	.71	.73
L	55	.92	.87	.82	.79	.73	.70	.73	.75
M	65	.83	.80	.76	.74	.71	.67	.69	.72
N	75	.68	.64	.62	.60	.55	.53	.56	.60
25	85	.69	.63	.63	.62	.59	.58	.61	.64
26	90	.84	.82	.80	.79	.76	.75	.79	.84
27	95	.99	.99	.97	.96	.93	.91	.97	1.04
28	97.5	1.09	1.09	1.07	1.07	1.02	1.02	1.09	1.16
[b] 16	15	.86	.78	.65	.56	.50	.45	.45	.46
[b] 29	80.3	1.24	1.24	1.22	1.22	1.22	1.24	1.31	1.41

[a] Angle of attack for maximum lift.
[b] Internal pressures.

TABLE IV.—PRESSURE COEFFICIENTS—Continued

(n) $\delta_N=9°$, $\delta_F=10°$

Orifice	x/c	Pressure coefficients for section angle of attack—								
		−4.1°	−2.0°	0°	2.0°	4.1°	6.1°	8.1°	[a] 9.1°	12.2°
1	0	0.94	1.22	0.93	0.47	0.62	1.01	1.85	1.08	1.07
2	1	.20	.39	.73	1.76	2.52	2.94	2.67	2.41	1.87
3	2	.35	.53	.84	1.23	2.54	2.95	2.68	2.41	1.87
4	3	.44	.61	.89	1.22	2.56	2.96	2.69	2.42	1.87
5	5	.57	.75	1.00	1.28	2.49	3.00	2.70	2.43	1.88
6	7.5	.73	.94	1.13	1.39	1.70	3.03	2.73	2.45	1.88
7	10	.84	1.07	1.23	1.45	1.61	2.90	2.75	2.47	1.90
8	12	.99	1.15	1.37	1.50	1.69	2.50	2.75	2.49	1.91
9	15	1.32	1.51	1.76	1.98	2.03	2.08	2.73	2.50	1.93
[b] 10	16.1	1.64	.82	.60	.59	.48	.40	.35	.36	.38
A	18.3	1.12	1.23	1.40	1.59	1.75	1.83	2.58	2.43	1.92
B	25	1.11	1.23	1.37	1.50	1.64	1.71	2.34	2.34	1.93
C	35	1.16	1.25	1.36	1.45	1.57	1.64	1.93	2.12	1.92
D	45	1.21	1.28	1.37	1.43	1.53	1.58	1.66	1.88	1.90
E	55	1.26	1.31	1.38	1.43	1.50	1.54	1.52	1.68	1.86
F	65	1.29	1.33	1.38	1.40	1.47	1.49	1.44	1.53	1.80
G	74	1.36	1.38	1.41	1.40	1.46	1.46	1.39	1.44	1.70
[b] 17	77.03	1.25	1.23	1.23	1.20	1.21	1.19	1.13	1.16	1.44
[b] 18	78.03	1.34	1.32	1.33	1.30	1.32	1.31	1.25	1.29	1.61
19	80	1.74	1.73	1.73	1.64	1.69	1.62	1.43	1.40	1.68
20	85	1.29	1.28	1.28	1.24	1.29	1.29	1.27	1.33	1.70
21	90	1.13	1.12	1.13	1.15	1.16	1.17	1.21	1.29	1.69
22	95	1.02	1.03	1.07	1.11	1.09	1.10	1.17	1.27	1.65
23	97.5	.98	1.00	1.05	1.10	1.06	1.07	1.14	1.25	1.61
24	100	.95	.98	1.02	1.06	1.04	1.04	1.12	1.22	1.55
11	1.3	1.61	1.58	.88	.50	.25	.11	.07	.08	.11
12	2.6	1.61	1.59	.85	.57	.35	.21	.16	.17	.19
13	5	1.63	1.53	.85	.64	.46	.33	.28	.28	.31
14	7.5	1.64	1.30	.83	.66	.51	.39	.34	.34	.37
15	11.4	1.65	.98	.76	.63	.51	.42	.37	.37	.40
H	18.1	1.64	.87	.77	.66	.56	.49	.45	.45	.48
I	25	1.38	.95	.88	.78	.69	.64	.57	.58	.62
J	35	1.07	1.00	.94	.85	.78	.71	.67	.68	.74
K	45	1.03	1.02	.96	.89	.83	.77	.74	.76	.83
L	55	1.01	1.00	.96	.90	.85	.80	.79	.81	.89
M	65	.91	.95	.93	.89	.85	.82	.80	.83	.92
N	75	.91	.87	.84	.81	.78	.75	.76	.79	.90
25	85	.88	.85	.83	.81	.78	.76	.79	.82	.90
26	90	.92	.90	.89	.89	.87	.85	.88	.92	1.11
27	95	.93	.93	.94	.95	.92	.91	.96	1.02	1.25
28	97.5	.94	.94	.96	.98	.95	.95	1.01	1.08	1.34
[b] 16	15	1.64	.81	.60	.58	.47	.39	.35	.36	.38
[b] 29	80.3	1.20	1.17	1.17	1.14	1.15	1.12	1.07	1.10	1.30

[a] Angle of attack for maximum lift.
[b] Internal pressures.

TABLE IV.—PRESSURE COEFFICIENTS—Continued

(o) $\delta_N=9°$, $\delta_F=22°$

Orifice	x/c	Pressure coefficients for section angle of attack—						
		−4.1°	−2.0°	0°	2.0°	4.1°	6.1°	*8.1°
1	0	1.44	1.42	0.48	0.55	1.18	2.23	2.29
2	1	.33	.60	1.11	2.36	2.84	2.92	2.44
3	2	.47	.73	1.15	2.39	2.85	2.94	2.45
4	3	.55	.80	1.16	2.36	2.87	2.94	2.46
5	5	.69	.92	1.24	1.92	2.91	2.96	2.47
6	7.5	.86	1.08	1.31	1.55	2.96	3.01	2.50
7	10	.96	1.17	1.42	1.57	2.46	3.02	2.51
8	12	1.11	1.32	1.56	1.72	2.00	3.00	2.52
9	15	1.48	1.71	1.97	2.10	1.92	2.90	2.54
b10	16.1	1.19	.62	1.16	.49	.41	.34	.33
A	18.3	1.24	1.38	1.59	1.75	1.81	2.63	2.51
B	25	1.23	1.36	1.51	1.64	1.72	2.23	2.44
C	35	1.26	1.37	1.48	1.58	1.66	1.81	2.29
D	45	1.30	1.39	1.47	1.55	1.61	1.66	2.08
E	55	1.35	1.42	1.47	1.54	1.57	1.60	1.88
F	65	1.37	1.42	1.47	1.50	1.52	1.55	1.72
G	74	1.40	1.43	1.46	1.47	1.47	1.51	1.61
b17	77.03	1.25	1.26	1.26	1.24	1.23	1.28	1.34
18	78.3	1.41	1.43	1.43	1.44	1.44	1.52	1.57
19	80	1.41	1.42	1.41	1.41	1.40	1.50	1.55
20	85	1.39	1.40	1.39	1.39	1.37	1.40	1.48
21	90	1.42	1.44	1.42	1.41	1.39	1.38	1.46
22	95	1.43	1.44	1.43	1.41	1.39	1.36	1.44
23	97.5	1.41	1.42	1.42	1.40	1.38	1.34	1.42
24	100	1.35	1.38	1.37	1.36	1.33	1.29	1.39
11	1.3	1.47	.97	.58	.31	.15	.06	.06
12	2.6	1.47	.92	.63	.41	.25	.14	.14
13	5	1.49	.89	.68	.50	.36	.25	.24
14	7.5	1.48	.85	.68	.54	.41	.33	.30
15	11.4	1.38	.78	.65	.53	.43	.36	.34
H	18.1	1.05	.77	.66	.58	.49	.42	.41
I	25	.91	.87	.77	.69	.61	.54	.53
J	35	.95	.90	.82	.76	.69	.63	.62
K	45	.95	.90	.84	.79	.73	.68	.68
L	55	.92	.87	.83	.78	.73	.70	.70
M	65	.85	.80	.77	.74	.71	.67	.68
N	75	.73	.65	.62	.60	.57	.53	.58
25	85	.73	.65	.64	.62	.60	.57	.60
26	90	.85	.82	.80	.79	.77	.74	.78
27	95	1.00	.98	.98	.96	.94	.91	.96
28	97.5	1.09	1.09	1.09	1.08	1.05	1.02	1.08
b16	15	1.18	.62	.60	.50	.40	.34	.33
b29	80.3	1.24	1.23	1.23	1.20	1.18	1.23	1.29

* Angle of attack for maximum lift.
b Internal pressures.

TABLE IV.—PRESSURE COEFFICIENTS—Continued

(p) $\delta_N=9°$, $\delta_F=42°$

Orifice	x/c	Pressure coefficients for section angle of attack—						
		−4.1°	−2.0°	0°	2.0°	4.1°	*6.1°	8.1°
1	0	1.00	0.34	0.52	1.47	2.41	2.57	2.25
2	1	.63	1.21	2.38	2.84	3.08	2.63	2.26
3	2	.77	1.17	2.41	2.86	3.09	2.63	2.27
4	3	.83	1.18	2.39	2.88	3.10	2.64	2.27
5	5	.95	1.26	1.99	2.92	3.12	2.65	2.28
6	7.5	1.08	1.33	1.63	2.94	3.17	2.66	2.28
7	10	1.21	1.45	1.59	2.41	3.18	2.68	2.30
8	12	1.36	1.60	1.75	1.96	3.10	2.71	2.32
9	15	1.77	2.02	2.14	1.95	2.86	2.74	2.34
b10	16.1	.58	.56	.45	.37	.32	.28	.29
A	18.3	1.44	1.57	1.79	1.84	2.45	2.70	2.33
B	25	1.41	1.60	1.69	1.77	2.01	2.66	2.34
C	35	1.45	1.55	1.65	1.70	1.77	2.49	2.32
D	45	1.47	1.56	1.63	1.67	1.71	2.26	2.24
E	55	1.53	1.58	1.62	1.65	1.67	2.00	2.14
F	65	1.56	1.60	1.61	1.62	1.63	1.80	2.01
G	74	1.61	1.64	1.62	1.59	1.60	1.68	1.90
b17	77.03	1.61	1.61	1.55	1.50	1.51	1.62	1.87
18	78.3	1.92	1.90	1.78	1.70	1.68	1.68	1.81
19	80	1.64	1.62	1.54	1.47	1.47	1.59	1.78
20	85	1.64	1.62	1.55	1.48	1.48	1.56	1.75
21	90	1.65	1.64	1.56	1.49	1.49	1.56	1.75
22	95	1.66	1.65	1.57	1.50	1.50	1.55	1.73
23	97.5	1.65	1.64	1.56	1.49	1.49	1.54	1.70
24	100	1.61	1.60	1.54	1.47	1.47	1.51	1.67
11	1.3	.89	.52	.28	.14	.05	.03	.04
12	2.6	.86	.57	.38	.23	.14	.11	.12
13	5	.83	.62	.47	.33	.24	.21	.22
14	7.5	.80	.63	.50	.38	.29	.26	.27
15	11.4	.72	.59	.50	.40	.33	.31	.31
H	18.1	.71	.60	.53	.45	.38	.36	.37
I	25	.79	.70	.62	.55	.49	.46	.48
J	35	.80	.73	.67	.60	.56	.53	.55
K	45	.78	.72	.68	.62	.58	.56	.59
L	55	.70	.67	.63	.59	.56	.55	.58
M	65	.57	.55	.53	.49	.48	.48	.52
N	75	.44	.37	.35	.32	.31	.29	.33
25	85	.38	.33	.32	.29	.29	.29	.32
26	90	.56	.55	.54	.52	.50	.50	.55
27	95	.84	.82	.80	.77	.76	.77	.83
28	97.5	1.03	1.01	.99	.94	.93	.94	1.04
b16	15	.57	.56	.45	.37	.32	.28	.29
b29	80.3	1.36	1.35	1.29	1.25	1.25	1.31	1.51

* Angle of attack for maximum lift.
b Internal pressures.

TABLE IV.—PRESSURE COEFFICIENTS—Continued

(q) $\delta_N=21°$, $\delta_F=42°$

Orifice	x/c	Pressure coefficients for section angle of attack—								
		−4.1°	−2.0°	0°	2.0°	4.1°	6.1°	8.1°	*10.2°	12.2°
1	0	1.19	0.94	1.02	0.28	0.88	2.09	3.24	3.87	2.84
2	1	.17	.43	.72	1.78	2.70	3.32	3.94	4.21	3.17
3	2	.32	.58	.85	1.28	2.73	3.35	3.97	4.22	3.18
4	3	.40	.67	.93	1.29	2.73	3.37	3.98	4.24	3.19
5	5	.57	.84	1.09	1.42	2.20	3.42	4.03	4.27	3.22
6	7.5	.80	1.05	1.20	1.56	1.93	2.42	4.10	4.32	3.27
7	10	.98	1.25	1.49	1.79	1.96	2.21	3.60	4.35	3.28
8	12	1.25	1.52	1.75	2.09	2.29	2.26	2.77	3.97	3.14
9	15	1.95	2.23	2.35	2.97	3.18	3.08	2.78	3.26	2.95
10	16.1	2.03	2.34	2.45	2.67	2.80	2.74	2.62	2.56	2.37
A	18.3	1.56	1.97	2.58	2.41	2.59	2.67	2.70	2.76	2.69
B	25	1.44	1.63	1.77	1.97	2.13	2.23	2.32	2.40	2.52
C	35	1.43	1.59	1.71	1.82	1.93	2.00	2.06	2.10	2.33
D	45	1.45	1.58	1.67	1.76	1.83	1.87	1.93	1.93	2.16
E	55	1.49	1.60	1.67	1.73	1.77	1.79	1.81	1.80	2.03
F	65	1.51	1.62	1.66	1.70	1.72	1.71	1.70	1.68	1.91
G	74	1.56	1.66	1.68	1.70	1.68	1.64	1.61	1.59	1.83
b17	77.03	1.55	1.65	1.64	1.57	1.60	1.54	1.50	1.51	1.78
18	78.3	1.82	1.90	1.90	1.87	1.80	1.68	1.62	1.60	1.80
19	80	1.58	1.65	1.62	1.61	1.57	1.49	1.46	1.46	1.73
20	85	1.59	1.65	1.62	1.61	1.58	1.49	1.46	1.45	1.70
21	90	1.60	1.67	1.65	1.63	1.59	1.50	1.47	1.47	1.69
22	95	1.59	1.67	1.66	1.64	1.60	1.51	1.48	1.47	1.67
23	97.5	1.58	1.66	1.64	1.62	1.59	1.50	1.47	1.47	1.66
24	100	1.57	1.62	1.60	1.60	1.55	1.49	1.46	1.45	1.63
11	1.3	1.19	.94	.73	.39	.20	.09	.03	.01	.02
12	2.6	1.19	.95	.68	.43	.27	.17	.09	.05	.07
13	5	1.20	.95	.63	.45	.33	.24	.17	.12	.14
14	7.5	1.20	.95	.57	.44	.34	.26	.20	.16	.18
15	11.4	1.21	.94	.45	.39	.30	.24	.19	.17	.18
H	18.1	1.23	.85	.40	.34	.28	.24	.20	.18	.19
I	25	1.26	.65	.56	.49	.43	.38	.33	.29	.31
J	35	1.16	.65	.64	.57	.51	.46	.42	.39	.41
K	45	.96	.68	.66	.60	.55	.51	.47	.44	.47
L	55	.82	.65	.62	.57	.54	.51	.47	.45	.48
M	65	.74	.56	.53	.49	.47	.44	.42	.40	.43
N	75	.68	.45	.37	.34	.32	.29	.28	.27	.29
25	85	.63	.43	.33	.30	.29	.27	.26	.26	.28
26	90	.69	.60	.53	.51	.50	.48	.47	.46	.50
27	95	.85	.83	.80	.78	.77	.73	.72	.71	.78
28	97.5	1.00	1.02	1.00	.98	.95	.92	.89	.88	.98
b16	15	1.23	.90	.37	.28	.31	.28	.22	.18	.20
b29	80.3	1.34	1.37	1.37	1.35	1.33	1.27	1.24	1.24	1.45

* Angle of attack for maximum lift.
b Internal pressures.

TABLE IV.—PRESSURE COEFFICIENTS—Concluded

(r) $\delta_N=27°$, $\delta_F=60°$

Orifice	x/c	Pressure coefficients for section angle of attack—								
		−4.1°	−2.0°	0°	2.0°	4.1°	6.1°	8.1°	*10.2°	12.2°
1	0	0.42	0.75	0.29	0.18	1.30	2.73	4.07	4.79	4.55
2	1	.21	.46	.82	2.13	2.87	3.56	4.26	4.80	4.32
3	2	.36	.62	.95	1.51	2.91	3.59	4.28	4.82	4.33
4	3	.45	.72	1.02	1.35	2.93	3.61	4.31	4.83	4.35
5	5	.64	.90	1.20	1.50	2.49	3.67	4.36	4.87	4.37
6	7.5	.94	1.18	1.48	1.80	2.13	3.00	4.36	4.92	4.40
7	10	1.13	1.42	1.71	2.02	2.18	2.40	3.62	4.73	4.41
8	12	1.48	1.81	2.13	2.47	2.69	2.68	2.91	3.82	3.97
9	15	2.69	3.21	3.68	4.20	4.44	4.33	3.88	3.49	3.33
10	16.1	2.99	3.54	4.16	4.68	4.88	4.70	4.26	3.72	3.21
A	18.3	1.78	2.05	2.30	2.57	2.79	2.93	3.02	3.06	2.86
B	25	1.63	1.83	2.02	2.20	2.35	2.46	2.57	2.63	2.54
C	35	1.59	1.74	1.88	2.00	2.11	2.19	2.26	2.30	2.25
D	45	1.61	1.72	1.83	1.93	1.99	2.05	2.08	2.10	2.05
E	55	1.64	1.74	1.82	1.88	1.92	1.94	1.96	1.94	1.91
F	65	1.71	1.74	1.80	1.87	1.86	1.85	1.84	1.81	1.80
G	74	1.84	1.69	1.76	1.90	1.83	1.70	1.69	1.67	1.71
17	77.03	2.29	2.16	2.14	2.13	2.06	2.02	2.05	2.03	1.99
18	78.3	1.88	1.91	1.89	1.88	1.85	1.80	1.78	1.67	1.68
19	80	1.79	1.95	1.94	1.92	1.87	1.80	1.72	1.61	1.66
20	85	1.81	1.86	1.85	1.83	1.78	1.72	1.65	1.60	1.65
21	90	1.81	1.85	1.83	1.82	1.78	1.70	1.66	1.60	1.64
22	95	1.82	1.83	1.82	1.80	1.77	1.70	1.65	1.60	1.64
23	97.5	1.82	1.81	1.81	1.78	1.76	1.69	1.64	1.59	1.63
24	100	1.82	1.75	1.76	1.76	1.72	1.66	1.61	1.58	1.62
11	1.3	.96	.75	.58	.30	.15	.04	.01	0	0
12	2.6	.96	.75	.54	.34	.21	.12	.06	.02	.03
13	5	.97	.75	.50	.36	.25	.18	.12	.08	.09
14	7.5	.98	.74	.45	.34	.25	.19	.14	.11	.11
15	11.4	.98	.73	.31	.30	.23	.17	.13	.11	.11
H	18.1	1.00	.67	.29	.24	.20	.16	.13	.12	.12
I	25	1.02	.51	.44	.37	.33	.28	.24	.22	.22
J	35	.91	.51	.50	.45	.40	.35	.32	.30	.30
K	45	.75	.53	.50	.45	.42	.37	.35	.33	.34
L	55	.63	.48	.44	.41	.38	.35	.33	.32	.33
M	65	.58	.40	.32	.29	.29	.26	.25	.25	.25
N	75	.52	.32	.26	.23	.22	.19	.18	.17	.18
25	85	.47	.28	.22	.20	.18	.15	.14	.14	.14
26	90	.49	.38	.29	.26	.25	.24	.23	.23	.24
27	95	.65	.62	.57	.55	.53	.51	.50	.48	.51
28	97.5	.84	.84	.81	.79	.77	.73	.71	.69	.72
b16	15	.98	.67	.18	.15	.19	.15	.12	.10	.10
b29	80.3	.68	.49	.49	.46	.46	.44	.42	.41	.42

* Angle of attack for maximum lift
b Internal pressures.

TABLE V.— $P_{bs}/c_{l_{bs}}$ DISTRIBUTION[1]

(a) Plain flap at δ=5°, 10°, and 15°

E →	0.05	0.10	0.15	0.20	0.25	0.30	0.35	0.40	0.45	0.50	0.55	0.60	0.65	0.70
$\frac{x/c}{1-E}$ (ahead of hinge) ↑	0	0	0	0	0	0	0	0	0	0	0	0	0	0
	.05	.15	.15	.16	.16	.17	.17	.18	.19	.20	.21	.22	.23	.25	.27
	.10	.22	.23	.23	.24	.25	.25	.26	.27	.29	.30	.32	.34	.36	.39
	.20	.33	.34	.34	.35	.36	.38	.39	.40	.42	.44	.46	.49	.52	.56
	.30	.43	.44	.45	.46	.47	.49	.50	.52	.54	.57	.60	.63	.67	.72
	.40	.54	.55	.56	.57	.58	.60	.62	.64	.67	.70	.73	.77	.82	.88
	.50	.66	.66	.67	.69	.71	.73	.75	.77	.80	.84	.88	.92	.98	1.05
	.60	.79	.80	.82	.83	.85	.88	.90	.93	.96	1.00	1.05	1.10	1.17	1.25
	.70	.97	.98	1.00	1.01	1.03	1.05	1.08	1.11	1.15	1.19	1.24	1.30	1.39	1.48
	.80	1.23	1.24	1.26	1.27	1.29	1.31	1.34	1.38	1.42	1.46	1.52	1.59	1.67	1.78
	.90	1.73	1.74	1.75	1.76	1.77	1.79	1.81	1.84	1.88	1.92	1.98	2.06	2.16	2.29
	1.00	8.74	6.04	4.89	4.40	4.01	3.71	3.50	3.35	3.23	3.15	3.11	3.06	3.04	3.02
$\frac{1-\frac{x}{c}}{E}$ (back of hinge) ↓	.90	6.45	4.48	3.78	3.32	2.99	2.77	2.60	2.48	2.39	2.32	2.26	2.22	2.19	2.16
	.80	4.96	3.51	2.92	2.57	2.31	2.12	2.00	1.90	1.81	1.74	1.69	1.64	1.60	1.57
	.70	3.85	2.72	2.23	1.97	1.77	1.64	1.53	1.44	1.37	1.32	1.27	1.22	1.19	1.16
	.60	3.09	2.18	1.78	1.57	1.41	1.30	1.21	1.14	1.08	1.04	1.00	.96	.93	.91
	.50	2.46	1.72	1.42	1.24	1.11	1.02	.95	.89	.85	.81	.77	.75	.72	.70
	.40	1.90	1.34	1.10	.96	.86	.78	.73	.69	.65	.62	.59	.57	.55	.53
	.30	1.40	.99	.81	.70	.63	.57	.53	.50	.47	.45	.43	.42	.40	.39
	.20	.92	.65	.53	.46	.41	.38	.35	.33	.31	.29	.28	.27	.26	.25
	.10	.48	.34	.27	.24	.21	.20	.18	.17	.16	.15	.15	.14	.13	.13
	.05	.32	.19	.16	.14	.12	.11	.10	.10	.09	.08	.08	.08	.07	.07
	0	0	0	0	0	0	0	0	0	0	0	0	0	0	0

(b) Plain flap at δ=20°

E →	0.05	0.10	0.15	0.20	0.25	0.30	0.35	0.40	0.45	0.50	0.55	0.60
$\frac{x/c}{1-E}$ (ahead of hinge) ↑	0	0	0	0	0	0	0	0	0	0	0	0
	.15	.15	.16	.16	.17	.17	.18	.19	.20	.21	.22	.23
	.22	.23	.23	.24	.25	.26	.26	.27	.29	.30	.32	.34
	.33	.34	.34	.35	.36	.38	.39	.40	.42	.44	.46	.49
	.43	.44	.45	.46	.47	.49	.50	.52	.54	.57	.60	.63
	.54	.55	.56	.57	.58	.60	.62	.64	.67	.70	.73	.77
	.66	.66	.67	.69	.71	.73	.75	.77	.80	.84	.88	.92
	.79	.80	.82	.83	.85	.88	.90	.93	.96	1.00	1.05	1.10
	.97	.98	1.00	1.01	1.03	1.05	1.08	1.11	1.15	1.19	1.24	1.30
	1.23	1.24	1.26	1.27	1.29	1.31	1.34	1.38	1.42	1.46	1.52	1.59
	1.73	1.74	1.75	1.76	1.77	1.79	1.81	1.84	1.88	1.92	1.98	2.06
	5.83	4.05	3.38	3.02	2.83	2.70	2.63	2.58	2.56	2.56	2.58	2.62
$\frac{1-\frac{x}{c}}{E}$ (back of hinge) ↓	5.08	3.53	2.98	2.61	2.36	2.18	2.05	1.96	1.88	1.83	1.78	1.75
	4.23	2.99	2.50	2.19	1.97	1.81	1.70	1.62	1.55	1.49	1.44	1.40
	3.71	2.63	2.16	1.90	1.71	1.58	1.48	1.39	1.32	1.27	1.22	1.18
	3.33	2.35	1.92	1.69	1.52	1.40	1.30	1.22	1.17	1.12	1.08	1.04
	2.98	2.09	1.73	1.50	1.35	1.24	1.15	1.08	1.03	.98	.94	.91
	2.65	1.87	1.54	1.34	1.19	1.09	1.02	.96	.91	.86	.83	.80
	2.32	1.63	1.34	1.16	1.04	.95	.88	.82	.78	.75	.72	.69
	1.93	1.35	1.11	.96	.86	.79	.73	.68	.65	.62	.59	.56
	1.39	.98	.79	.69	.62	.57	.53	.50	.47	.45	.43	.41
	1.16	.70	.58	.50	.45	.40	.38	.35	.33	.31	.30	.28
	0	0	0	0	0	0	0	0	0	0	0	0

(c) Plain flap at δ=30°

E →	0.05	0.10	0.15	0.20	0.25	0.30	0.35	0.40	0.45	0.50
$\frac{x/c}{1-E}$ (ahead of hinge) ↑	0	0	0	0	0	0	0	0	0	0
	.05	.15	.15	.16	.16	.17	.17	.18	.19	.20	.21
	.10	.22	.23	.23	.24	.25	.25	.26	.27	.29	.30
	.20	.33	.34	.34	.35	.36	.38	.39	.40	.42	.44
	.30	.43	.44	.45	.46	.47	.49	.50	.52	.54	.57
	.40	.54	.55	.56	.57	.58	.60	.62	.64	.67	.70
	.50	.66	.66	.67	.69	.71	.73	.75	.77	.80	.84
	.60	.79	.80	.82	.83	.85	.88	.90	.93	.96	1.00
	.70	.97	.98	1.00	1.01	1.03	1.05	1.08	1.11	1.15	1.19
	.80	1.23	1.24	1.26	1.27	1.29	1.31	1.34	1.38	1.42	1.46
	.90	1.67	1.68	1.69	1.70	1.71	1.73	1.73	1.74	1.77	1.80
	1.00	4.50	3.12	2.66	2.36	2.22	2.13	2.08	2.05	2.01	1.99
$\frac{1-\frac{x}{c}}{E}$ (back of hinge) ↓	.90	4.61	3.20	2.70	2.37	2.15	2.01	1.90	1.83	1.77	1.73
	.80	4.34	3.07	2.56	2.24	2.02	1.86	1.75	1.66	1.59	1.52
	.70	4.08	2.89	2.37	2.09	1.88	1.73	1.62	1.52	1.45	1.40
	.60	3.82	2.69	2.20	1.94	1.74	1.60	1.49	1.40	1.34	1.28
	.50	3.55	2.49	2.05	1.79	1.61	1.47	1.37	1.29	1.22	1.17
	.40	3.25	2.29	1.88	1.64	1.46	1.34	1.25	1.17	1.11	1.06
	.30	2.89	2.04	1.68	1.45	1.29	1.18	1.10	1.03	.98	.93
	.20	2.44	1.73	1.41	1.22	1.09	1.00	.93	.87	.82	.78
	.10	1.81	1.27	1.03	.90	.81	.74	.69	.65	.61	.58
	.05	1.53	.92	.76	.66	.59	.53	.49	.46	.44	.41
	0	0	0	0	0	0	0	0	0	0	0

(d) Plain flap at δ=40°

E →	0.05	0.10	0.15	0.20	0.25	0.30	0.35	0.40
$\frac{x/c}{1-E}$ (ahead of hinge) ↑	0	0	0	0	0	0	0	0
	.15	.15	.16	.16	.17	.17	.18	.19
	.22	.23	.23	.24	.25	.25	.26	.27
	.33	.34	.35	.36	.38	.39	.40	.42
	.43	.44	.45	.46	.47	.49	.51	.52
	.54	.55	.56	.57	.58	.60	.62	.64
	.66	.66	.68	.69	.71	.73	.75	.77
	.79	.80	.82	.83	.85	.88	.90	.93
	.97	.98	1.00	1.01	1.03	1.05	1.08	1.11
	1.23	1.23	1.25	1.26	1.28	1.30	1.33	1.36
	1.58	1.59	1.60	1.61	1.61	1.62	1.62	1.63
	4.10	2.90	2.42	2.12	1.99	1.88	1.81	1.76
$\frac{1-\frac{x}{c}}{E}$ (back of hinge) ↓	4.24	3.01	2.52	2.23	2.02	1.88	1.78	1.72
	4.29	3.04	2.53	2.22	2.00	1.84	1.73	1.66
	4.27	3.02	2.48	2.18	1.96	1.81	1.70	1.60
	4.14	2.91	2.39	2.10	1.89	1.74	1.62	1.52
	3.92	2.75	2.27	1.98	1.77	1.62	1.51	1.42
	3.64	2.56	2.11	1.83	1.64	1.50	1.40	1.31
	3.28	2.31	1.90	1.64	1.47	1.34	1.24	1.17
	2.82	1.98	1.62	1.40	1.26	1.15	1.07	1.00
	2.11	1.48	1.20	1.05	.95	.87	.81	.76
	1.79	1.08	.89	.77	.69	.63	.58	.54
	0	0	0	0	0	0	0	0

(e) Plain flap at δ=50°

E →	0.5	0.10	0.15	0.20	0.25	0.30	0.35	0.40
$\frac{x/c}{1-E}$ (ahead of hinge) ↑	0	0	0	0	0	0	0	0
	.05	.15	.15	.16	.16	.17	.17	.18	.19
	.10	.22	.23	.23	.24	.25	.25	.26	.27
	.20	.33	.34	.35	.35	.36	.38	.39	.40
	.30	.43	.44	.45	.46	.47	.49	.51	.52
	.40	.54	.55	.56	.57	.58	.60	.62	.64
	.50	.66	.66	.68	.69	.71	.73	.75	.77
	.60	.79	.80	.82	.83	.85	.88	.90	.93
	.70	.97	.98	1.00	1.03	1.05	1.08	1.11	1.14
	.80	1.21	1.22	1.23	1.25	1.26	1.29	1.32	1.35
	.90	1.54	1.55	1.56	1.57	1.57	1.57	1.57	1.57
	1.00	3.81	2.68	2.27	2.00	1.86	1.77	1.71	1.67
$\frac{1-\frac{x}{c}}{E}$ (back of hinge) ↓	.90	4.18	2.90	2.45	2.15	1.95	1.81	1.72	1.66
	.80	4.25	3.00	2.50	2.20	1.98	1.82	1.72	1.64
	.70	4.27	3.02	2.48	2.18	1.96	1.81	1.70	1.59
	.60	4.21	2.97	2.43	2.14	1.92	1.77	1.65	1.55
	.50	4.07	2.86	2.36	2.06	1.84	1.69	1.57	1.48
	.40	3.86	2.71	2.24	1.95	1.73	1.59	1.48	1.39
	.30	3.52	2.49	2.04	1.76	1.58	1.44	1.34	1.25
	.20	3.06	2.15	1.76	1.53	1.37	1.25	1.16	1.09
	.10	2.34	1.64	1.33	1.16	1.05	.96	.90	.84
	.05	2.02	1.22	1.00	.87	.78	.70	.65	.61
	0	0	0	0	0	0	0	0	0

(f) Plain flap at δ=60°

E →	0.05	0.10	0.15	0.20	0.25	0.30	0.35	0.40
$\frac{x/c}{1-E}$ (ahead of hinge) ↑	0	0	0	0	0	0	0	0
	.15	.15	.16	.16	.17	.17	.18	.19
	.22	.23	.23	.24	.25	.25	.26	.27
	.33	.34	.35	.35	.36	.38	.39	.40
	.43	.44	.45	.46	.47	.49	.51	.52
	.54	.55	.56	.57	.58	.60	.62	.64
	.66	.67	.68	.69	.71	.73	.75	.77
	.79	.80	.82	.83	.85	.88	.90	.93
	.97	.98	.99	1.01	1.02	1.05	1.07	1.10
	1.20	1.21	1.22	1.24	1.25	1.28	1.29	1.32
	1.52	1.53	1.54	1.55	1.54	1.53	1.51	1.50
	3.84	2.59	2.22	1.97	1.81	1.71	1.63	1.59
$\frac{1-\frac{x}{c}}{E}$ (back of hinge) ↓	4.04	2.80	2.36	2.08	1.88	1.76	1.68	1.62
	4.16	2.94	2.45	2.15	1.94	1.78	1.68	1.59
	4.27	3.02	2.48	2.18	1.96	1.81	1.70	1.59
	4.27	3.01	2.46	2.17	1.95	1.79	1.67	1.57
	4.18	2.93	2.42	2.11	1.89	1.73	1.62	1.52
	4.01	2.82	2.33	2.02	1.80	1.65	1.54	1.45
	3.71	2.62	2.15	1.86	1.66	1.52	1.41	1.32
	3.27	2.29	1.88	1.63	1.46	1.33	1.24	1.16
	2.51	1.76	1.43	1.25	1.13	1.03	.96	.90
	2.18	1.31	1.08	.93	.84	.76	.71	.66
	0	0	0	0	0	0	0	0

[1] Modified form of table III, ref. 9; the normal-force coefficient was taken to be essentially the same as the lift coefficient.